Search for massive, long-lived particles using multitrack displaced vertices or displaced lepton pairs in *pp* collisions at $\sqrt{s} = 8$ TeV with the ATLAS detector

G. Aad *et al.*[*]
(ATLAS Collaboration)

(Received 21 April 2015; revised manuscript received 19 August 2015; published 13 October 2015)

Many extensions of the Standard Model posit the existence of heavy particles with long lifetimes. This article presents the results of a search for events containing at least one long-lived particle that decays at a significant distance from its production point into two leptons or into five or more charged particles. This analysis uses a data sample of proton-proton collisions at $\sqrt{s} = 8$ TeV corresponding to an integrated luminosity of 20.3 fb^{-1} collected in 2012 by the ATLAS detector operating at the Large Hadron Collider. No events are observed in any of the signal regions, and limits are set on model parameters within supersymmetric scenarios involving R-parity violation, split supersymmetry, and gauge mediation. In some of the search channels, the trigger and search strategy are based only on the decay products of individual long-lived particles, irrespective of the rest of the event. In these cases, the provided limits can easily be reinterpreted in different scenarios.

DOI: 10.1103/PhysRevD.92.072004 PACS numbers: 12.60.Jv, 13.85.Rm, 14.80.Ly, 14.80.Pq

I. INTRODUCTION

Several extensions to the Standard Model (SM) predict the production at the Large Hadron Collider (LHC) of heavy particles with lifetimes of order picoseconds to nanoseconds (e.g., see Ref. [1] and references therein). At the LHC experiments, the decay of a long-lived particle (LLP) with lifetime in this range could be observed as a displaced vertex (DV), with daughter particles produced at a significant distance from the interaction point (IP) of the incoming proton beams. Particle decays may be suppressed by small couplings or high mass scales, thus resulting in long lifetimes. An example of a small-coupling scenario is supersymmetry with R-parity violation (RPV) [2,3]. The present (largely indirect) constraints on RPV couplings allow the decay of the lightest supersymmetric particle (LSP) as it traverses a particle detector at the LHC. In general gauge-mediated supersymmetry breaking (GGM) scenarios [4], the next-to-lightest supersymmetric particle (NLSP) decays into an SM particle and the LSP, which is a very light gravitino. The NLSP width is suppressed by the large supersymmetry-breaking scale, and may be such that its decay leads to the formation of a DV. Within split supersymmetry [5,6], gluino ($\tilde{g}$) decay is suppressed by the high mass of the squarks. Long-lived gluinos then hadronize into heavy "R-hadrons" that may decay at a detectable distance from their production point. Additional scenarios with LLPs include hidden-valley [7], dark-sector gauge bosons [8], and stealth supersymmetry [9]. Some of the models are disfavored [10] by the recent observation of a Higgs boson at $m_H \approx 125$ GeV [11,12].

This article presents the results of a search for DVs that arise from decays of long-lived, heavy particles, at radial distances of millimeters to tens of centimeters from the proton-proton IP in the ATLAS detector at the LHC. Two types of signatures are considered. In the dilepton signature, the vertex is formed from at least two lepton candidates (with "lepton" referring to an electron or a muon), with opposite electric charges. In the multitrack signature, the DV must contain at least five charged-particle tracks. This signature is divided into four different final states, in which the DV must be accompanied by a high-transverse-momentum (high-p_{T}) muon or electron candidate that originates from the DV, jets, or missing transverse momentum ($E_{\mathrm{T}}^{\mathrm{miss}}$). These signatures are labeled DV + muon, DV + electron, DV + jets, and DV + $E_{\mathrm{T}}^{\mathrm{miss}}$, respectively. In all signatures, at least one DV is required per event. In all cases, the expected background is much less than one event.

The multitrack results improve on the previous ATLAS searches for this signature [13,14] in several ways. The LHC center-of-mass energy is increased to 8 TeV, and the integrated luminosity is more than 4 times larger. While the previous search required only a high-p_{T} muon trigger, the current search also uses high-p_{T} electron, jets, or $E_{\mathrm{T}}^{\mathrm{miss}}$ triggers. Furthermore, the detector volume used for the search has been enlarged by more than a factor of 3.

This is the first search for high-mass, displaced lepton pairs at ATLAS. A previous ATLAS search [15] considered pairs of muons that were highly collimated due to the low

[*]Full author list given at the end of the article.

mass of the decaying particle. ATLAS has also searched for long-lived particles that decay inside the hadronic calorimeter [16,17], the inner detector, or the muon spectrometer [18], or that traverse the entire detector [19].

Related searches have been performed at other experiments. The CMS Collaboration has searched for decays of a long-lived particle into a final state containing two electrons, two muons [20,21], an electron and a muon [22], or a quark-antiquark pair [23]. The LHCb Collaboration has searched for long-lived particles that decay into jet pairs [24]. The Belle Collaboration has searched for long-lived heavy neutrinos [25], and the *BABAR* Collaboration has searched for displaced vertices formed of two charged particles [26]. The D0 Collaboration has searched for displaced lepton pairs [27] and $b\bar{b}$ pairs [28], and the CDF Collaboration has searched for long-lived particles decaying to Z bosons [29]. LLPs have also been searched for by the ALEPH Collaboration at LEP [30].

This article is organized as follows. First, the ATLAS detector and event samples used are described in Secs. II and III, respectively. The event reconstruction and vertex selection criteria are given in Sec. IV, while the signal efficiency is detailed in Sec. V. The background estimation is given in Sec. VI, with the systematic uncertainties on background and signal in Sec. VII. Finally, the search results are given in Sec. VIII, along with their interpretations in various supersymmetric scenarios.

II. THE ATLAS DETECTOR

The ATLAS experiment[1] [31] is a multipurpose detector at the LHC. The detector consists of several layers of subdetectors. From the IP outwards, there is an inner tracking detector (ID), electromagnetic and hadronic calorimeters, and a muon spectrometer (MS).

The ID is immersed in a 2 T axial magnetic field and extends from a radius of about 45 mm to 1100 mm and to $|z|$ of about 3100 mm. It provides tracking and vertex information for charged particles within the pseudorapidity region $|\eta| < 2.5$. At small radii, silicon pixel layers and stereo pairs of silicon microstrip detectors provide high-resolution position measurements. The pixel system consists of three barrel layers, and three forward disks on either side of the IP. The barrel pixel layers, which are positioned at radii of 50.5 mm, 88.5 mm, and 122.5 mm, are of particular relevance to this work. The silicon microstrip tracker (SCT) comprises four double layers in the barrel and nine forward disks on either side. The radial position of the innermost (outermost) SCT barrel layer is 30.3 cm (52.0 cm). A further tracking system, a transition-radiation tracker (TRT), is positioned at larger radii, with coverage up to $|\eta| = 2.0$. This device has two hit thresholds, the higher of which is used to assist in the identification of electrons through the production of transition radiation within the TRT.

The calorimeter provides coverage over the range $|\eta| < 4.9$. It consists of a lead/liquid-argon electromagnetic calorimeter, a hadronic calorimeter comprising a steel and scintillator-tile system in the barrel region, and a liquid-argon system with copper and tungsten absorbers in the end caps.

The MS provides muon identification and contributes to the muon momentum measurement. This device has a coverage in pseudorapidity of $|\eta| < 2.7$ and is a three-layer system of gas-filled tracking chambers. The pseudorapidity region $|\eta| < 2.4$ is additionally covered by separate trigger chambers, used by the hardware trigger for the first level of triggering (level-1). The MS is immersed in a magnetic field that is produced by a set of toroid magnets, one for the barrel and one each for the two end caps.

Online event selection is performed with a three-level trigger system. It is composed of a hardware-based level-1 trigger that uses information from the MS trigger chambers and the calorimeters, followed by two software-based trigger levels.

III. DATA AND SIMULATED EVENTS

The data used in this analysis were collected in 2012 at a pp center-of-mass energy of $\sqrt{s} = 8$ TeV. After the application of detector and data-quality requirements, the integrated luminosity of the data sample is 20.3 fb^{-1}. The uncertainty on the integrated luminosity is $\pm 2.8\%$. It is derived following the same methodology as that detailed in Ref. [32]. With respect to the origin of the ATLAS coordinate system at the center of the detector, the mean position of the pp collision, averaged throughout the collected data sample, is $\langle x \rangle = -0.3$ mm, $\langle y \rangle = 0.7$ mm, $\langle z \rangle = -7.7$ mm. The root-mean-square spread of the z distribution of the collisions is $\sigma_z = 47.7$ mm, and the spreads in the x and y directions are less than 0.1 mm.

Samples of simulated Monte Carlo (MC) events are used to study the reconstruction and trigger efficiency for signal events within RPV, split supersymmetry, and GGM scenarios. In each simulated event, two gluinos or two squarks are created in the pp collision. Both of these primary particles undergo decay chains described by the same set of effective operators. In the simulated GGM and RPV scenarios, the LLP is the lightest neutralino $\tilde{\chi}_1^0$. In the split-supersymmetry scenario, the LLP is the gluino. Diagrams representing the simulated processes are shown in Fig. 1.

[1]ATLAS uses a right-handed coordinate system with its origin at the nominal IP in the center of the detector and the z axis along the beam pipe. The x axis points from the IP to the center of the LHC ring, and the y axis points upward. Cylindrical coordinates (r, ϕ) are used in the transverse plane, ϕ being the azimuthal angle around the beam pipe. The pseudorapidity is defined in terms of the polar angle θ as $\eta = -\ln\tan(\theta/2)$.

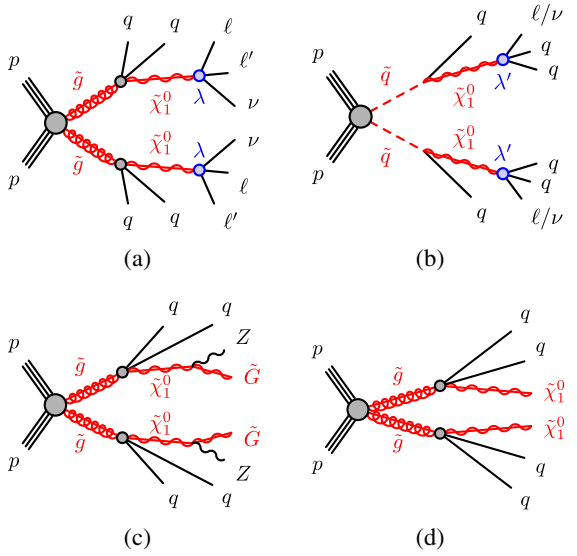

FIG. 1 (color online). Diagrams representing some of the processes under study, corresponding to the simulated event samples. In RPV scenarios, the long-lived neutralino may decay via the (a) λ_{ijk} or (b) λ'_{ijk} couplings. (c) Long-lived neutralino decay in a GGM scenario. (d) Long-lived R-hadron decay in a split-supersymmetry scenario. The quarks and leptons shown may have different flavors. Filled circles indicate effective interactions.

All samples are generated with the AUET2B ATLAS underlying-event tune [33] and the CTEQ6L1 parton distribution function (PDF) set [34]. Events are generated consistently with the position of the pp luminous region and weighted so as to yield the correct z distribution of the collisions. Each generated event is processed with the GEANT4-based [35] ATLAS detector simulation [36] and treated in the same way as the collision data. The samples include a realistic modeling of the effects of multiple pp collisions per bunch crossing observed in the data, obtained by overlaying additional simulated pp events generated using PYTHIA8 [37], on top of the hard scattering events, and reweighting events such that the distribution of the number of interactions per bunch crossing matches that in the data.

In what follows, the notation $P \to A[L \to F]$ denotes an MC sample in which a primary particle P produced in the pp collision decays into a long-lived particle L and additional particles denoted A. The decay of the LLP into final state F is enclosed in square brackets. Samples where the primary particle is long-lived are denoted with $[L \to F]$. In both cases, masses may be indicated with parentheses, as in $[L(100\ \text{GeV}) \to F]$. The symbol q indicates a u- or d-quark unless otherwise specified, and ℓ indicates an electron or a muon. Charge conjugation of fermions is to be understood where appropriate.

RPV samples of the type $\tilde{g} \to qq[\tilde{\chi}_1^0 \to \ell\ell'\nu]$ are produced with HERWIG++ 2.6.3 [38]. Decays of the neutralino into a neutrino and light leptons, which may be e^+e^-, $\mu^+\mu^-$, or $e^\pm\mu^\mp$, take place due to the nonzero values of the RPV couplings λ_{121} and λ_{122} [2].

RPV samples of $\tilde{q} \to q[\tilde{\chi}_1^0 \to \ell qq/\nu qq]$ are generated with PYTHIA6.426.2 [39]. The $\tilde{\chi}_1^0$ decay into two light quarks and an electron, muon, or neutrino is governed by the nonzero RPV coupling λ'_{i11}. Samples containing heavy-flavor quarks, $\tilde{q} \to q[\tilde{\chi}_1^0 \to \ell qb]$ (produced with $\lambda'_{i13} \neq 0$) and $\tilde{q} \to q[\tilde{\chi}_1^0 \to \ell cb]$ (corresponding to $\lambda'_{i23} \neq 0$) are also generated, in order to study the impact of long-lived charm and bottom hadrons on the efficiency of DV reconstruction. A $\tilde{g} \to qq[\tilde{\chi}_1^0 \to \ell qq]$ sample is used to quantify the effect of prompt NLSP decays on the reconstruction efficiency, by comparing with the corresponding model with squark production.

PYTHIA6.426.2 is used to produce GGM samples denoted $\tilde{g} \to qq[\tilde{\chi}_1^0 \to \tilde{G}Z]$, in which the NLSP $\tilde{\chi}_1^0$ is a Higgsino-like neutralino. Both the leptonic and hadronic decays of the Z boson are considered.

Within a split-supersymmetry scenario, PYTHIA6.427 is used to simulate production and hadronization of a primary, long-lived gluino. GEANT4 simulates the propagation of the R-hadron through the detector [40], and PYTHIA decays the R-hadron into a stable neutralino plus two quarks (u, d, s, c, or b), a gluon, or two top quarks. The resulting samples are denoted $[\tilde{g} \to qq\tilde{\chi}_1^0]$, $[\tilde{g} \to g\tilde{\chi}_1^0]$, or $[\tilde{g} \to tt\tilde{\chi}_1^0]$, respectively.

Signal cross sections are calculated to next-to-leading order in the strong coupling constant, adding the resummation of soft gluon emission at next-to-leading-logarithmic accuracy (NLO + NLL) [41–45]. The nominal cross section and its uncertainty are taken from an envelope of cross-section predictions using different PDF sets and factorization and renormalization scales, as described in Ref. [46].

In addition to these signal samples, MC samples of QCD dijet events, Drell-Yan events, and cosmic-ray muons are used for estimating some systematic uncertainties and some of the smaller background rates, as well as for validation of aspects of the background-estimation methods.

IV. EVENT RECONSTRUCTION AND SELECTION

The event-reconstruction and selection procedures are designed, based on MC and experience from previous analyses [13,14], to strongly suppress background and accommodate robust background-estimation methods (described in Sec. VI), while efficiently accepting signal events over a broad range of LLP masses, lifetimes, and velocities.

The initial event selection is performed with a combination of triggers that require the presence of lepton candidates, jets, or $E_{\mathrm{T}}^{\mathrm{miss}}$. This selection is described in Sec. IV A.

Off-line selection criteria for leptons, jets, and $E_{\mathrm{T}}^{\mathrm{miss}}$ (see Sec. IV B) are used to further filter events for off-line processing, as described in Sec. IV C.

Events satisfying the filter requirements undergo a CPU-intensive process termed "retracking," aimed at efficient reconstruction of tracks with large impact parameter (d_0) with respect to the transverse position of any primary vertex (PV) of particles formed from the pp collision. Retracking is described in Sec. IV D.

At the final event-selection stage, the presence of a pp collision is ensured by first requiring the event to have a PV formed from at least five tracks and situated in the longitudinal range $|z| < 200$ mm, consistent with the IP.

The final selection is based on the reconstruction of a multitrack DV or dilepton DV, described in Secs. IV E and IV F, respectively.

A. Trigger requirements

Events must satisfy trigger requirements based on muon, electron, jets, or $E_{\mathrm{T}}^{\mathrm{miss}}$ criteria.

Where muon triggers are used, a muon candidate is required by the trigger algorithm to be identified in the MS with transverse momentum $p_{\mathrm{T}} > 50$ GeV. Its pseudorapidity must be in the MS-barrel region $|\eta| < 1.07$, to reduce the trigger rate from fake muons due to beam background in the end cap region.

Photon triggers are used for channels requiring electron candidates, since the ID track of a high-d_0 electron may not be reconstructed. These require only a high-energy deposit in the electromagnetic calorimeter and have no veto or selection based on ID tracks. Photon triggers provide significantly less background rejection than muon triggers. Therefore, the trigger used for final states involving electrons requires either a single photon candidate with $p_{\mathrm{T}} > 120$ GeV or two photon candidates with $p_{\mathrm{T}} > 40$ GeV each.

The trigger requirement for the DV + $E_{\mathrm{T}}^{\mathrm{miss}}$ search is $E_{\mathrm{T}}^{\mathrm{miss}} > 80$ GeV. The DV + jets trigger requires four jets with $p_{\mathrm{T}} > 80$ GeV, five jets with $p_{\mathrm{T}} > 55$ GeV, or six jets with $p_{\mathrm{T}} > 45$ GeV.

B. Off-line object definition

The reconstruction and selection criteria for $E_{\mathrm{T}}^{\mathrm{miss}}$, muon, electron, and jet candidates are described in what follows. These object definitions are used by the off-line filter (Sec. IV C) and the final analysis (Secs. IV E and IV F).

1. Muon selection

Muon candidates are required to be reconstructed in both the MS and the ID. The ID track associated with the muon candidate is required to have at least four SCT hits, but the number of required hits is reduced if the track crosses nonoperational sensors. Furthermore, the track must satisfy an $|\eta|$-dependent requirement on the number of TRT hits. No pixel hit requirement is applied to the muon-candidate track, which is different from the standard ATLAS muon-reconstruction algorithm [47].

2. Photon and electron selection

Photon and electron candidates are identified with criteria based on the fraction of the candidate energy deposited in the hadronic calorimeter and on the shape of the electromagnetic shower. In addition, electron candidates must be in the pseudorapidity region $|\eta| < 2.47$ and must satisfy requirements on the number of TRT hits associated with the ID track, the fraction of high-threshold TRT hits, and the pseudorapidity difference between the electron-candidate track and the associated calorimeter cluster. In contrast to the standard ATLAS electron-selection requirements [48], no requirement on the number of silicon hits is applied.

3. Jet and $E_{\mathrm{T}}^{\mathrm{miss}}$ selection

Jet candidates are reconstructed using the anti-k_t jet clustering algorithm [49,50] with a radius parameter $R = 0.6$. The inputs to this algorithm are the energies of clusters [51,52] of calorimeter cells seeded by those with energy significantly above the measured noise. Jet momenta are constructed by performing a four-vector sum over these cell clusters, treating each cell as a four-momentum with zero mass. Jets are initially calibrated to the electromagnetic energy scale, which correctly measures the energy deposited in the calorimeter by electromagnetic showers [51]. Further jet-energy scale corrections are derived from MC simulation and data, and used to calibrate the energies of jets to the scale of their constituent particles [51]. Jets are required to satisfy $|\eta| < 4.5$ after all corrections are applied.

A special category of jets is termed "trackless" jets. These are reconstructed as above, except that the anti-k_t radius parameter is $R = 0.4$, the jet pseudorapidity is in the range $|\eta| < 2.5$, and the scalar sum of the transverse momenta of the tracks in the jet is required to satisfy $\sum_{\mathrm{tr}} p_{\mathrm{T}} < 5$ GeV. Trackless jets may arise from decays of LLPs that take place far from the PV, where track-reconstruction efficiency is low.

The measurement of the missing transverse momentum $E_{\mathrm{T}}^{\mathrm{miss}}$ is based on the calibrated transverse momenta of all jet and lepton candidates, as well as all calorimeter energy clusters not associated with such objects [53,54].

C. Off-line–filter requirements

Events are selected for retracking and subsequent off-line analysis based on off-line filters that require one of the following:

(i) A muon candidate with $p_{\mathrm{T}} > 50$ GeV, an electron candidate with $p_{\mathrm{T}} > 110$ GeV, or a photon candidate with $p_{\mathrm{T}} > 130$ GeV. Electron candidates, and muon candidates that are associated with an ID track at this stage, are required to have $d_0 > 1.5$ mm. The sample selected by this criterion contains 8.5×10^6 events.

(ii) A pair of candidate electrons, photons, or an electron-photon pair, with p_{T} thresholds between 38 and 48 GeV per object, and electron impact parameter satisfying $d_0 > 2.0$ mm or $d_0 > 2.5$ mm depending on the channel. This criterion selects 2.4×10^6 events.

(iii) Either two 50 GeV trackless jets and $E_{\mathrm{T}}^{\mathrm{miss}} > 100$ GeV (selecting 1.9×10^4 events) or one 45 GeV trackless jet and between four and six jets passing the same p_{T} thresholds as those applied in the trigger, listed in Sec. IV A (selecting 4.6×10^5 events).

D. Retracking

In standard ATLAS tracking [31], several algorithms are used to reconstruct charged-particle tracks. In the silicon-seeded approach, combinations of hits in the pixel and SCT detectors are used to form initial track candidates (seeds) that are then extended into the TRT. Another algorithm starts from track segments formed of TRT hits, and extrapolates back into the SCT, adding any silicon hits that are compatible with the reconstructed trajectory. Both of these methods place constraints on the transverse and longitudinal impact parameters of track candidates that result in a low efficiency for tracks originating from a DV, many of which have large d_0.

To recover some of these lost tracks, the silicon-seeded tracking algorithm is rerun off-line, using only hits that are not associated with existing tracks, for the events that satisfy the trigger and filter requirements (Secs. IV A and IV C). This retracking procedure is performed with the looser requirement $d_0 < 300$ mm and $|z_0| < 1500$ mm. Furthermore, retracking requires a track to have at least five detector hits that are not shared with other tracks, while the corresponding requirement in standard silicon-seeded tracking is at least six hits. To reduce the rate of false seed tracks, it is required that these additional tracks have $p_{\mathrm{T}} > 1$ GeV, while the standard-tracking requirement is $p_{\mathrm{T}} > 400$ MeV.

The remainder of the analysis proceeds with both the standard-tracking tracks and retracking tracks. To realize the benefits of retracking for lepton candidates, the lepton-identification algorithms are rerun with the retracking tracks.

E. Multitrack vertex reconstruction and final selection

1. Multitrack vertex reconstruction

Tracks used for DV reconstruction are required to satisfy $p_{\mathrm{T}} > 1$ GeV and to have at least two SCT hits, to ensure high track quality. The requirement $d_0 > 2$ mm is also applied, rejecting at least 97% of tracks originating from a PV. The tracks are rejected if they have no TRT hits and fewer than two pixel hits, in order to remove fake tracks.

The selected tracks are used to construct a multitrack DV by means of an algorithm based on the incompatibility-graph approach [55].

The algorithm starts by finding two-track seed vertices from all pairs of tracks. Seed vertices that have a vertex fit χ^2 of less than 5.0 (for 1 degree of freedom) are retained. If the seed vertex is inside the innermost pixel layer, both tracks must have a hit in this layer. If the vertex is between the first and second (second and third) pixel layers, both tracks must have a hit in either the second or third pixel layer (third pixel layer or the SCT). A seed vertex is rejected if any of its tracks have hits at radial positions smaller than that of the vertex. The interesting case of a charged LLP is not precluded by this selection, as the track formed by the LLP itself fails the $d_0 > 2$ mm requirement, and is therefore not included in the seed vertex. To ensure consistency between the position of the seed vertex and the direction $\hat{p}$ of the three-momentum vector of the seed-vertex tracks, the requirement $\vec{d} \cdot \hat{p} > -20$ mm is applied, where $\vec{d} = \vec{r}_{\mathrm{DV}} - \vec{r}_{\mathrm{PV}}$ is referred to as the "distance vector" between the position of the DV and that of the first PV. The first PV is defined as the PV with the largest $\sum p_{\mathrm{T}}^2$, where the sum is over tracks associated with the PV.

Multitrack vertices are formed from combinations of seed vertices in an iterative process, as follows. If a track is assigned to several vertices, the vertex DV_1 with respect to which it has the largest χ^2 is identified. If this χ^2 is larger than 6, the track is removed from DV_1. Otherwise, the algorithm finds the vertex DV_2 that has the smallest value of D/σ_D, where D is the distance between DV_1 and DV_2, and σ_D is the estimated uncertainty on D. If $D/\sigma_D < 3$, a single vertex is formed from all the tracks of both vertices. If this is not the case, the track is removed from DV_1. This process continues until no track is associated with more than one vertex. Finally, vertices are combined and refitted if they are separated by less than 1 mm. No requirement is made on the total charge of the tracks forming a vertex.

2. Vertex selection

The reduced χ^2 of the DV fit is required to be smaller than 5.0. The DV position must be within the fiducial region $r_{\mathrm{DV}} < 300$ mm, $|z_{\mathrm{DV}}| < 300$ mm, where r_{DV} and z_{DV} are the radial and longitudinal DV positions with respect to the origin. To minimize background due to tracks originating from the PVs, the transverse distance $\Delta_{xy} = \sqrt{(x_{\mathrm{DV}} - x_{\mathrm{PV}})^2 + (y_{\mathrm{DV}} - y_{\mathrm{PV}})^2}$ between the DV and any of the PVs is required to be at least 4 mm. Here x and y are the transverse coordinates of a given vertex, with the subscripts PV and DV denoting the type of vertex.

DVs that are situated within regions of dense detector material are vetoed using a three-dimensional map of the detector within the fiducial region. The map is constructed in an iterative process, beginning with geometrically simple detector elements that are fully accounted for in the MC

simulation. Subsequently, detailed structures, as well as the positioning and thickness of the simple elements, are obtained from the spatial distribution of vertices obtained from the data, taking advantage of the known ϕ periodicity of the detector to reduce statistical uncertainties. The vertices used to construct the map are required to be formed from fewer than five tracks, in order to avoid the signal region defined below. The invariant mass of these vertices, assuming massless tracks, must be greater than 50 MeV, to suppress vertices from photon conversions, which have low spatial resolution due to the small opening angle between the electrons, as well as electron scattering. Vertices arising from decays of K_S^0 mesons are removed with an invariant-mass criterion. The transverse-plane projection of the positions of vertices that occur inside the material regions is shown in Fig. 2.

As the final step in multitrack DV selection, the number of tracks forming the DV is required to satisfy $N_{\mathrm{tr}} \geq 5$, and the invariant mass m_{DV} of all the tracks in the vertex must be greater than 10 GeV. In calculating m_{DV}, each track is taken to have the mass of the charged pion. Candidate vertices that pass (fail) the $m_{\mathrm{DV}} > 10$ GeV requirement are hereafter referred to as being high-m_{DV} (low-m_{DV}) vertices.

The typical position resolution of the DV in the multitrack signal MC samples is tens of microns for r_{DV} and about 200 μm for z_{DV} near the IP. For vertices beyond the outermost pixel layer, which is located at a radius of 122.5 mm, the typical resolution is several hundred microns for both coordinates.

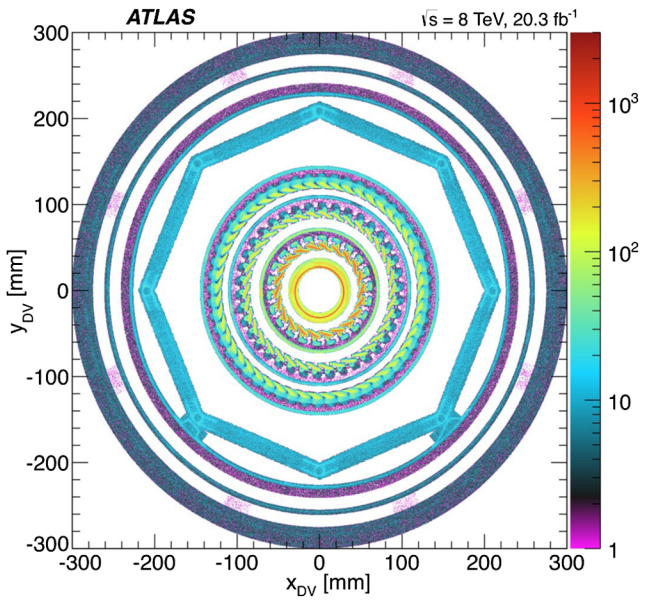

FIG. 2 (color online). Transverse-plane density (in arbitrary units) of vertices with fewer than five tracks in material regions that are excluded by the material veto in the region $|z| < 300$ mm. The innermost circle corresponds to the beam pipe. This is surrounded by the three pixel layers. The octagonal shape and outermost circles are due to support structures separating the pixel and SCT detectors.

3. DV + lepton selection

In the DV + muon search, the muon candidate is required to have triggered the event and have transverse momentum $p_{\mathrm{T}} > 55$ GeV, which is well into the region where the trigger efficiency is approximately independent of the muon momentum. The muon candidate is further required to be in the range $|\eta| < 1.07$ and have transverse impact parameter $d_0 > 1.5$ mm. A cosmic-ray muon traversing the entire ATLAS detector is reconstructed as two back-to-back muon candidates. To reject cosmic-ray background, events are discarded if they contain two muon candidates with $\Delta R_{\mathrm{cosmic}} = \sqrt{(\pi - \Delta\phi)^2 - (\eta_1 + \eta_2)^2} < 0.04$, where η_1 and η_2 are the pseudorapidities of the two reconstructed muon candidates and $\Delta\phi$ is their angular separation in the azimuthal plane. This has a negligible impact on the signal efficiency.

In the DV + electron search, the electron candidate is required to have triggered the event and to satisfy $p_{\mathrm{T}} > 125$ GeV and $d_0 > 1.5$ mm.

To ensure that the lepton candidate is associated with the reconstructed DV, the distance of closest approach of the selected muon or electron candidate to the DV is required to be less than 0.5 mm. This requirement ensures that the reconstructed DV gave rise to the muon or electron candidate that triggered the event, and so the selection efficiency for each LLP decay is independent of the rest of the event. This facilitates a straightforward calculation of the event-selection efficiency for scenarios with different numbers of LLPs. The aforementioned selections are collectively referred to as the vertex-selection criteria. Events containing one or more vertices satisfying these criteria are accepted.

4. DV + jets and DV + $E_{\mathrm{T}}^{\mathrm{miss}}$ selection

The DV + jets selection requires one of the following: four jets with $p_{\mathrm{T}} > 90$ GeV; five jets with $p_{\mathrm{T}} > 65$ GeV; or six jets with $p_{\mathrm{T}} > 55$ GeV. All jets considered in these selection criteria are required to have $|\eta| < 2.8$. DV + jet candidate events are discarded if they contain any candidate jet failing to satisfy quality criteria designed to suppress detector noise and noncollision backgrounds [56,57]. This has a negligible effect on the signal efficiency. In the DV + $E_{\mathrm{T}}^{\mathrm{miss}}$ search, the requirement $E_{\mathrm{T}}^{\mathrm{miss}} > 180$ GeV is applied. For these selection criteria, the trigger efficiency is approximately independent of the $E_{\mathrm{T}}^{\mathrm{miss}}$ and the jet transverse momenta.

F. Dilepton selection

In the dilepton search, muon candidates are required to satisfy $p_{\mathrm{T}} > 10$ GeV, $|\eta| < 2.5$, and $d_0 > 2$ mm. For electron candidates, the requirements are $p_{\mathrm{T}} > 10$ GeV

and $d_0 > 2.5$ mm. A lepton candidate is discarded if its ID track is in the pseudorapidity region $|\eta| < 0.02$, where the background-estimation procedure is observed to be unreliable (see Sec. VI).

To avoid double counting of vertices, lepton candidates used to form a dilepton DV must not have the same ID track as another lepton candidate. If two muon candidates or two electron candidates do share an ID track, the candidate that has the lower transverse momentum is discarded. If muon and electron candidates share an ID track, the electron candidate is discarded. Cosmic-ray muons, even those that interact while traversing the detector, are rejected by requiring that all lepton-candidate pairs satisfy $\Delta R_{\text{cosmic}} > 0.04$.

A dilepton DV is formed from at least two opposite-charge tracks identified as two electrons, two muons, or an electron and a muon. Any number of additional tracks may be included in the vertex. At this stage, it is verified that the dilepton selection criteria applied at the trigger and filter level (see Secs. IV A and IV C) are satisfied by the two lepton candidates forming the DV. Finally, the dilepton DV is required to satisfy the DV selection criteria specified in Sec. IV E 2, except for the requirement on the number of tracks, which is $N_{\text{tr}} \geq 2$. As in the DV + lepton case, the dilepton-DV selection relies only on the leptons in the DV and is independent of the rest of the event.

V. SIGNAL EFFICIENCY

In the dilepton and DV + lepton searches, where the selection criteria rely only on the particles produced in the DV, the vertex-level efficiency ϵ_{DV} is defined to be the product of acceptance and efficiency for reconstructing one signal DV, produced in the given search model, with all the trigger, filter, and final selection criteria. The event-level efficiency ϵ_{ev}, defined as the probability for an event containing two DVs to be identified with at least one DV satisfying all the selection criteria, is then obtained from the relation

$$\epsilon_{\text{ev}} = 2\mathcal{B}\epsilon_{\text{DV}} - \mathcal{B}^2\epsilon_{\text{DV}}^2, \tag{1}$$

where $\mathcal{B}$ is the LLP branching fraction into the specific search channel. In the DV + jets and DV + $E_{\text{T}}^{\text{miss}}$ searches, only the event-level efficiency is defined, since the selection criteria involve the entire event.

The efficiency for reconstructing a multitrack or dilepton DV with the above selection criteria depends strongly on the efficiencies for track reconstruction and track selection, which are affected by several factors: (1) The number of tracks originating from the DV and their total invariant mass increase with the LLP mass. (2) More tracks fail the minimal-d_0 requirement for small r_{DV}, or when the LLP is highly boosted. (3) The efficiency for reconstructing tracks decreases with increasing values of d_0. (4) When an LLP decays at a radius somewhat smaller than that of a pixel layer, many tracks share hits on that pixel layer, failing to meet the track-selection criteria. The resulting impact on efficiency can be seen in Fig. 3 at radii around 45 mm, 80 mm, and 115 mm.

The efficiency for reconstructing a multitrack DV is reduced when the LLP decays to charm or bottom hadrons, resulting in two or more nearby DVs. Each of these DVs has a high probability of failing to meet the N_{tr} and m_{DV} criteria, resulting in low efficiency if these DVs are not merged. This happens less at large values of r_{DV}, where DVs are more readily merged due to the worse position resolution.

The vertex-level efficiency does not depend appreciably on whether the primary particle is a squark or a gluino.

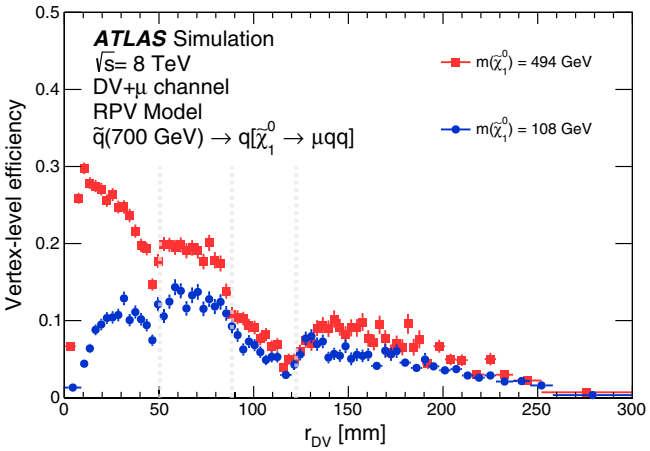

(a)

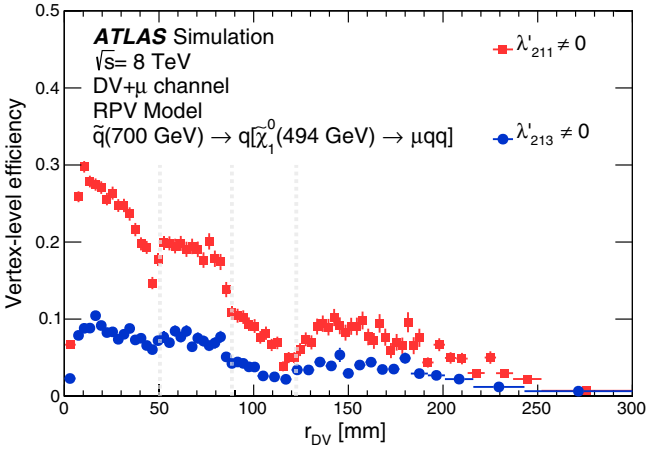

(b)

FIG. 3 (color online). Comparisons of the vertex-level efficiency as a function of the vertex radial position r_{DV} for different RPV samples. The vertical gray lines show the position of the first, second, and third pixel layers. (a) For the $\tilde{q} \to q[\tilde{\chi}_1^0 \to \mu qq]$ (λ'_{211}) samples with $m_{\tilde{q}} = 700$ GeV, comparing two cases of different LLP masses: $m_{\tilde{\chi}_1^0} = 494$ GeV, and $m_{\tilde{\chi}_1^0} = 108$ GeV. (b) For the $\tilde{q} \to q[\tilde{\chi}_1^0 \to \mu qq]$ (λ'_{211}) and $\tilde{q} \to q[\tilde{\chi}_1^0 \to \mu qb]$ (λ'_{213}) samples, indicated by the relevant nonzero RPV couplings.

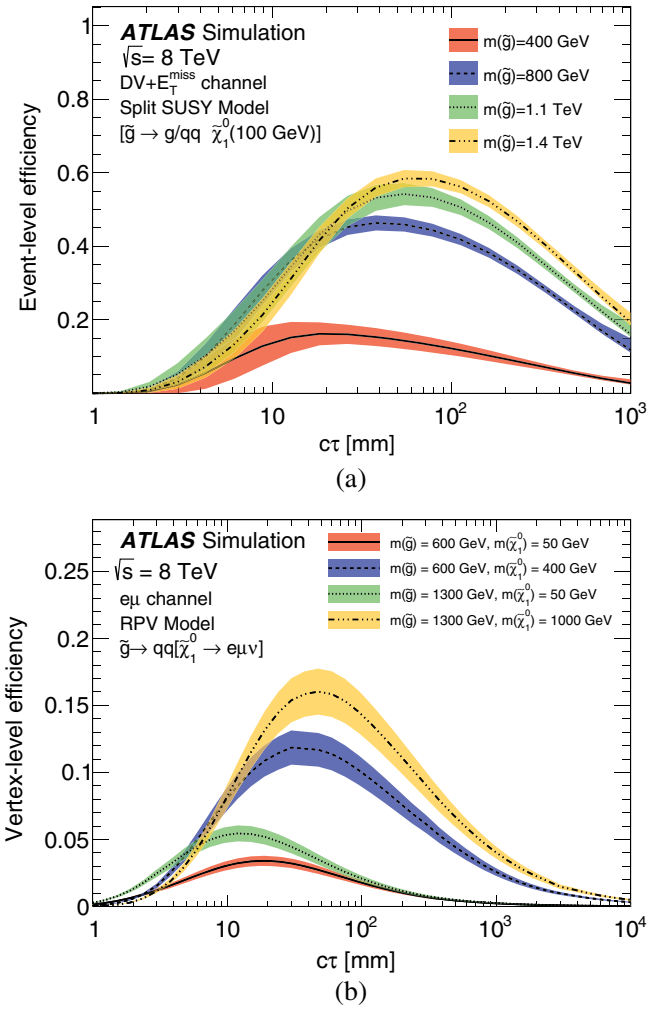

FIG. 4 (color online). (a) The event-level efficiency as a function of $c\tau$ for split-supersymmetry $[\tilde{g} \to g/qq\tilde{\chi}_1^0(100\ \mathrm{GeV})]$ samples with various gluino masses, reconstructed in the DV + $E_{\mathrm{T}}^{\mathrm{miss}}$ channel. (b) The vertex-level efficiency for the RPV $\tilde{g} \to qq[\tilde{\chi}_1^0 \to e\mu\nu]$ samples with combinations of gluino and neutralino masses, reconstructed in the $e\mu$ dilepton channel. The total uncertainties on the efficiencies are shown as bands (see Sec. VII).

However, the nature of the primary particle determines the number of jets, and hence impacts the event-level efficiency in the DV + jets and DV + $E_{\mathrm{T}}^{\mathrm{miss}}$ channels.

Examples of the impact of LLP boost, mass, and heavy-flavor decays on the vertex-level efficiency are shown in Fig. 3 for $\tilde{q} > q[\tilde{\chi}_1^0 \to \mu qq]$ samples. As an example of the benefits of retracking, it is worthwhile to note that without retracking, the vertex-level efficiency for the $m(\tilde{\chi}_1^0) = 494$ GeV, $\lambda'_{211} \neq 0$ sample shown in this figure is about 1% at $r_{\mathrm{DV}} = 80$ mm and is negligible for larger radii.

Events in each MC sample are generated with a fixed value of the LLP lifetime τ_{MC}. To obtain the vertex-level efficiency for a different lifetime τ, each LLP is given a weight

$$W_{\mathrm{DV}}(t,\tau) = \frac{\tau_{\mathrm{MC}}}{\tau}\exp\left(\frac{t}{\tau_{\mathrm{MC}}} - \frac{t}{\tau}\right), \tag{2}$$

where t is the true proper decay time of the generated LLP. The vertex-level efficiency is then the sum of weights for LLPs that satisfy all the criteria in the sample. The same procedure is applied when calculating the event-level efficiency, except that the entire event is weighted by

$$W_{\mathrm{evt}}(t_1,t_2,\tau) = W_{\mathrm{DV}}(t_1,\tau)W_{\mathrm{DV}}(t_2,\tau), \tag{3}$$

where t_1 and t_2 are the true proper decay times of the two LLPs in the event. Examples of the resulting dependence of ϵ_{DV} and ϵ_{ev} on the average proper decay distance $c\tau$ are shown in Fig. 4. For most models considered in this analysis, the peak efficiency is typically greater than 5%, and it occurs in the range $10 \lesssim c\tau \lesssim 100$ mm.

VI. BACKGROUND ESTIMATION

The expected number of background vertices is estimated from the collision data for each channel. Since the number of events satisfying the final selection criteria is very small, the general approach is to first obtain a high-statistical-precision assessment of the probability for background-vertex formation using a large data control sample. That probability is then scaled by the size of the signal-candidate sample relative to that of the control sample.

A. Multitrack-vertex background estimation

Background vertices that are due to accidental spatial crossing of tracks in a jet, particle interactions with material, or heavy-flavor decays have low values of m_{DV} and/or N_{tr} and thus fail the selection requirements. Such vertices may contribute to high-m_{DV}, high-N_{tr} background vertices via two mechanisms.

(i) The dominant source of backgrounds are low-m_{DV} vertices that are accidentally crossed by an unrelated, high-p_{T} track at large angle [$\mathcal{O}$(1 radian)] to the other tracks in the vertex. This is referred to as the accidental-crossing background.

(ii) A much smaller background contribution is due to merged vertices. In this case, two low-m_{DV} vertices are less than 1 mm apart, and thus may be combined by the vertex-reconstruction algorithm into a single vertex that satisfies the N_{tr} and m_{DV} criteria.

The expected background levels from the two sources are estimated from the data. In order for the background estimate to have high statistical precision, it is performed with a large sample containing all events that have undergone retracking. This includes the events selected for this search, as described in Sec. IV C, as well as events used for other ATLAS analyses. The sample is divided into three subsamples, referred to as the muon stream, the electron stream, and the jets + $E_{\mathrm{T}}^{\mathrm{miss}}$ stream, with the name

indicating the type of trigger used to select the events. The background level is estimated separately in each of these streams with the methods described below, and the results are used for the DV + muon, DV + electron, and DV + jets and DV + $E_{\mathrm{T}}^{\mathrm{miss}}$ signal regions, respectively.

To obtain the final background estimate in the signal region, the background estimate in each stream is multiplied by a final-selection scale factor F^{stream}, which is the fraction of events in the given stream that satisfy the final event-selection criteria, other than the DV selection criteria. The values of these fractions are 0.08%, 5.0%, 1.45%, and 0.04%, for the DV + muon, DV + electron, DV + jet, and DV + $E_{\mathrm{T}}^{\mathrm{miss}}$ searches, respectively. This use of F^{stream} assumes that the average number of vertices per event, $N_{\mathrm{ev}}^{\mathrm{DV}}$, is independent of the selection criteria. Based on the change in $N_{\mathrm{ev}}^{\mathrm{DV}}$ when the final selection criteria are applied, an upward bias correction of 60% is applied to the estimated background level in the DV + electron channel (the correction is included in the $F^{\mathrm{stream}} = 5.0\%$ value quoted above). The other channels have negligible bias. A 10% systematic uncertainty is estimated for all channels from the statistical uncertainty of the bias estimate.

1. Background from accidental vertex-track crossings

The accidental-crossing background is estimated separately in six radial regions, ordered from the inside out. Region 1 is inside the beam pipe. Regions 2, 3, and 4 correspond to the volumes just before each of the three pixel layers. Regions 5 and 6 are outside the pixel layers. Region 5 extends outwards to $r_{\mathrm{DV}} = 180$ mm, where there is essentially no detector material, while Region 6 covers the volume from $180 < r_{\mathrm{DV}} < 300$ mm. In each region, a study of the m_{DV} distribution of N_{tr}-track vertices, where $N_{\mathrm{tr}} = 3$ through 6, leads to identification of two types of background vertices, as follows.

The first type, which dominates the low-m_{DV} range, is due to accidental track crossings in Region 1, and particle-material interactions in the other regions. This contribution to the m_{DV} spectrum is referred to as collimated-tracks background, reflecting the typically small angle between the tracks. The m_{DV} distribution $P_{N_{\mathrm{tr}}}^{\mathrm{coll}}(m_{\mathrm{DV}})$ for this contribution is modeled from the N_{tr}-track vertices for which the average three-dimensional angle between every pair of tracks is less than 0.5. In Fig. 5, $P_3^{\mathrm{coll}}(m_{\mathrm{DV}})$ is seen to fully account for 3-track vertices with m_{DV} less than about 3 GeV. However, it does not account for vertices with higher masses, particularly the signal region, $m_{\mathrm{DV}} > 10$ GeV.

The high-m_{DV} part of the m_{DV} distribution is dominated by the second contribution, referred to as "DV + track." In this case, a $(N_{\mathrm{tr}} - 1)$-track vertex is crossed by an unrelated track at a large angle with respect to the momentum vector of the vertex tracks. To construct a model of the DV + track m_{DV} distribution of N_{tr}-track vertices, every $(N_{\mathrm{tr}} - 1)$-track

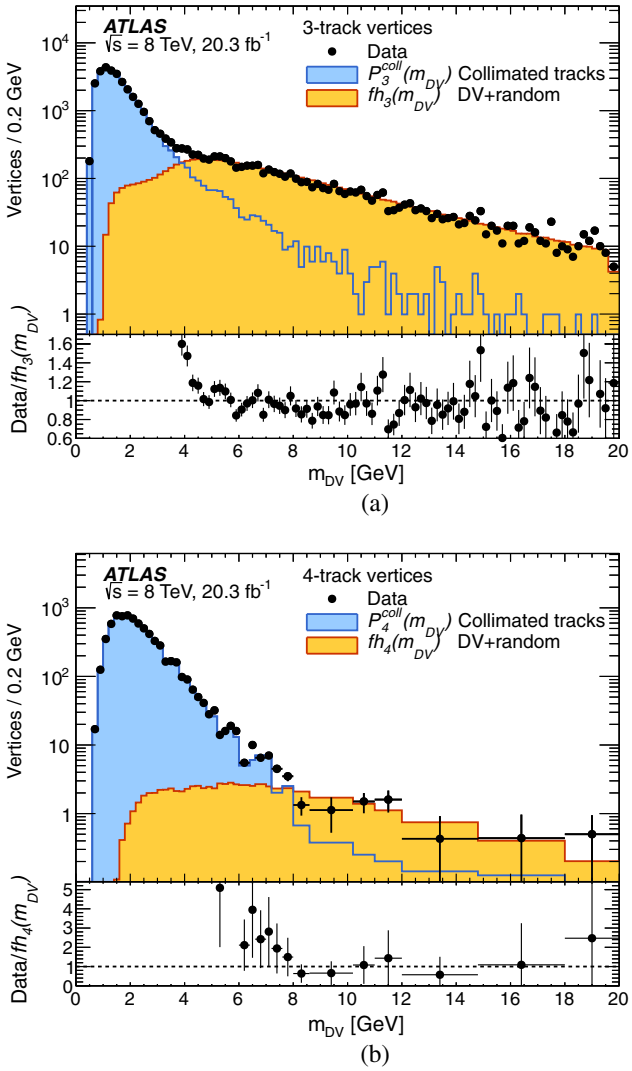

FIG. 5 (color online). The mass distribution for (a) 3-track and (b) 4-track vertices (data points) from the jets + $E_{\mathrm{T}}^{\mathrm{miss}}$ stream in Region 6, overlaid with the model $fh_3(m_{\mathrm{DV}})$ of Eq. (5) (yellow-shaded histogram) at high mass. The lower panel of each plot shows the ratio of the data to this model. The model for the collimated-track contribution $P_3^{\mathrm{coll}}(m_{\mathrm{DV}})$ (blue-shaded histogram), which is correlated with the low-mass data but not used for estimating the signal-region background, is also shown.

vertex, referred to as an "acceptor" vertex, is paired with a "donated" track that is taken from a "donor" vertex in another event. This is done for $N_{\mathrm{tr}} - 1$ in the range 2–5, where acceptor vertices with five tracks are required to have mass below 10 GeV, to avoid the signal region.

The pairing of a vertex and a track is performed with the following procedure. The donor vertex must satisfy all the DV selection criteria, except that the requirement on its mass is not applied, and it may have as few as two tracks. To ensure that the donated track is able to accurately model the effects of a large-angle crossing, it is required that the donor vertex be from the same radial region as the acceptor vertex, and that there is a large angle between the direction

of the donated track and the distance vector of the donor vertex.

In all regions apart from Region 1, the momentum vector of the donated track is then rotated, so that its azimuthal and polar angles ($\Delta\phi_{\text{donor}}$ and $\Delta\theta_{\text{donor}}$) with respect to the distance vector of the acceptor vertex match those that it originally had with respect to the donor vertex. This ensures that the contribution of the donated track to the acceptor vertex mass correctly reflects the accidental-crossing probability as a function of $\Delta\eta_{\text{donor}}$ and $\Delta\phi_{\text{donor}}$.

Then, the four-momentum of the acceptor vertex and the rotated four-momentum of the track are added, obtaining the m_{DV} value of the N_{tr}-track vertex that would have been formed from an accidental crossing of the acceptor vertex and the rotated donated track. The resulting m_{DV} distribution for the N_{pairs} DV + track pairs found in each region is denoted $h_{N_{\text{tr}}}(m_{\text{DV}})$, such that

$$\int_0^\infty h_{N_{\text{tr}}}(m_{\text{DV}})dm_{\text{DV}} = N_{\text{pairs}}. \tag{4}$$

Tracks from donor vertices in Region 1 are treated differently, since they tend to have high pseudorapidity, which impacts their DV-crossing probability more than their $\Delta\phi_{\text{donor}}$ and $\Delta\theta_{\text{donor}}$ values. Therefore, a Region-1 track is not rotated before its four-momentum is added to that of the acceptor vertex.

The high-m_{DV} distribution for N_{tr}-track vertices is then modeled by

$$P_{N_{\text{tr}}}(m_{\text{DV}}) = f h_{N_{\text{tr}}}(m_{\text{DV}}), \tag{5}$$

where

$$f = \frac{N_3^{10\text{ GeV}}}{\int_{10\text{ GeV}}^\infty h_3(m_{\text{DV}})dm_{\text{DV}}} \tag{6}$$

is the scale factor that normalizes the model to the data, and $N_3^{10\text{ GeV}}$ is the number of 3-track vertices with $m_{\text{DV}} > 10$ GeV. The model-predicted number of N_{tr}-track background vertices with $m_{\text{DV}} > 10$ GeV for a given stream and region is given by

$$N_{N_{\text{tr}}}^{\text{stream}} = \int_{10\text{ GeV}}^\infty P_{N_{\text{tr}}}(m_{\text{DV}})dm_{\text{DV}}. \tag{7}$$

The model describes the high-m_{DV} background distribution in data well, as seen in Fig. 5 for jets + $E_{\text{T}}^{\text{miss}}$-stream 3-track and 4-track vertices in Region 6. Also shown is the collimated-track contribution, which accounts for the low-m_{DV} part of the distribution. Using 4-track vertices to validate Eq. (7), the prediction for each of the three streams and six regions is compared with the observed number of vertices. The comparison, summarized in Fig. 6, shows good agreement within the statistical precision.

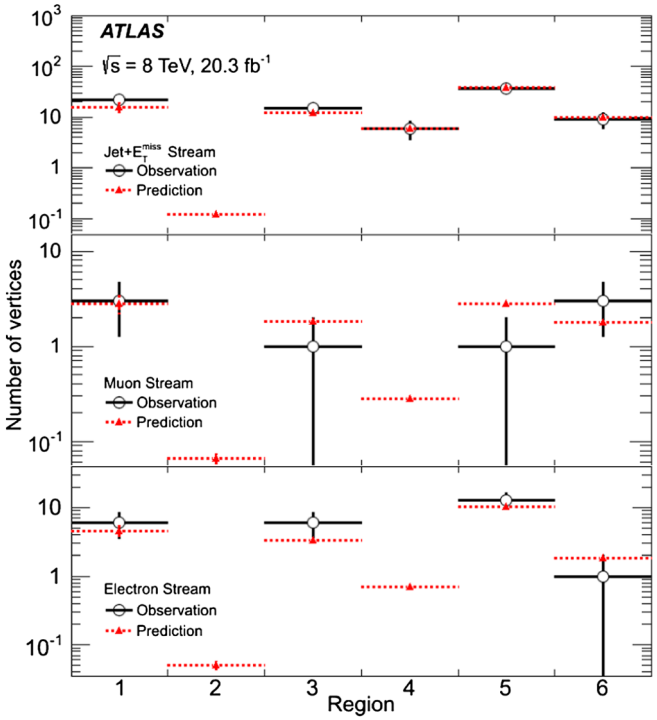

FIG. 6 (color online). Summary of the number of observed (black open circles) 4-track, high-m_{DV} vertices in each of the radial regions and filter-selection streams and the predicted number (red triangles), from Eq. (7). In Region 1, the prediction includes the contribution from merging of two 2-track vertices (see Sec. VI A 2). The error bars on the prediction are too small to be visible, and in some bins no events are observed.

The final numbers of expected background vertices, after multiplying $N_{N_{\text{tr}}}^{\text{stream}}$ by the scale factor F^{stream}, are shown in Table I.

2. Background due to merged vertices

In the last step of DV reconstruction (see Sec. IV E 1), vertices are combined if they are separated by less than 1 mm. To estimate the background arising from this procedure, the distribution of the distance $d_{2\text{DV}}$ between two 2-track or 3-track vertices is studied. Each of the selected vertices is required to satisfy the DV selection criteria of Sec. IV E 2 except the m_{DV} and N_{tr} requirements,

TABLE I. Estimated numbers of background vertices satisfying all of the multitrack signal selection criteria, which arise from a low-mass DV accidentally crossed by an unrelated track. In each entry, the first uncertainty is statistical, and the second is systematic (see Sec. VII).

Channel	No. of background vertices ($\times 10^{-3}$)
DV + jet	$410 \pm 7 \pm 60$
DV + $E_{\text{T}}^{\text{miss}}$	$10.9 \pm 0.2 \pm 1.5$
DV + muon	$1.5 \pm 0.1 \pm 0.2$
DV + electron	$207 \pm 9 \pm 29$

and their combined mass is required to be greater than 10 GeV. To obtain a sufficient number of vertices for studying the d_{2DV} distribution, the distribution is reconstructed from a much larger sample of vertex pairs, where each vertex in the pair is found in a different event. This is referred to as the "model" sample.

To validate the d_{2DV} distribution of the model sample, it is compared to that of vertices that occur in the same event, referred to as the "same-event" sample. It is found that the z positions of vertices in the same event are correlated, since more vertices are formed in high-track-multiplicity regions corresponding to jets. This effect is absent in the model sample. As a result, the distributions of the longitudinal distance between the vertices in the model and the same-event samples differ by up to 30% at low values of d_{2DV}. To correct for this difference, each vertex pair in the model sample is weighted so as to match the z component distribution of the same-event sample. After weighting, the model distribution of the three-dimensional distance d_{2DV} agrees well with that of the same-event sample in the entire study range of $d_{2DV} < 120$ mm. This is demonstrated in Fig. 7 for pairs of 2-track vertices and for the case of a 2-track vertex paired with a 3-track vertex.

The background level for the analysis requirement of $N_{tr} \geq 5$ tracks is estimated from vertex pairs where one vertex has two tracks and the other has three tracks. The area under the model distribution in the range $d_{2DV} < 1$ mm yields a background prediction of 0.02 ± 0.02 events in each of the DV + lepton channels, and 0.03 ± 0.03 events in the DV + jets and DV + E_T^{miss} channels. After multiplication by F^{stream}, this background is negligible relative to the accidental-crossing background, described in Sec. VI A 1. Background from the merging of two 3-track vertices or a 2-track and a 4-track vertex is deemed much smaller still.

B. Dilepton-vertex background estimation

Background DVs in the dilepton search may arise from two sources:

(i) The dominant background is due to accidental spatial crossings of unrelated lepton candidates that happen to come close enough to satisfy the vertex-reconstruction criteria.

(ii) Minor backgrounds, due to tracks originating from the PV wrongly associated with a DV, decays of SM long-lived particles, or cosmic-ray muons. The levels of background from these sources are determined to be negligible relative to the accidental-crossing background.

1. Background from accidental lepton crossing

The level of the accidental-crossing background is estimated by determining the crossing probability, defined as the probability for two unrelated lepton-candidate tracks to be spatially nearby and reconstructed as a vertex. Pairs of opposite-charge lepton candidates are formed, where each lepton candidate in a pair is from a different event and satisfies the lepton-selection criteria. The momentum vector of one of the two lepton candidates, selected at random, is rotated through all azimuthal angles by a step $\delta\phi$. At each rotation step, the two lepton candidates are subjected to a vertex fit and the DV selection criteria. If the pair satisfies the selection criteria, it is assigned a weighted probability $\delta\phi/2\pi$. Averaging the weighted probabilities over all pairs

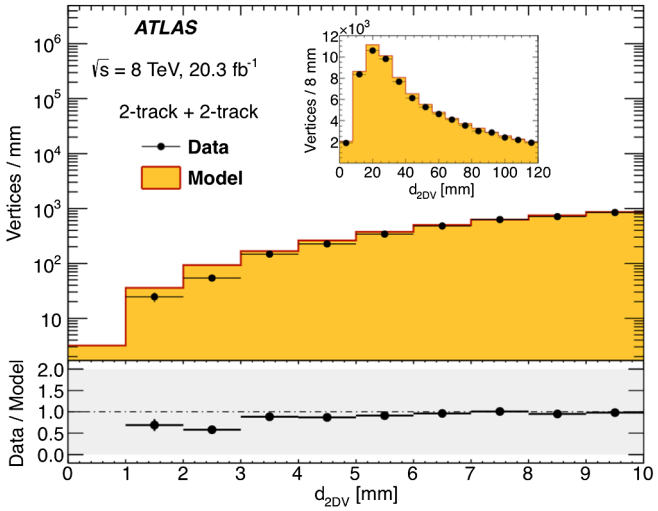

(a)

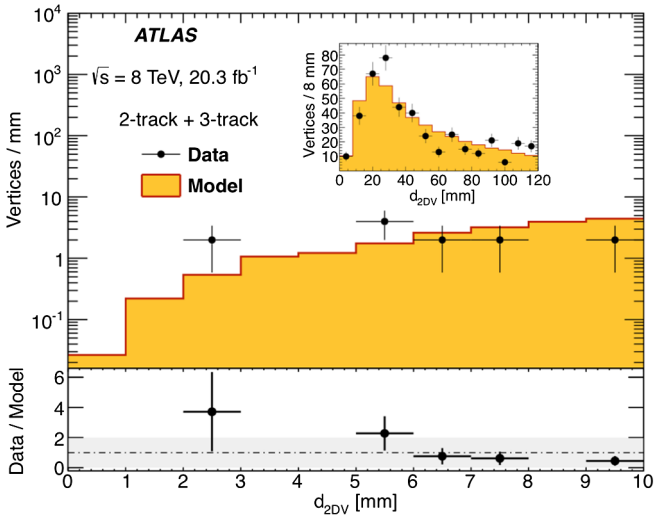

(b)

FIG. 7 (color online). The distribution of the distance d_{2DV} between (a) two 2-track vertices and (b) a 2-track vertex and a 3-track vertex with a combined mass above 10 GeV for the jets + E_T^{miss} stream data (data points) and in the model sample, in which the two vertices are in different events (histogram). A conservative 100% uncertainty on the model is shown in the data/model ratio plot. The inset shows the d_{2DV} distance up to values of 120 mm. The merged-vertex background estimate is determined from the area under the model distribution in the range $d_{2DV} < 1$ mm in (b).

TABLE II. Estimated numbers of background vertices satisfying all of the dilepton signal selection criteria, arising from random combinations of lepton candidates. In each entry, the first uncertainty is statistical, and the second is systematic (see Sec. VII).

Channel	No. of background vertices ($\times 10^{-3}$)
e^+e^-	$1.0 \pm 0.2^{+0.3}_{-0.6}$
$e^\pm\mu^\mp$	$2.4 \pm 0.9^{+0.8}_{-1.5}$
$\mu^+\mu^-$	$2.0 \pm 0.5^{+0.3}_{-1.4}$

gives the probability for a lepton-candidate pair to accidentally form a vertex. The probability is observed to be independent of $\delta\phi$ for $\delta\phi < 0.03$. To obtain the final background estimate, this probability is multiplied by the number $N_{\ell\ell}$ of data events containing two opposite-charge lepton candidates that satisfy the lepton-selection criteria. This procedure yields the background predictions shown in Table II. Compared with these predictions, the background level for a 3-track vertex, where at least two of the tracks are lepton candidates, is negligible.

The validity of this method for estimating the number of dilepton DVs, including the assumption that the tracks are uncorrelated, is verified in several ways. Using $Z \to \mu^+\mu^-$ and $t\bar{t}$ MC samples, the procedure is applied to vertices formed from two lepton candidates, a lepton candidate and another track, or two tracks that are not required to be lepton candidates. It is observed that the method correctly predicts the accidental-crossing background to within about 10%. The background-estimation method is tested also on pairs of tracks in the data, excluding pairs of lepton candidates, with a variety of selection criteria. The predicted and observed numbers of background vertices are again found to agree to within 10% for all selection criteria. The method also reproduces well the distributions of $m_{\rm DV}$, $r_{\rm DV}$, $z_{\rm DV}$, $\hat{d}\cdot\hat{p}$, and the azimuthal angle between the two lepton candidates, in both MC simulation and data. As an example, Fig. 8 shows the $m_{\rm DV}$ and $r_{\rm DV}$ distributions observed for data vertices composed of two nonlepton tracks and the distributions predicted by pairing two tracks in different events. Some differences between the model and the data are seen at certain radii (e.g., $r_{\rm DV} < 50$ mm and $250 < r_{\rm DV} < 270$ mm), but these do not substantially affect the total number of DVs and are covered by the assigned systematic uncertainty (see Sec. VII A 2). The prediction is accurate down to DV masses of 6 GeV, well below the DV selection criterion of 10 GeV. At smaller masses, contributions from other background sources become significant.

This background-estimation method ignores the possibility of angular correlations between the leptons forming a background vertex. The associated systematic uncertainty is described in Sec. VII A 2.

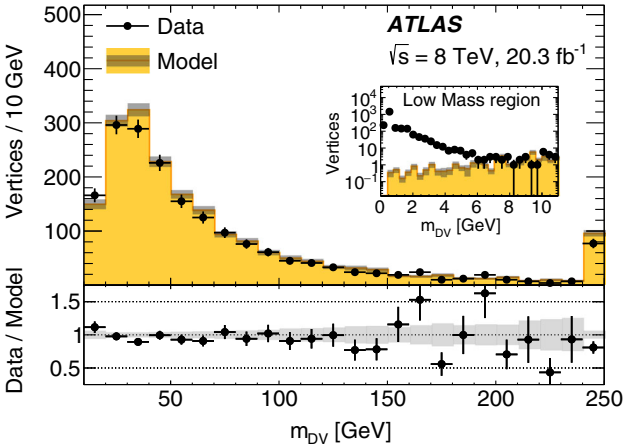

(a)

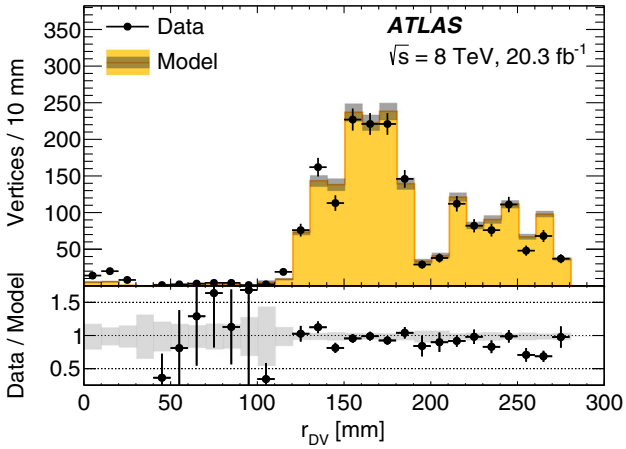

(b)

FIG. 8 (color online). Distributions of the (a) vertex mass and (b) vertex position radius for vertices composed of two nonlepton tracks in the data sample (data points), and the predicted model distribution obtained from vertices formed by combining tracks from two different data events (shaded histograms). The ratio of the data to the model distributions is shown below each plot. The gray bands indicate the statistical uncertainties for the predicted distributions. The inset shows the mass distribution in the low-mass region, elsewhere $m_{\rm DV} > 10$ GeV is required. In (a), the highest bin shows the histogram overflow.

2. Minor backgrounds

Backgrounds from the following sources are found to be negligible relative to the accidental-crossing background, and are therefore neglected.

A potential source of background is prompt production of hard lepton pairs, notably from $Z \to \ell^+\ell^-$ decays. Requiring $\Delta_{xy} < 4$ mm and removing the $m_{\rm DV} > 10$ GeV requirement yields no dilepton-vertex candidates, so the data show no evidence for prompt background. Therefore, MC simulation is used to estimate the probability for leptons originating from $Z \to \ell^+\ell^-$ decays to satisfy the minimum-d_0 requirements, the probability for such leptons to satisfy the vertex requirements, and the

probability for a $Z \to \ell^+\ell^-$ event to pass the analysis kinematic requirements. Multiplying the product of these probabilities by the number of $Z \to \ell^+\ell^-$ events produced at ATLAS yields an estimate of 10^{-5} $Z \to \mu^+\mu^-$ events and 10^{-4} $Z \to e^+e^-$ events in the $\Delta_{xy} < 4$ mm sideband. Thus, the background from this source is negligible.

Background from cosmic-ray muons is studied with the ΔR_{cosmic} distribution of the two highest-p_{T} muon candidates in each event, which satisfy the selection criteria except the $\Delta R_{\text{cosmic}} > 0.04$ requirement. The distribution drops rapidly as ΔR_{cosmic} increases, with the highest pair having $\Delta R_{\text{cosmic}} = 0.014$. The pairs that also satisfy the DV selection criteria constitute less than 7% of this sample and have a similar ΔR_{cosmic} distribution, terminating at $\Delta R_{\text{cosmic}} \sim 0.0045$. Therefore, it is concluded that the rate for cosmic-ray background muons satisfying the $\Delta R_{\text{cosmic}} > 0.04$ requirement is several orders of magnitude below the accidental-crossing background. In the case of a partially reconstructed cosmic-ray muon crossing a reconstructed lepton candidate from a pp collision, the two tracks are uncorrelated and any contribution to the background is already accounted for in the results shown in Table II.

Background from decays of known long-lived hadrons is studied from vertices in which only one track is required to be a lepton candidate. It is found to be negligible, due to the small probability for a hadron to be misidentified as a lepton candidate and the mass resolution of the detector.

VII. SYSTEMATIC UNCERTAINTIES AND CORRECTIONS

The dominant systematic uncertainties are those associated with the efficiency for reconstructing displaced electrons and with the jet and $E_{\text{T}}^{\text{miss}}$ selection criteria. Since the background level is low, uncertainties on the background estimation have a minor effect on the results of the analysis. The methods for evaluation of the systematic uncertainties are described in detail below.

A. Background-estimation uncertainties

1. Multitrack DV background uncertainties

The choice of the $m_{\text{DV}} > 10$ GeV mass range for determining the scale factor f (see Sec. VI A 1), as well as differences between the m_{DV} distribution of the vertices and that of the model, are a source of systematic uncertainty on the background prediction. To estimate this uncertainty, f is obtained in the modified mass ranges $m_{\text{DV}} > 5$ GeV and $m_{\text{DV}} > 15$ GeV. The resulting 10% change in the background prediction for DVs passing the final selection requirements is used as a systematic uncertainty. An additional uncertainty of 10% is estimated from the variation of F^{stream} as the selection criteria are varied (see Sec. VI A 1). Compared with these uncertainties, the uncertainty on the much smaller merged-vertex background level is negligible.

2. Dilepton background uncertainties

The background-estimation procedure for the dilepton search (see Sec. VI B 1) normalizes the background to the number $N_{\ell\ell}$ of events containing two lepton candidates that could give rise to a DV that satisfies the selection criteria. Contrary to the underlying assumption of the background estimation, the two lepton candidates may be correlated, impacting their probability for forming a high-m_{DV} vertex. To study the impact of such correlation, $N_{\ell\ell}$ is recalculated twice, placing requirements on the azimuthal angle between the two lepton candidates, $\Delta\phi_{\ell\ell}$, of $0.5 < \Delta\phi_{\ell\ell} < \pi$ and $0 < \Delta\phi_{\ell\ell} < \pi - 0.5$. The resulting variation yields the relative uncertainty estimates on $N_{\ell\ell}$ of $^{+0\%}_{-54\%}$, $^{+19\%}_{-49\%}$, and $^{+13\%}_{-50\%}$ for the $\mu^+\mu^-$, $e^\pm\mu^\mp$, and e^+e^- channels, respectively.

An uncertainty of 15% on the background prediction is estimated from the validation studies performed using MC simulation and data, described in Sec. VI B 1. The resulting systematic uncertainties are shown in Table II.

B. Signal-efficiency uncertainties and corrections

1. Trigger efficiency

The muon trigger efficiency is studied with a "tag-and-probe" method, in which the invariant-mass distribution of pairs of tracks is fitted to the sum of a $Z \to \mu^+\mu^-$ peak and a background contribution. To reduce the background, one of the muon candidates (the "tag") is required to be identified as a muon. The muon-trigger efficiency is determined from the fraction of $Z \to \mu^+\mu^-$ decays in which the other muon candidate (the "probe") satisfies the trigger criteria. Based on the results of this study in data and MC simulation, a correction of $\Delta\epsilon = -2.5\%$ is applied to the MC-predicted trigger efficiency. A total uncertainty of $\sigma_\epsilon = 1.7\%$ is estimated by comparing the trigger efficiency as a function of the muon candidate p_{T} in data and MC simulation, and by comparing the results of the tag-and-probe method, applied to Drell-Yan MC, with MC generator-level information. Similar studies of the trigger selections used for the electron channels lead to $\Delta\epsilon = -1.5\%$ and $\sigma_\epsilon = 0.8\%$ for the $p_{\text{T}} > 120$ GeV photon trigger, and $\Delta\epsilon = -0.5\%$, $\sigma_\epsilon = 2.1\%$ for the two-photon $p_{\text{T}} > 40$ GeV trigger. The jets and $E_{\text{T}}^{\text{miss}}$ triggers are fully efficient after the off-line cuts.

2. Off-line track-reconstruction efficiency

The uncertainty associated with the reconstruction efficiency for tracks that originate far from the IP is estimated by comparing the decay radius distributions for K_S^0 mesons in data and MC simulation. The comparison is carried out with the ratio

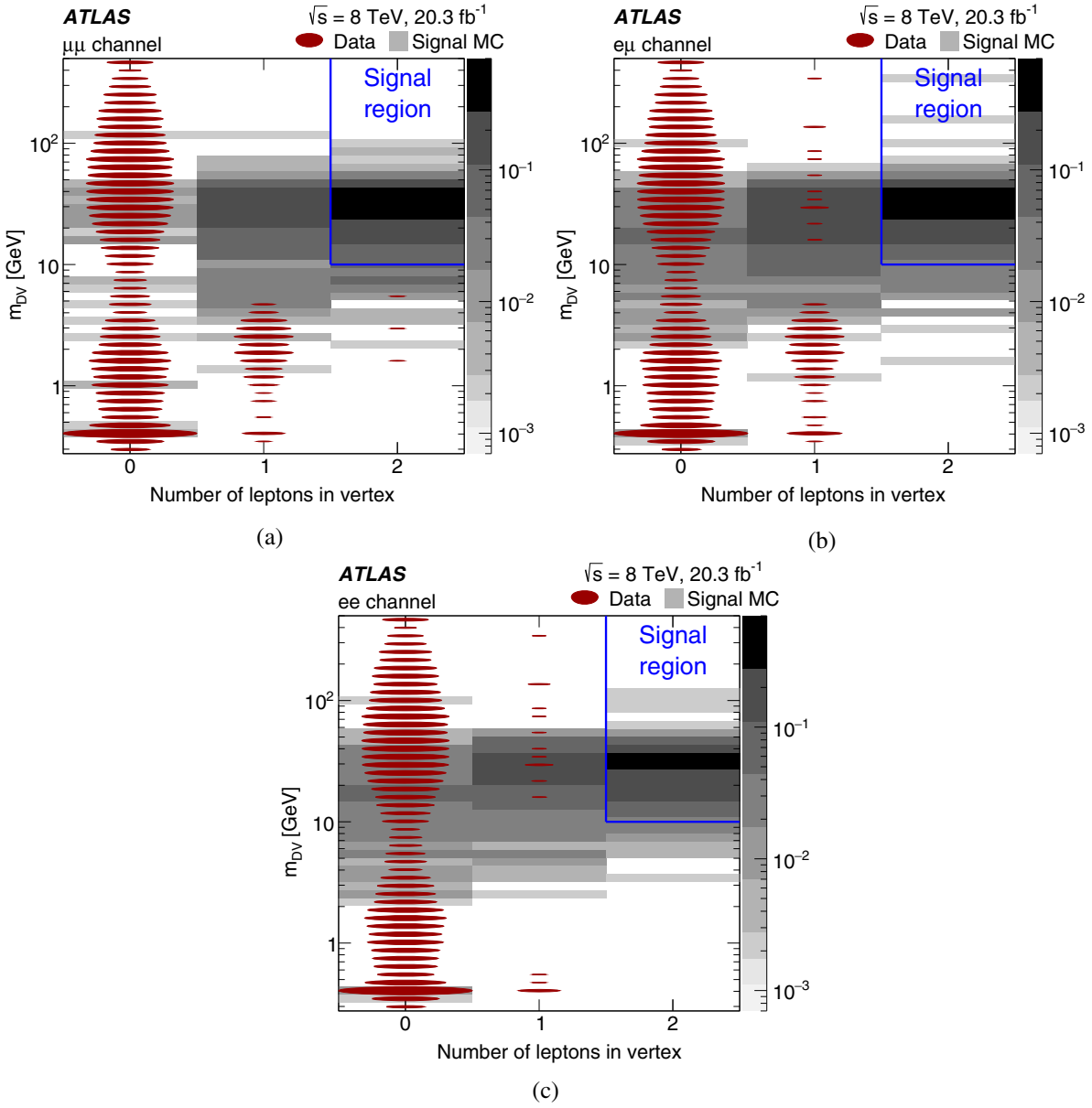

FIG. 9 (color online). The distribution of dilepton-vertex candidates in terms of the vertex mass versus the number of lepton candidates in the vertex, in the (a) $\mu^+\mu^-$, (b) $e^\pm\mu^\mp$, and (c) e^+e^- search channels. The data distributions are shown with red ovals, the area of the oval being proportional to the logarithm of the number of vertex candidates in that bin. The gray squares show the $\tilde{g}(600\ \text{GeV}) \to qq[\tilde{\chi}_1^0(50\ \text{GeV}) \to \mu\mu\nu/e\mu\nu/ee\nu]$ signal MC sample. The shape of the background m_{DV} distribution arises partly from the lepton-candidate p_{T} requirements. The signal region defined by the two-lepton and $m_{\text{DV}} \to 10$ GeV requirements is indicated.

$$\rho_i(K_S^0) = \frac{N_i^{\text{data}}(K_S^0)}{N_i^{\text{MC}}(K_S^0)}, \tag{8}$$

where $i = 1, \ldots, 4$ labels four radial regions between 5 mm and 40 mm, and $N_i^{\text{data/MC}}(K_S^0)$ is the number of K_S^0 mesons in radial region i in data/MC simulation, obtained by fitting the two-track mass distributions. In the calculation of $N_i^{\text{MC}}(K_S^0)$, the K_S^0 candidates in MC are weighted so that their $|\eta|$ and p_{T} distributions match those seen in the data. The ratio $\rho_i(K_S^0)$ is constructed separately for $|\eta| < 1$ and $|\eta| \geq 1$. The difference $\Delta\rho_i(K_S^0) = \rho_i(K_S^0) - \rho_1(K_S^0)$ quantifies the radial dependence of the data-MC discrepancy. The discrepancy is largest in the outermost radial region, with $\Delta\rho_4(K_S^0) = -0.03$ for $|\eta| < 1$ and $\Delta\rho_4(K_S^0) = -0.2$ for $|\eta| \geq 1$. The statistical uncertainties on $\rho_i(K_S^0)$ are negligible compared to these discrepancies.

To propagate this maximal discrepancy into a conservative uncertainty on the signal efficiency, DV daughter tracks are randomly removed from signal-MC vertices before performing the vertex fit. The single-track removal probability is taken to be $\Delta\rho_4(K_S^0)/2$ in each of the

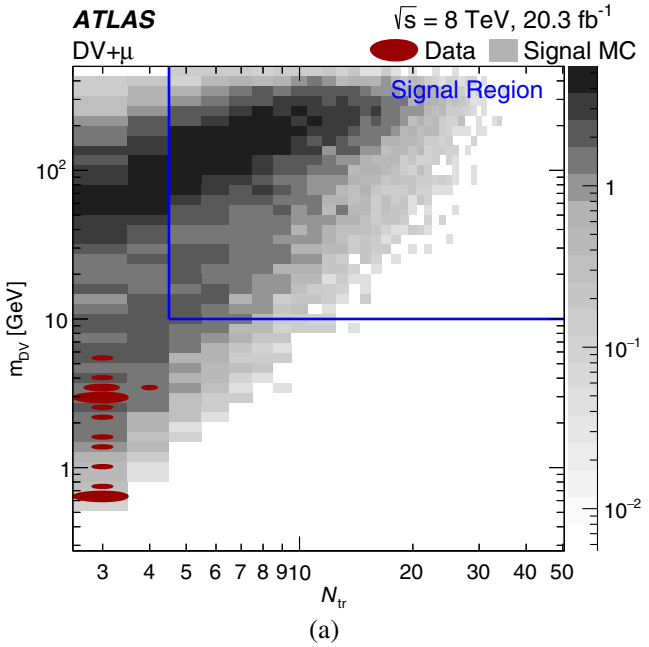

FIG. 10 (color online). The distribution of (a) DV + muon and (b) DV + electron candidates in terms of the vertex mass versus the number of tracks in the vertex. The data distribution is shown with red ovals, the area of each oval being proportional to the logarithm of the number of vertex candidates in that bin. The gray squares show the $\tilde{q}(700\ \mathrm{GeV}) \to q[\tilde{\chi}_1^0(494\ \mathrm{GeV}) \to \ell qq]$ RPV signal MC sample. The signal region $N_{\mathrm{tr}} \geq 5$, $m_{\mathrm{DV}} \to 10$ GeV is indicated.

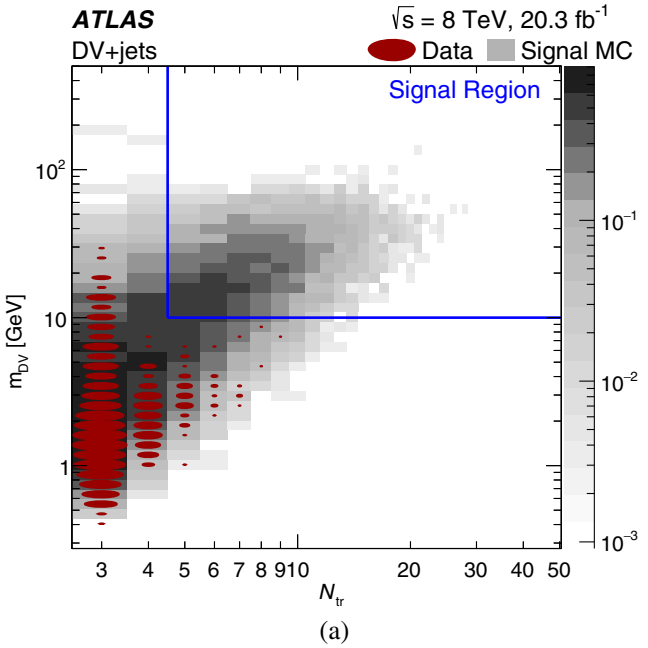

FIG. 11 (color online). The distribution of (a) DV + jets and (b) DV + $E_{\mathrm{T}}^{\mathrm{miss}}$ candidates in terms of the vertex mass versus the number of tracks in the vertex. The data distribution is shown with red ovals, the area of each oval being proportional to the logarithm of the number of vertex candidates in that bin. The gray squares show the $\tilde{g}(1.1\,\mathrm{TeV}) \to qq[\tilde{\chi}_1^0(400\,\mathrm{GeV}) \to \tilde{G}Z]$ GGM signal MC sample in (a) and the $[\tilde{g}(1.4\ \mathrm{TeV}) \to \tilde{\chi}_1^0(100\ \mathrm{GeV})qq/g]$ split-supersymmetry sample in (b). The signal region $N_{\mathrm{tr}} \geq 5$, $m_{\mathrm{DV}} > 10$ GeV is indicated.

two $|eta|$ regions. The resulting change in the DV efficiency is taken as the tracking-efficiency systematic uncertainty. This uncertainty is evaluated separately for each value of $c\tau$, and is generally around 1%.

3. Off-line lepton-identification efficiency

The lepton-identification efficiency uncertainty is determined in ATLAS using $Z \to \ell\ell$ decays and is typically less than 1%. For this analysis, an additional

TABLE III. Model-independent 95% confidence-level upper limits on the visible cross section for new physics in each of our searches.

Channel	Upper limit on visible cross section [fb]
DV + jet	0.14
DV + $E_{\mathrm{T}}^{\mathrm{miss}}$	0.15
DV + muon	0.15
DV + electron	0.15
e^+e^-	0.14
$\mu^+\mu^-$	0.14
$e^\pm\mu^\mp$	0.15

uncertainty associated with identification of high-d_0 leptons is evaluated.

For muons, this is done by comparing a cosmic-ray muon simulation to cosmic-ray muon candidates in data. The events are required to pass the muon trigger and to have two muon candidates that fail the muon veto (see Sec. IV B 1). The MC muons are weighted so that their η and ϕ distributions are in agreement with those of the data. Comparing the ratio of the muon candidate d_0 distributions in data and in MC simulation yields a d_0-dependent efficiency correction that is between 1% and 2.5%, with an average value of 1.5%. The uncertainty associated with this procedure is taken from the statistical uncertainty, and is 2% on average.

Unlike in the case of cosmic-ray muons, there is no easily identifiable, high-rate source of large-d_0 electrons. Therefore, the performance of the simulation is validated by comparing the electron-identification efficiency $\epsilon_e(z_0)$ as a function of the longitudinal impact parameter z_0 of the

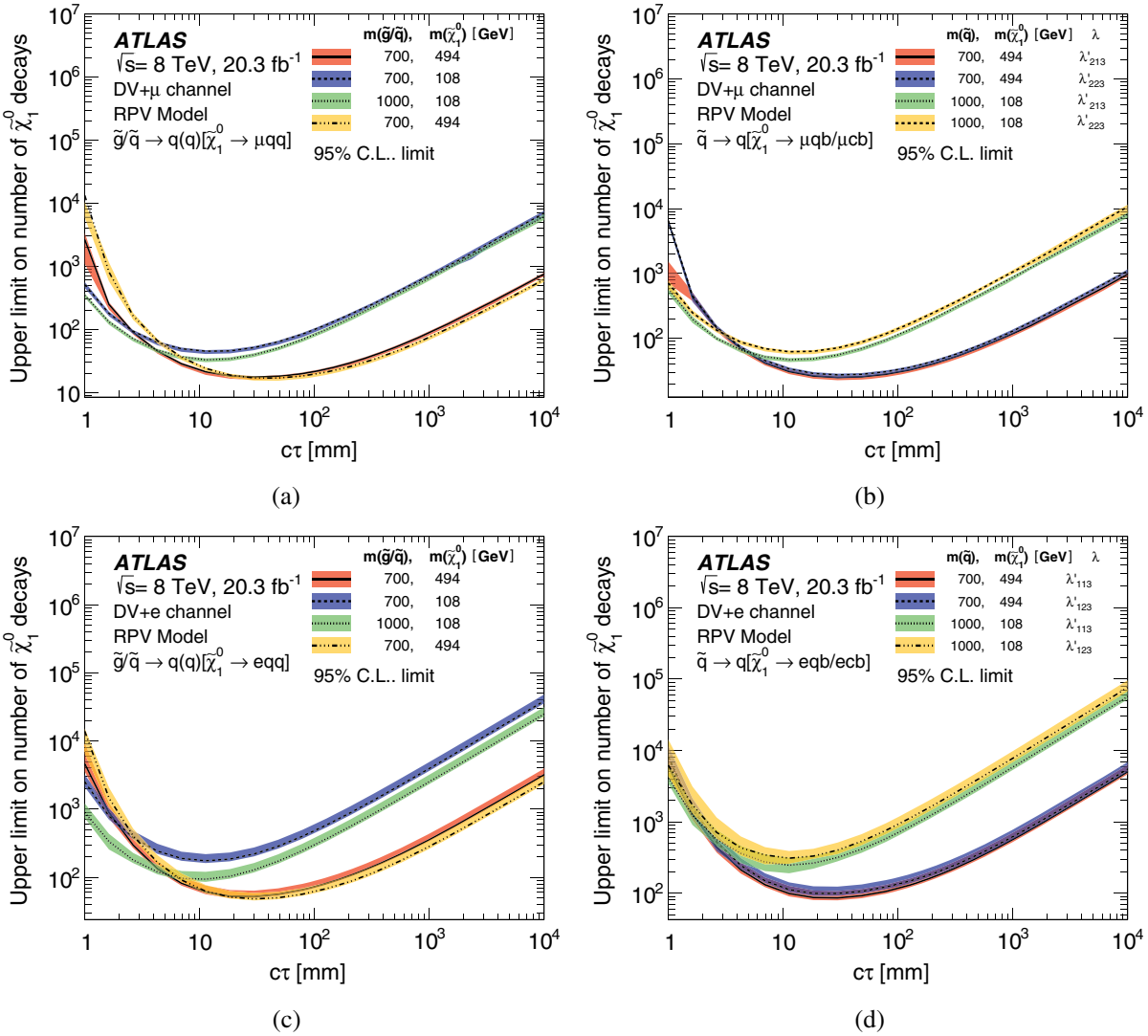

FIG. 12 (color online). RPV-scenario upper limits at 95% confidence level on the number of neutralinos in 20.3 fb^{-1} that decay into (a) μqq (with q indicating a u- or d-quark), (b) μqb and μcb (indicated by the nonzero RPV couplings λ'_{213} and λ'_{223}, respectively), (c) eqq, and (d) eqb and ecb (λ'_{113} and λ'_{123}, respectively). The upper limits account for the vertex-level efficiency for each value of the neutralino proper decay distance $c\tau$. The different curves show the results for different masses of the primary gluino or squark and of the long-lived neutralino, while the shaded bands indicate $\pm 1\sigma$ variations in the expected limit.

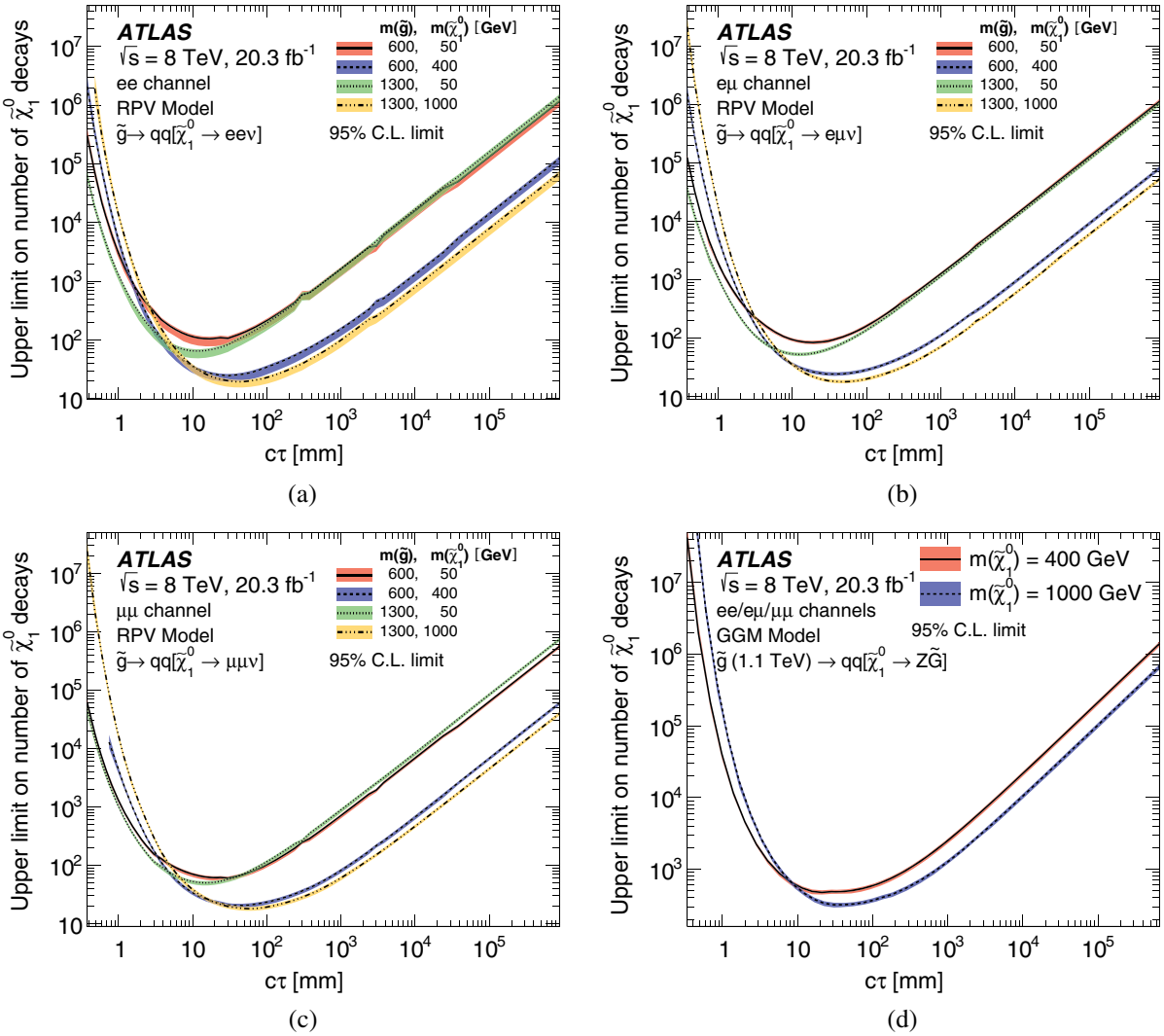

FIG. 13 (color online). Upper limits at 95% confidence level on the number of neutralinos in 20.3 fb^{-1} that decay into (a) $ee\nu$ in the RPV model, (b) $e\mu\nu$ in the RPV model, (c) $\mu\mu\nu$ in the RPV model, and (d) $Z\tilde{G}$ in the GGM model. The upper limits account for the vertex-level efficiency for each value of the neutralino proper decay distance $c\tau$. The different curves show the results for different masses of the primary gluino and of the long-lived neutralino, while the shaded bands indicate $\pm 1\sigma$ variations in the expected limit. In some cases limits are terminated for $c\tau \lesssim 1$ mm due to limited statistical precision.

electron candidate in data and MC simulation, measured with the tag-and-probe method using $Z \to e^+e^-$ events. It is observed that $\epsilon_e(z_0)$ is consistent in data and in MC simulation to better than 1% for $|z_0| < 250$ mm, beyond which there are too few events for an accurate measurement. Furthermore, the value of ϵ_e obtained with the tag-and-probe method is consistent to within 1% with that determined from MC generator-level information. This data-MC agreement in $\epsilon_e(z_0)$ is taken as an indication that the d_0 dependence of the efficiency, $\epsilon_e(d_0)$, is also well described by simulation. In signal MC samples, the function $\epsilon_e(d_0)$ varies by about 10% due to kinematic correlations between d_0 and factors that affect the efficiency, such as the value of r_{DV} and the boost of the LLP. To account for the possibility of an additional d_0 dependence that may not be well simulated, a systematic uncertainty of 10% on the electron-identification efficiency is assigned. This conservative uncertainty weakens the upper limits by less than 1%.

4. Jets and $E_{\mathrm{T}}^{\mathrm{miss}}$ reconstruction

The impact on the signal efficiency of uncertainties in the jet-energy scale calibration and jet-energy resolution is evaluated following the methods described in Refs. [57] and [58], respectively. An additional uncertainty on the jet p_{T} is evaluated for jets that originate from the decay of an LLP, by linearly parametrizing the p_{T} mismeasurement in MC simulation as a function of r_{DV} and z_{DV}. The only significant dependence observed is a relative p_{T}

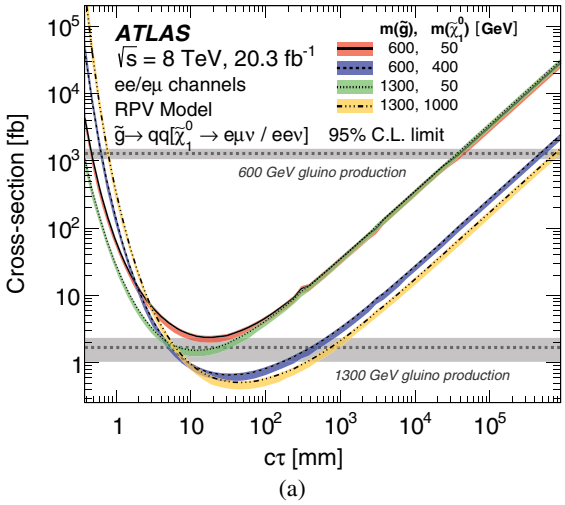

(a)

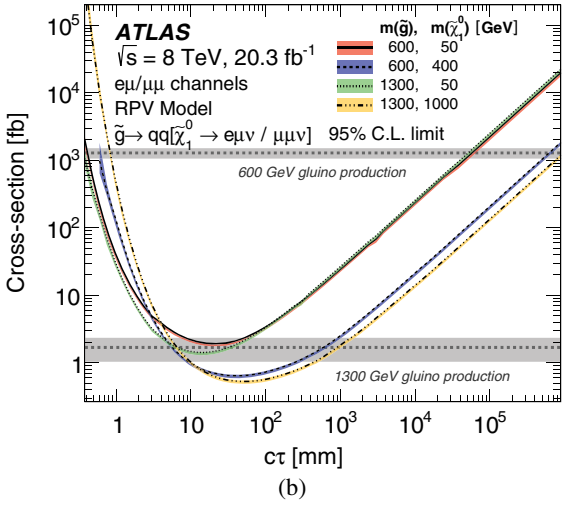

(b)

FIG. 14 (color online). The 95% confidence-level upper limits, obtained from the dilepton search, on the production cross section for a pair of gluinos of different masses that decay into two quarks and a long-lived neutralino in different models: (a) the RPV scenario with a pure λ_{121} coupling, (b) the RPV scenario with a pure λ_{122} coupling. All relevant final-state lepton-flavor combinations are used. The shaded bands around the observed limits indicate $\pm 1\sigma$ variations in the expected limit, while the horizontal bands show the theoretical cross sections and their uncertainties. In some cases limits are terminated for $c\tau \lesssim 1$ mm due to limited statistical precision.

mismeasurement of $(4 \pm 1) \times 10^{-5}(r_{\mathrm{DV}}/\mathrm{mm})$, which is propagated to the jet-selection efficiency as a systematic uncertainty. To account for possible mismodeling of trackless jets, an uncertainty is obtained by varying the requirement on $\sum_{\mathrm{tr}} p_{\mathrm{T}}$ for these jets. Systematic uncertainties in the $E_{\mathrm{T}}^{\mathrm{miss}}$ measurement are evaluated with the methods described in Refs. [53,54] and propagated to the efficiency uncertainty. The impact of uncertainties in the simulation of initial-state radiation is estimated by varying the p_{T} distribution of the primary particles according to the distribution observed in MADGRAPH5 [59]

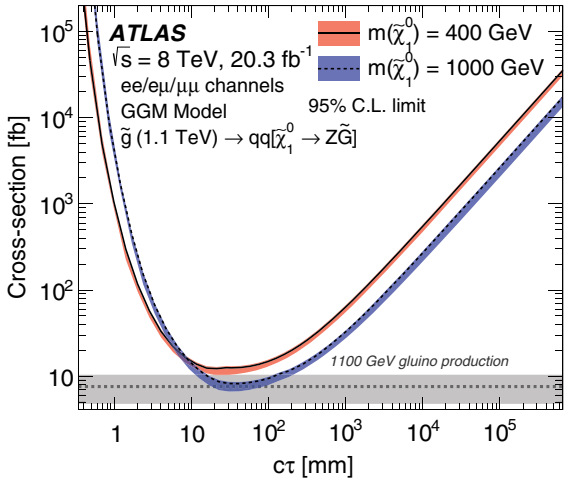

FIG. 15 (color online). The 95% confidence-level upper limits, obtained from the dilepton search, on the production cross section for a pair of gluinos of mass 1.1 TeV that decay into two quarks and a long-lived neutralino in the GGM scenario for two values of the neutralino mass. For further details see Fig. 14.

samples. The resulting efficiency uncertainty varies between 2% and 10%.

5. Multiple pp interactions

The dependence of the reconstruction efficiency on the number of pp interactions per bunch crossing is studied by varying the average number of interactions per LHC bunch crossing in the simulation by 4%. This value reflects uncertainties in the detector acceptance, trigger efficiency, and modeling of additional pp interactions. The resulting relative uncertainty is typically of order 1% or less.

VIII. RESULTS

Figure 9 shows the distribution of m_{DV} versus the number of associated lepton candidates in the selected data sample before the final selection requirements on these variables are applied. The distributions of m_{DV} versus the number of tracks in the vertex obtained for the multitrack-DV search are shown in Figs. 10 and 11. No events are seen in the signal region for any of the seven channels. In addition, no same-charge dilepton vertices are seen with $m_{\mathrm{DV}} > 10$ GeV. The distributions expected for some of the signal samples are also shown for comparison.

Given the lack of a signal observation, 95% confidence-level upper limits on the total visible cross section for new physics are shown in Table III.

Furthermore, for each of the physics scenarios considered, 95% confidence-level upper limits on the signal yields and production cross sections are calculated for different values of the proper decay distance $c\tau$ of the LLP and presented in the figures in this section. The limits are calculated using the CL_S prescription [60] with the profile likelihood used as the test statistic, using the

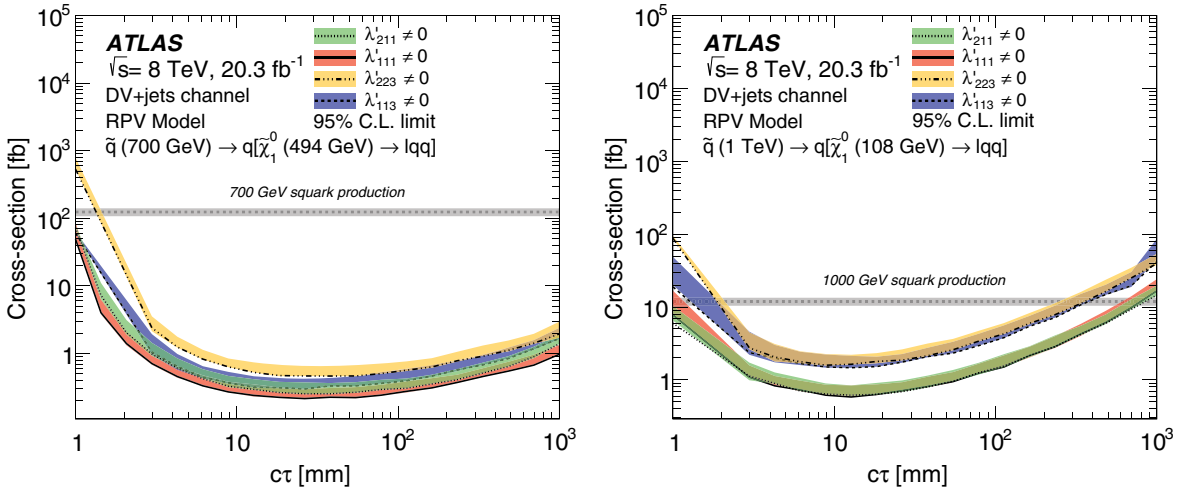

FIG. 16 (color online). The 95% confidence-level upper limits, obtained from the DV + jets search, on the production cross section for a pair of squarks in the RPV scenario, with the neutralino decaying to a lepton and two quarks, according to the nonzero λ' couplings indicated in each case. The squark and neutralino masses are (a) 700 GeV and 494 GeV or (b) 1 TeV and 108 GeV, respectively, representing the results for different neutralino masses and boosts. For further details see Fig. 14.

HistFitter [61] framework. Uncertainties on the signal efficiency and background expectation are included as nuisance parameters, and the CL_S values are calculated by generating ensembles of pseudoexperiments corresponding to the background-only and signal-plus-background hypotheses.

Since less than one background event is expected in all cases and no events are observed, the observed limits are very close to the expected limits.

In the case of the dilepton and DV + lepton searches, where the trigger and reconstruction depend almost exclusively on the signal DV, upper limits on the number of vertices produced in 20.3 fb^{-1} of data are presented for each channel, accounting for the vertex-level efficiency at each value of $c\tau$. Figure 12 shows these number limits for the DV + lepton search signatures. The limits are given separately for different masses of the long-lived neutralino and the primary squark or gluino, as well as for different λ'_{ijk} couplings, which give rise to light- or heavy-flavor quarks in the final state (see Sec. V for a discussion of the heavy-flavor and mass impact on efficiency). The number limits for the dilepton search signatures are shown in Fig. 13 for the final states ee, $\mu\mu$, $e\mu$, as well as for the combination of $Z \to ee$, $Z \to \mu\mu$, and $Z \to \tau\tau$.

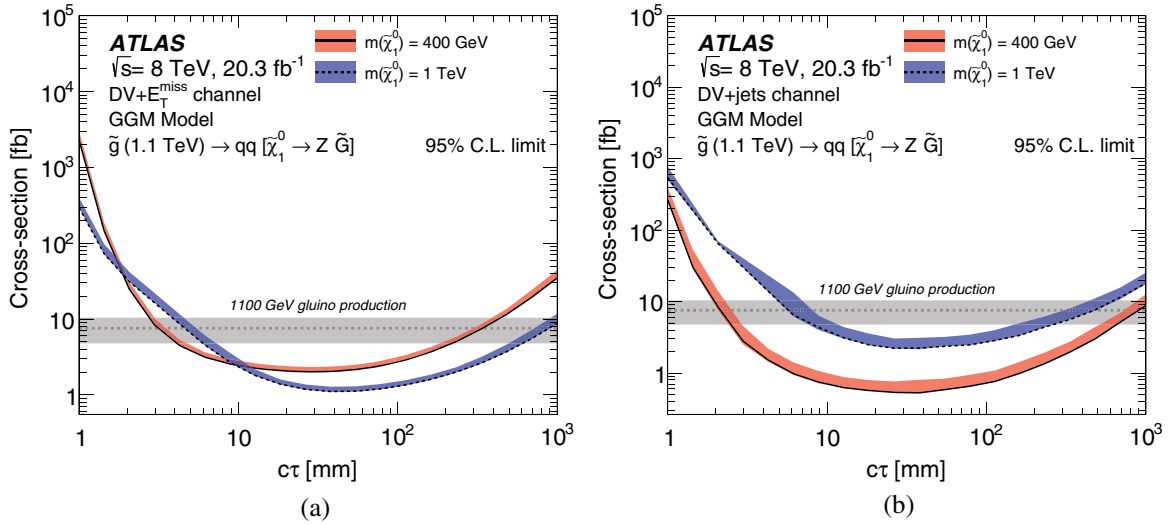

FIG. 17 (color online). The 95% confidence-level upper limits, obtained from the (a) DV + $E_{\mathrm{T}}^{\mathrm{miss}}$ and (b) DV + jets searches, on the production cross section for a pair of gluinos of mass 1.1 TeV that decay into two quarks and a long-lived neutralino in the GGM scenario. For further details see Fig. 14.

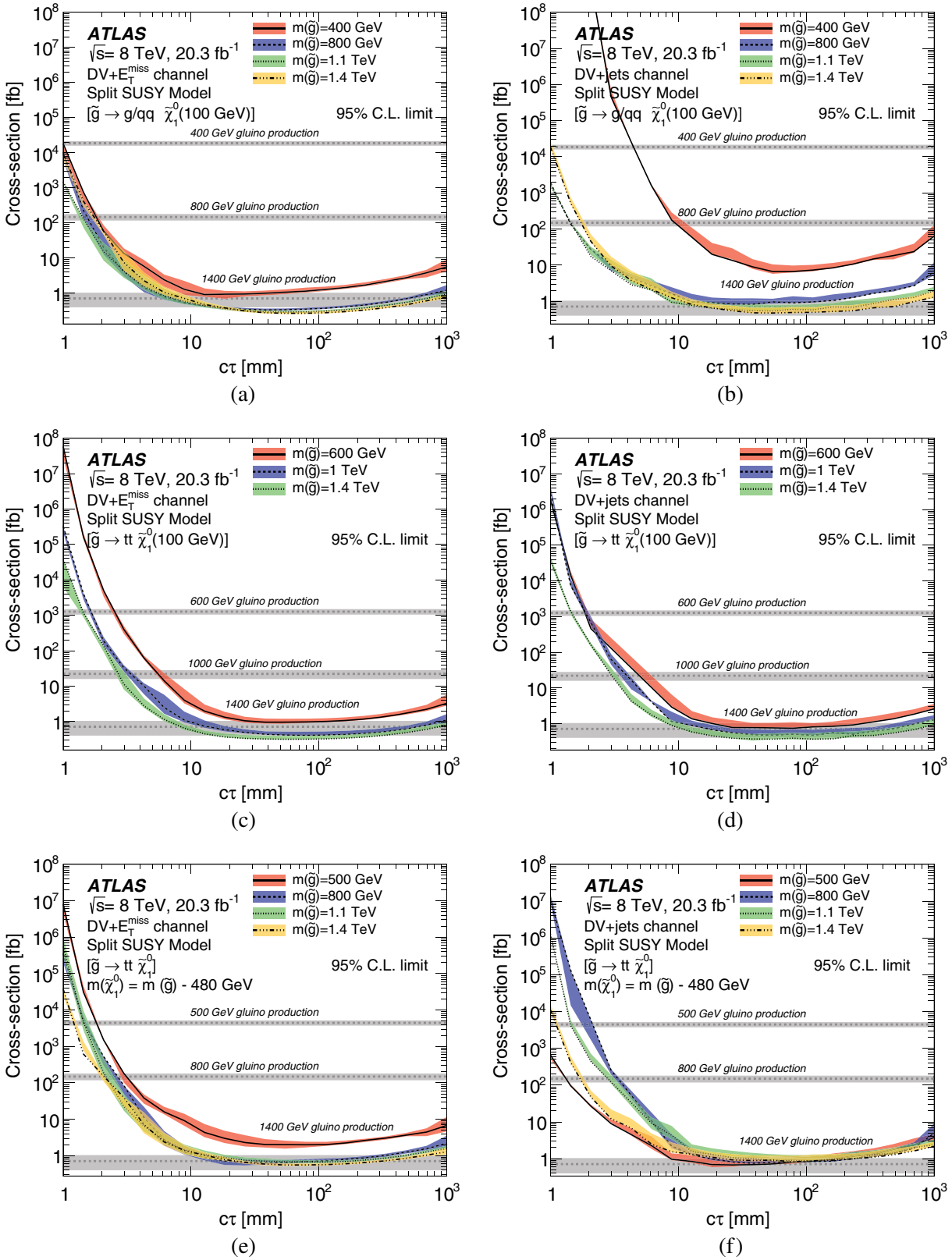

FIG. 18 (color online). The 95% confidence-level upper limits, obtained from the (a), (c), (e) DV + $E_{\mathrm{T}}^{\mathrm{miss}}$ and (b), (d), (f) DV + jets searches, on the cross section for gluino pair production in the split-supersymmetry model, with the gluino decaying to a neutralino plus either (a), (b) a gluon or a light-quark pair or (c), (d), (e), (f) a pair of top quarks. The mass of the neutralino is 100 GeV in (a), (b), (c), (d) and is 480 GeV smaller than the gluino mass in (e), (f). For further details see Fig. 14.

In addition, limits on the production cross sections for events are presented for the different simulated scenarios.

Figures 14 and 15 show cross-section upper limits obtained with the dilepton-DV search. Upper limits are shown for gluino-pair production in the RPV scenario, with neutralino decays determined by the choice of nonzero RPV coupling λ_{121} or λ_{122}, as well as within the GGM scenario with leptonic decays of the Z boson. For example, the RPV scenario is excluded for gluino mass $m_{\tilde{g}} = 600$ GeV, neutralino mass $m_{\tilde{\chi}_1^0} = 400$ GeV, and neutralino proper decay distance in the range $0.7 < c\tau < 3 \times 10^5$ mm.

Cross-section upper limits obtained with the multitrack-DV search are shown in the remaining figures. These limits are calculated up to proper decay distances of $c\tau = 1$ m, to avoid inaccuracies associated with reweighting events to very high lifetimes when the efficiency depends on both LLPs in the event.

Figure 16 shows the upper limits on the production cross section of two squarks in the RPV scenario, with different squark and neutralino masses, as well as different λ' parameters governing the neutralino decay. These limits are obtained with the DV + jets search, which results in tighter limits than the DV + lepton searches for this scenario. These results exclude a $m_{\tilde{q}} = 1$ TeV squark for $m_{\tilde{\chi}_1^0} = 108$ GeV and $2.5 < c\tau < 200$ mm with either light- or heavy-quark neutralino decays. Figure 17 shows the cross-section upper limits for gluino-pair production within the GGM scenario, using hadronic Z decays. The scenario is excluded, for instance, for $m_{\tilde{g}} = 1.1$ TeV and $m_{\tilde{\chi}_1^0} = 400$ GeV in the proper decay distance range $3 < c\tau < 500$ mm.

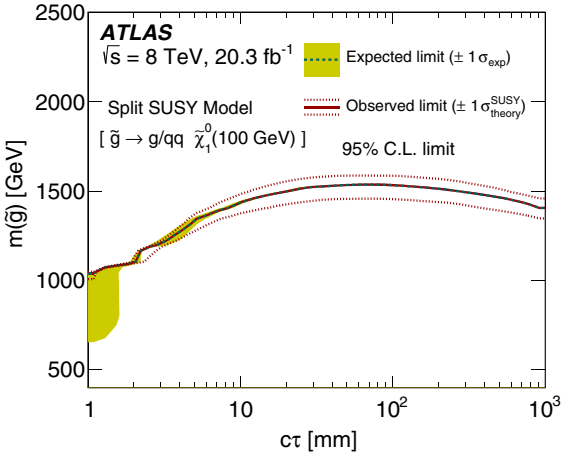

FIG. 19 (color online). The 95% confidence-level excluded regions lie below the curves shown in the mass-versus-$c\tau$ plane for the split-supersymmetry samples, with the gluino decaying into a gluon or light quarks, plus a 100 GeV neutralino. The shaded bands indicate $\pm 1\sigma$ variations in the expected limit, while the dotted lines indicate the effect of varying the production cross section by 1 standard deviation. The expected and observed limits are identical.

Figure 18 shows the upper limits on gluino-pair production cross section in the split-supersymmetry model. These limits are obtained from the results of the DV + $E_{\mathrm{T}}^{\mathrm{miss}}$ and DV + jets searches. The sensitivity is greater for the cases with $m_{\tilde{\chi}_1^0} = 100$ GeV than for those with $m_{\tilde{\chi}_1^0} = m_{\tilde{g}} - 480$ GeV, and the DV + $E_{\mathrm{T}}^{\mathrm{miss}}$ search performs better than DV + jets in these scenarios, excluding $m_{\tilde{g}} < 1400$ GeV in the range of proper decay lengths 15 mm $< c\tau < 300$ mm.

In Figs. 19 and 20, the region of gluino mass versus proper decay distance that is excluded by these limits is shown. The limit for each point in parameter space is taken from the channel that is expected to yield the most stringent limit, which is DV + $E_{\mathrm{T}}^{\mathrm{miss}}$ for most points. For the region

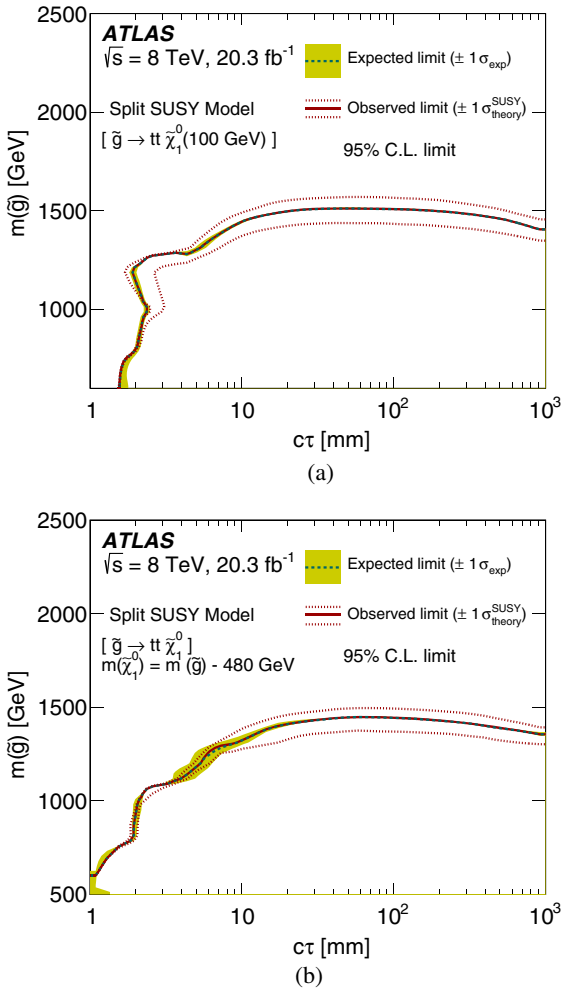

FIG. 20 (color online). The 95% confidence-level excluded regions lie below the curves shown in the mass-versus-$c\tau$ plane for the split-supersymmetry samples, with the gluino decaying into (a) a top quark pair and a 100 GeV neutralino, or (b) a top quark pair and a neutralino with a mass that is 480 GeV smaller than the gluino mass. The shaded bands indicate $\pm 1\sigma$ variations in the expected limit, while the dotted lines indicate the effect of varying the production cross section by 1 standard deviation. The expected and observed limits are identical.

of parameter space where the sensitivity is greatest, $20\ \text{mm} < c\tau < 250\ \text{mm}$ and $m_{\tilde{\chi}_1^0} = 100\ \text{GeV}$, gluino masses of $m_{\tilde{g}} < 1500\ \text{GeV}$ are excluded. This range of masses is comparable to or slightly larger than those excluded by prompt searches [62], searches for long-lived R-hadrons stopped in the ATLAS calorimeter [17], or searches for stable, massive, charged particles [19].

IX. SUMMARY AND CONCLUSIONS

This article reports on a search for long-lived particles decaying into two leptons or five or more charged particles. In the latter case, events are selected using associated lepton candidates, jets, or missing transverse momentum. The main signature of the search is a displaced vertex with an invariant mass greater than 10 GeV. This signature corresponds to a wide variety of new-physics models, many of which have not been searched for previously. The search uses the full data sample of pp collisions collected by the ATLAS detector at the LHC with a center-of-mass energy of $\sqrt{s} = 8$ TeV and an integrated luminosity of 20.3 fb^{-1}. Less than one background event is expected in each of the channels, and no events are observed. Upper limits are provided on the number of long-lived particle decays in the data sample and on the cross section for production of particles that give rise to the search signatures in a variety of supersymmetric models. These upper limits exclude significant regions of the parameter space of new-physics models with particle masses within reach of the LHC.

ACKNOWLEDGMENTS

We thank CERN for the very successful operation of the LHC, as well as the support staff from our institutions without whom ATLAS could not be operated efficiently. We acknowledge the support of ANPCyT, Argentina; YerPhI, Armenia; ARC, Australia; BMWFW and FWF, Austria; ANAS, Azerbaijan; SSTC, Belarus; CNPq and FAPESP, Brazil; NSERC, NRC, and CFI, Canada; CERN; CONICYT, Chile; CAS, MOST, and NSFC, China; COLCIENCIAS, Colombia; MSMT CR, MPO CR, and VSC CR, Czech Republic; DNRF, DNSRC, and Lundbeck Foundation, Denmark; EPLANET, ERC, and NSRF, European Union; IN2P3-CNRS, CEA-DSM/IRFU, France; GNSF, Georgia; BMBF, DFG, HGF, MPG, and AvH Foundation, Germany; GSRT and NSRF, Greece; RGC, Hong Kong SAR, China; ISF, MINERVA, GIF, I-CORE, and Benoziyo Center, Israel; INFN, Italy; MEXT and JSPS, Japan; CNRST, Morocco; FOM and NWO, Netherlands; BRF and RCN, Norway; MNiSW and NCN, Poland; GRICES and FCT, Portugal; MNE/IFA, Romania; MES of Russia and NRC KI, Russian Federation; JINR; MSTD, Serbia; MSSR, Slovakia; ARRS and MIZŠ, Slovenia; DST/NRF, South Africa; MINECO, Spain; SRC and Wallenberg Foundation, Sweden; SER, SNSF, and Cantons of Bern and Geneva, Switzerland; NSC, Taiwan; TAEK, Turkey; STFC, the Royal Society, and Leverhulme Trust, United Kingdom; DOE and NSF, United States of America. The crucial computing support from all WLCG partners is acknowledged gratefully, in particular from CERN and the ATLAS Tier-1 facilities at TRIUMF (Canada), NDGF (Denmark, Norway, Sweden), CC-IN2P3 (France), KIT/GridKA (Germany), INFN-CNAF (Italy), NL-T1 (Netherlands), PIC (Spain), ASGC (Taiwan), RAL (UK), and BNL (USA) and in the Tier-2 facilities worldwide.

[1] M. Fairbairn, A. C. Kraan, D. A. Milstead, T. Sjöstrand, P. Skands, and T. Sloan, Stable massive particles at colliders, Phys. Rep. **438**, 1 (2007).
[2] R. Barbier *et al.*, R-parity violating supersymmetry, Phys. Rep. **420**, 1 (2005).
[3] B. C. Allanach, M. A. Bernhardt, H. K. Dreiner, C. H. Kom, and P. Richardson, Mass Spectrum in R-Parity Violating mSUGRA and Benchmark Points, Phys. Rev. D **75**, 035002 (2007).
[4] S. Dimopoulos, M. Dine, S. Raby, and S. D. Thomas, Experimental Signatures of Low-Energy Gauge Mediated Supersymmetry Breaking, Phys. Rev. Lett. **76**, 3494 (1996).
[5] J. L. Hewett, B. Lillie, M. Masip, and T. G. Rizzo, Signatures of long-lived gluinos in split supersymmetry, J. High Energy Phys. 09 (2004) 070.
[6] A. Arvanitaki, N. Craig, S. Dimopoulos, and G. Villadoro, Mini-Split, J. High Energy Phys. 02 (2013) 126.
[7] M. J. Strassler and K. M. Zurek, Echoes of a hidden valley at hadron colliders, Phys. Lett. B **651**, 374 (2007).
[8] P. Schuster, N. Toro, and I. Yavin, Terrestrial and Solar Limits on Long-Lived Particles in a Dark Sector, Phys. Rev. D **81**, 016002 (2010).
[9] J. Fan, M. Reece, and J. T. Ruderman, Stealth Supersymmetry, J. High Energy Phys. 11 (2011) 012.
[10] A. Arbey, M. Battaglia, A. Djouadi, F. Mahmoudi, and J. Quevillon, Implications of a 125 GeV Higgs for supersymmetric models, Phys. Lett. B **708**, 162 (2012).
[11] ATLAS Collaboration, Observation of a new particle in the search for the Standard Model Higgs boson with the ATLAS detector at the LHC, Phys. Lett. B **716**, 1 (2012).
[12] CMS Collaboration, Observation of a new boson at a mass of 125 GeV with the CMS experiment at the LHC, Phys. Lett. B **716**, 30 (2012).

[13] ATLAS Collaboration, Search for displaced vertices arising from decays of new heavy particles in 7 TeV pp collisions at ATLAS, Phys. Lett. B **707**, 478 (2012).
[14] ATLAS Collaboration, Search for long-lived, heavy particles in final states with a muon and multi-track displaced vertex in proton-proton collisions at $\sqrt{s} = 7$ TeV with the ATLAS detector, Phys. Lett. B **719**, 280 (2013).
[15] ATLAS Collaboration, Search for displaced muonic lepton jets from light Higgs boson decay in proton-proton collisions at $\sqrt{s} = 7$ TeV with the ATLAS detector, Phys. Lett. B **721**, 32 (2013).
[16] ATLAS Collaboration, Search for pair-produced long-lived neutral particles decaying in the ATLAS hadronic calorimeter in pp collisions at $\sqrt{s} = 8$ TeV, Phys. Lett. B **743**, 15 (2015).
[17] ATLAS Collaboration, Search for long-lived stopped R-hadrons decaying out-of-time with pp collisions using the ATLAS detector, Phys. Rev. D **88**, 112003 (2013).
[18] ATLAS Collaboration, Search for long-lived, weakly interacting particles that decay to displaced hadronic jets in proton-proton collisions at $\sqrt{s} = 8$ TeV with the ATLAS detector, Phys. Rev. D **92**, 012010 (2015).
[19] ATLAS Collaboration, Searches for heavy long-lived charged particles with the ATLAS detector in proton-proton collisions at $\sqrt{s} = 8$ TeV, J. High Energy Phys. 01 (2015) 068.
[20] CMS Collaboration, Search in leptonic channels for heavy resonances decaying to long-lived neutral particles, J. High Energy Phys. 02 (2013) 085.
[21] V. Khachatryan *et al.* (CMS Collaboration), Search for long-lived particles that decay into final states containing two electrons or two muons in proton-proton collisions at $\sqrt{s} = 8$ TeV, Phys. Rev. D **91**, 052012 (2015).
[22] CMS Collaboration, Search for "Displaced Supersymmetry" in Events with an Electron and A Muon with Large Impact Parameters, Phys. Rev. Lett. **114**, 061801 (2015).
[23] CMS Collaboration, Search for long-lived neutral particles decaying to quark-antiquark pairs in proton-proton collisions at $\sqrt{s} = 8$ TeV, Phys. Rev. D **91**, 012007 (2015).
[24] LHCb Collaboration, Search for long-lived particles decaying to jet pairs, Eur. Phys. J. C **75**, 152 (2015).
[25] D. Liventsev *et al.* (Belle Collaboration), Search for heavy neutrinos at Belle, Phys. Rev. D **87**, 071102 (2013).
[26] J. P. Lees *et al.* (*BABAR* Collaboration), Search for Long-Lived Particles in e^+e^- Collisions, Phys. Rev. Lett. **114**, 171801 (2015).
[27] V. M. Abazov *et al.* (D0 Collaboration), Search for Neutral, Long-Lived Particles Decaying into Two Muons in $p\bar{p}$ Collisions at $\sqrt{s} = 1.96$ TeV, Phys. Rev. Lett. **97**, 161802 (2006).
[28] V. M. Abazov *et al.* (D0 Collaboration), Search for Resonant Pair Production of Neutral Long-Lived Particles Decaying to $b\bar{b}$ in $p\bar{p}$ Collisions at $\sqrt{s} = 1.96$ TeV, Phys. Rev. Lett. **103**, 071801 (2009).
[29] F. Abe *et al.* (CDF Collaboration), Search for long-lived parents of Z^0 bosons in $p\bar{p}$ collisions at $\sqrt{s} = 1.8$ TeV, Phys. Rev. D **58**, 051102 (1998).
[30] A. Heister *et al.* (ALEPH Collaboration), Search for gauge mediated SUSY breaking topologies in e^+e^- collisions at center-of-mass energies up to 209 GeV, Eur. Phys. J. C **25**, 339 (2002).
[31] ATLAS Collaboration, The ATLAS Experiment at the CERN Large Hadron Collider, J. Instrum. **3**, S08003 (2008).
[32] ATLAS Collaboration, Improved luminosity determination in pp collisions at $\sqrt{s} = 7$ TeV using the ATLAS detector at the LHC, Eur. Phys. J. C **73**, 2518 (2013).
[33] ATLAS Collaboration, ATLAS tunes of PYTHIA 6 and Pythia 8 for MC11, Report No. ATL-PHYS-PUB-2011-009, http://cds.cern.ch/record/1363300/, 2011.
[34] P. M. Nadolsky, H.-L. Lai, Q.-H. Cao, J. Huston, J. Pumplin, D. Stump, Wu-Ki Tung, and C.-P. Yuan, Implications of CTEQ global analysis for collider observables, Phys. Rev. D **78**, 013004 (2008).
[35] S. Agostinelli *et al.* (GEANT4 Collaboration), GEANT4: A Simulation toolkit, Nucl. Instrum. Methods Phys. Res., Sect. A **506**, 250 (2003).
[36] ATLAS Collaboration, The ATLAS Simulation Infrastructure, Eur. Phys. J. C **70**, 823 (2010).
[37] T. Sjöstrand, S. Mrenna, and P. Z. Skands, A Brief Introduction to PYTHIA 8.1, Comput. Phys. Commun. **178**, 852 (2008).
[38] M. Bähr *et al.*, Herwig + + Physics and Manual, Eur. Phys. J. C **58**, 639 (2008).
[39] T. Sjöstrand, S. Mrenna, and P. Z. Skands, PYTHIA 6.4 Physics and Manual, J. High Energy Phys. 05 (2006) 026.
[40] R. Mackeprang and D. Milstead, An Updated Description of Heavy-Hadron Interactions in GEANT-4, Eur. Phys. J. C **66**, 493 (2010).
[41] W. Beenakker, R. Höpker, M. Spira, and P. M. Zerwas, Squark and gluino production at hadron colliders, Nucl. Phys. **B492**, 51 (1997).
[42] A. Kulesza and L. Motyka, Threshold Resummation for Squark-Antisquark and Gluino-Pair Production at the LHC, Phys. Rev. Lett. **102**, 111802 (2009).
[43] A. Kulesza and L. Motyka, Soft gluon resummation for the production of gluino-gluino and squark-antisquark pairs at the LHC, Phys. Rev. D **80**, 095004 (2009).
[44] W. Beenakker, S. Brensing, M. Krämer, A. Kulesza, E. Laenen, and I. Niessen, Soft-gluon resummation for squark and gluino hadroproduction, J. High Energy Phys. 12 (2009) 041.
[45] W. Beenakker, S. Brensing, M. Krämer, A. Kulesza, E. Laenen, L. Motyka, and I. Niessen, Squark and Gluino Hadroproduction, Int. J. Mod. Phys. A **26**, 2637 (2011).
[46] M. Krämer, A. Kulesza, R. v. d. Leeuw, M. Mangano, S. Padhi, T. Plehn, and X. Portell, Supersymmetry production cross sections in pp collisions at $\sqrt{s} = 7$ TeV, arXiv:1206.2892.
[47] ATLAS Collaboration, Measurement of the muon reconstruction performance of the ATLAS detector using 2011 and 2012 LHC proton-proton collision data, Eur. Phys. J. C **74**, 3130 (2014).
[48] ATLAS Collaboration, Electron and photon energy calibration with the ATLAS detector using LHC Run 1 data, Eur. Phys. J. C **74**, 3071 (2014).
[49] M. Cacciari, G. P. Salam, and G. Soyez, The anti-k_t jet clustering algorithm, J. High Energy Phys. 04 (2008) 063.
[50] M. Cacciari and G. P. Salam, Dispelling the N^3 myth for the k_t jet-finder, Phys. Lett. B **641**, 57 (2006).
[51] ATLAS Collaboration, Jet energy measurement with the ATLAS detector in proton-proton collisions at $\sqrt{s} = 7$ TeV, Eur. Phys. J. C **73**, 2304 (2013).

[52] W. Lampl, S. Laplace, D. Lelas, P. Loch, H. Ma, S. Menke, S. Rajagopalan, D. Rousseau, S. Snyder, and G. Unal, Calorimeter clustering algorithms: Description and performance, Report No. ATL-LARG-PUB-2008-002, http://cds.cern.ch/record/1099735/, 2008.

[53] ATLAS Collaboration, Performance of Missing Transverse Momentum Reconstruction in Proton-Proton Collisions at 7 TeV with ATLAS, Eur. Phys. J. C **72**, 1844 (2012).

[54] ATLAS Collaboration, Performance of Missing Transverse Momentum Reconstruction in ATLAS studied in Proton-Proton Collisions recorded in 2012 at 8 TeV, Report No. ATLAS-CONF-2013-082, http://cds.cern.ch/record/1570993/, 2013.

[55] S. R. Das, On a new approach for finding all the modified cut-sets in an incompatibility graph, IEEE Trans. Comput. **C-22**, 187 (1973).

[56] ATLAS Collaboration, Characterisation and mitigation of beam-induced backgrounds observed in the ATLAS detector during the 2011 proton-proton run, J. Instrum. **8**, P07004 (2013).

[57] ATLAS Collaboration, Jet energy measurement and its systematic uncertainty in proton-proton collisions at $\sqrt{s} = 7$ TeV with the ATLAS detector, Eur. Phys. J. C **75**, 17 (2015).

[58] ATLAS Collaboration, Jet energy resolution in proton-proton collisions at $\sqrt{s} = 7$ TeV recorded in 2010 with the ATLAS detector, Eur. Phys. J. C **73**, 2306 (2013).

[59] J. Alwall, M. Herquet, F. Maltoni, O. Mattelaer, and T. Stelzer, MadGraph 5 : Going Beyond, J. High Energy Phys. 06 (2011) 128.

[60] A. L. Read, Presentation of search results: The CL(s) technique, J. Phys. G **28**, 2693 (2002).

[61] M. Baak, G. J. Besjes, D. Côté, A. Koutsman, J. Lorenz, and D. Short, HistFitter software framework for statistical data analysis, Eur. Phys. J. C **75**, 153 (2015).

[62] ATLAS Collaboration, Search for squarks and gluinos with the ATLAS detector in final states with jets and missing transverse momentum using $\sqrt{s} = 8$ TeV proton–proton collision data, J. High Energy Phys. 09 (2014) 176.

G. Aad,[85] B. Abbott,[113] J. Abdallah,[151] O. Abdinov,[11] R. Aben,[107] M. Abolins,[90] O. S. AbouZeid,[158] H. Abramowicz,[153] H. Abreu,[152] R. Abreu,[30] Y. Abulaiti,[146a,146b] B. S. Acharya,[164a,164b,b] L. Adamczyk,[38a] D. L. Adams,[25] J. Adelman,[108] S. Adomeit,[100] T. Adye,[131] A. A. Affolder,[74] T. Agatonovic-Jovin,[13] J. A. Aguilar-Saavedra,[126a,126f] S. P. Ahlen,[22] F. Ahmadov,[65,c] G. Aielli,[133a,133b] H. Akerstedt,[146a,146b] T. P. A. Åkesson,[81] G. Akimoto,[155] A. V. Akimov,[96] G. L. Alberghi,[20a,20b] J. Albert,[169] S. Albrand,[55] M. J. Alconada Verzini,[71] M. Aleksa,[30] I. N. Aleksandrov,[65] C. Alexa,[26a] G. Alexander,[153] T. Alexopoulos,[10] M. Alhroob,[113] G. Alimonti,[91a] L. Alio,[85] J. Alison,[31] S. P. Alkire,[35] B. M. M. Allbrooke,[18] P. P. Allport,[74] A. Aloisio,[104a,104b] A. Alonso,[36] F. Alonso,[71] C. Alpigiani,[76] A. Altheimer,[35] B. Alvarez Gonzalez,[30] D. Álvarez Piqueras,[167] M. G. Alviggi,[104a,104b] B. T. Amadio,[15] K. Amako,[66] Y. Amaral Coutinho,[24a] C. Amelung,[23] D. Amidei,[89] S. P. Amor Dos Santos,[126a,126c] A. Amorim,[126a,126b] S. Amoroso,[48] N. Amram,[153] G. Amundsen,[23] C. Anastopoulos,[139] L. S. Ancu,[49] N. Andari,[30] T. Andeen,[35] C. F. Anders,[58b] G. Anders,[30] J. K. Anders,[74] K. J. Anderson,[31] A. Andreazza,[91a,91b] V. Andrei,[58a] S. Angelidakis,[9] I. Angelozzi,[107] P. Anger,[44] A. Angerami,[35] F. Anghinolfi,[30] A. V. Anisenkov,[109,d] N. Anjos,[12] A. Annovi,[124a,124b] M. Antonelli,[47] A. Antonov,[98] J. Antos,[144b] F. Anulli,[132a] M. Aoki,[66] L. Aperio Bella,[18] G. Arabidze,[90] Y. Arai,[66] J. P. Araque,[126a] A. T. H. Arce,[45] F. A. Arduh,[71] J-F. Arguin,[95] S. Argyropoulos,[42] M. Arik,[19a] A. J. Armbruster,[30] O. Arnaez,[30] V. Arnal,[82] H. Arnold,[48] M. Arratia,[28] O. Arslan,[21] A. Artamonov,[97] G. Artoni,[23] S. Asai,[155] N. Asbah,[42] A. Ashkenazi,[153] B. Åsman,[146a,146b] L. Asquith,[149] K. Assamagan,[25] R. Astalos,[144a] M. Atkinson,[165] N. B. Atlay,[141] B. Auerbach,[6] K. Augsten,[128] M. Aurousseau,[145b] G. Avolio,[30] B. Axen,[15] M. K. Ayoub,[117] G. Azuelos,[95,e] M. A. Baak,[30] A. E. Baas,[58a] C. Bacci,[134a,134b] H. Bachacou,[136] K. Bachas,[154] M. Backes,[30] M. Backhaus,[30] E. Badescu,[26a] P. Bagiacchi,[132a,132b] P. Bagnaia,[132a,132b] Y. Bai,[33a] T. Bain,[35] J. T. Baines,[131] O. K. Baker,[176] P. Balek,[129] T. Balestri,[148] F. Balli,[84] E. Banas,[39] Sw. Banerjee,[173] A. A. E. Bannoura,[175] H. S. Bansil,[18] L. Barak,[30] S. P. Baranov,[96] E. L. Barberio,[88] D. Barberis,[50a,50b] M. Barbero,[85] T. Barillari,[101] M. Barisonzi,[164a,164b] T. Barklow,[143] N. Barlow,[28] S. L. Barnes,[84] B. M. Barnett,[131] R. M. Barnett,[15] Z. Barnovska,[5] A. Baroncelli,[134a] G. Barone,[49] A. J. Barr,[120] F. Barreiro,[82] J. Barreiro Guimarães da Costa,[57] R. Bartoldus,[143] A. E. Barton,[72] P. Bartos,[144a] A. Bassalat,[117] A. Basye,[165] R. L. Bates,[53] S. J. Batista,[158] J. R. Batley,[28] M. Battaglia,[137] M. Bauce,[132a,132b] F. Bauer,[136] H. S. Bawa,[143,f] J. B. Beacham,[111] M. D. Beattie,[72] T. Beau,[80] P. H. Beauchemin,[161] R. Beccherle,[124a,124b] P. Bechtle,[21] H. P. Beck,[17,g] K. Becker,[120] M. Becker,[83] S. Becker,[100] M. Beckingham,[170] C. Becot,[117] A. J. Beddall,[19c] A. Beddall,[19c] V. A. Bednyakov,[65] C. P. Bee,[148] L. J. Beemster,[107] T. A. Beermann,[175] M. Begel,[25] J. K. Behr,[120] C. Belanger-Champagne,[87] P. J. Bell,[49] W. H. Bell,[49] G. Bella,[153] L. Bellagamba,[20a] A. Bellerive,[29] M. Bellomo,[86] K. Belotskiy,[98] O. Beltramello,[30] O. Benary,[153] D. Benchekroun,[135a] M. Bender,[100] K. Bendtz,[146a,146b] N. Benekos,[10] Y. Benhammou,[153] E. Benhar Noccioli,[49] J. A. Benitez Garcia,[159b] D. P. Benjamin,[45] J. R. Bensinger,[23] S. Bentvelsen,[107]

L. Beresford,[120] M. Beretta,[47] D. Berge,[107] E. Bergeaas Kuutmann,[166] N. Berger,[5] F. Berghaus,[169] J. Beringer,[15] C. Bernard,[22] N. R. Bernard,[86] C. Bernius,[110] F. U. Bernlochner,[21] T. Berry,[77] P. Berta,[129] C. Bertella,[83] G. Bertoli,[146a,146b] F. Bertolucci,[124a,124b] C. Bertsche,[113] D. Bertsche,[113] M. I. Besana,[91a] G. J. Besjes,[106] O. Bessidskaia Bylund,[146a,146b] M. Bessner,[42] N. Besson,[136] C. Betancourt,[48] S. Bethke,[101] A. J. Bevan,[76] W. Bhimji,[46] R. M. Bianchi,[125] L. Bianchini,[23] M. Bianco,[30] O. Biebel,[100] S. P. Bieniek,[78] M. Biglietti,[134a] J. Bilbao De Mendizabal,[49] H. Bilokon,[47] M. Bindi,[54] S. Binet,[117] A. Bingul,[19c] C. Bini,[132a,132b] C. W. Black,[150] J. E. Black,[143] K. M. Black,[22] D. Blackburn,[138] R. E. Blair,[6] J.-B. Blanchard,[136] J. E. Blanco,[77] T. Blazek,[144a] I. Bloch,[42] C. Blocker,[23] W. Blum,[83,a] U. Blumenschein,[54] G. J. Bobbink,[107] V. S. Bobrovnikov,[109,d] S. S. Bocchetta,[81] A. Bocci,[45] C. Bock,[100] M. Boehler,[48] J. A. Bogaerts,[30] A. G. Bogdanchikov,[109] C. Bohm,[146a] V. Boisvert,[77] T. Bold,[38a] V. Boldea,[26a] A. S. Boldyrev,[99] M. Bomben,[80] M. Bona,[76] M. Boonekamp,[136] A. Borisov,[130] G. Borissov,[72] S. Borroni,[42] J. Bortfeldt,[100] V. Bortolotto,[60a,60b,60c] K. Bos,[107] D. Boscherini,[20a] M. Bosman,[12] J. Boudreau,[125] J. Bouffard,[2] E. V. Bouhova-Thacker,[72] D. Boumediene,[34] C. Bourdarios,[117] N. Bousson,[114] A. Boveia,[30] J. Boyd,[30] I. R. Boyko,[65] I. Bozic,[13] J. Bracinik,[18] A. Brandt,[8] G. Brandt,[54] O. Brandt,[58a] U. Bratzler,[156] B. Brau,[86] J. E. Brau,[116] H. M. Braun,[175,a] S. F. Brazzale,[164a,164c] K. Brendlinger,[122] A. J. Brennan,[88] L. Brenner,[107] R. Brenner,[166] S. Bressler,[172] K. Bristow,[145c] T. M. Bristow,[46] D. Britton,[53] D. Britzger,[42] F. M. Brochu,[28] I. Brock,[21] R. Brock,[90] J. Bronner,[101] G. Brooijmans,[35] T. Brooks,[77] W. K. Brooks,[32b] J. Brosamer,[15] E. Brost,[116] J. Brown,[55] P. A. Bruckman de Renstrom,[39] D. Bruncko,[144b] R. Bruneliere,[48] A. Bruni,[20a] G. Bruni,[20a] M. Bruschi,[20a] L. Bryngemark,[81] T. Buanes,[14] Q. Buat,[142] P. Buchholz,[141] A. G. Buckley,[53] S. I. Buda,[26a] I. A. Budagov,[65] F. Buehrer,[48] L. Bugge,[119] M. K. Bugge,[119] O. Bulekov,[98] D. Bullock,[8] H. Burckhart,[30] S. Burdin,[74] B. Burghgrave,[108] S. Burke,[131] I. Burmeister,[43] E. Busato,[34] D. Büscher,[48] V. Büscher,[83] P. Bussey,[53] C. P. Buszello,[166] J. M. Butler,[22] A. I. Butt,[3] C. M. Buttar,[53] J. M. Butterworth,[78] P. Butti,[107] W. Buttinger,[25] A. Buzatu,[53] R. Buzykaev,[109,d] S. Cabrera Urbán,[167] D. Caforio,[128] V. M. Cairo,[37a,37b] O. Cakir,[4a] P. Calafiura,[15] A. Calandri,[136] G. Calderini,[80] P. Calfayan,[100] L. P. Caloba,[24a] D. Calvet,[34] S. Calvet,[34] R. Camacho Toro,[49] S. Camarda,[42] P. Camarri,[133a,133b] D. Cameron,[119] L. M. Caminada,[15] R. Caminal Armadans,[12] S. Campana,[30] M. Campanelli,[78] A. Campoverde,[148] V. Canale,[104a,104b] A. Canepa,[159a] M. Cano Bret,[76] J. Cantero,[82] R. Cantrill,[126a] T. Cao,[40] M. D. M. Capeans Garrido,[30] I. Caprini,[26a] M. Caprini,[26a] M. Capua,[37a,37b] R. Caputo,[83] R. Cardarelli,[133a] T. Carli,[30] G. Carlino,[104a] L. Carminati,[91a,91b] S. Caron,[106] E. Carquin,[32a] G. D. Carrillo-Montoya,[8] J. R. Carter,[28] J. Carvalho,[126a,126c] D. Casadei,[78] M. P. Casado,[12] M. Casolino,[12] E. Castaneda-Miranda,[145b] A. Castelli,[107] V. Castillo Gimenez,[167] N. F. Castro,[126a,h] P. Catastini,[57] A. Catinaccio,[30] J. R. Catmore,[119] A. Cattai,[30] J. Caudron,[83] V. Cavaliere,[165] D. Cavalli,[91a] M. Cavalli-Sforza,[12] V. Cavasinni,[124a,124b] F. Ceradini,[134a,134b] B. C. Cerio,[45] K. Cerny,[129] A. S. Cerqueira,[24b] A. Cerri,[149] L. Cerrito,[76] F. Cerutti,[15] M. Cerv,[30] A. Cervelli,[17] S. A. Cetin,[19b] A. Chafaq,[135a] D. Chakraborty,[108] I. Chalupkova,[129] P. Chang,[165] B. Chapleau,[87] J. D. Chapman,[28] D. G. Charlton,[18] C. C. Chau,[158] C. A. Chavez Barajas,[149] S. Cheatham,[152] A. Chegwidden,[90] S. Chekanov,[6] S. V. Chekulaev,[159a] G. A. Chelkov,[65,i] M. A. Chelstowska,[89] C. Chen,[64] H. Chen,[25] K. Chen,[148] L. Chen,[33d,j] S. Chen,[33c] X. Chen,[33f] Y. Chen,[67] H. C. Cheng,[89] Y. Cheng,[31] A. Cheplakov,[65] E. Cheremushkina,[130] R. Cherkaoui El Moursli,[135e] V. Chernyatin,[25,a] E. Cheu,[7] L. Chevalier,[136] V. Chiarella,[47] J. T. Childers,[6] G. Chiodini,[73a] A. S. Chisholm,[18] R. T. Chislett,[78] A. Chitan,[26a] M. V. Chizhov,[65] K. Choi,[61] S. Chouridou,[9] B. K. B. Chow,[100] V. Christodoulou,[78] D. Chromek-Burckhart,[30] M. L. Chu,[151] J. Chudoba,[127] A. J. Chuinard,[87] J. J. Chwastowski,[39] L. Chytka,[115] G. Ciapetti,[132a,132b] A. K. Ciftci,[4a] D. Cinca,[53] V. Cindro,[75] I. A. Cioara,[21] A. Ciocio,[15] Z. H. Citron,[172] M. Ciubancan,[26a] A. Clark,[49] B. L. Clark,[57] P. J. Clark,[46] R. N. Clarke,[15] W. Cleland,[125] C. Clement,[146a,146b] Y. Coadou,[85] M. Cobal,[164a,164c] A. Coccaro,[138] J. Cochran,[64] L. Coffey,[23] J. G. Cogan,[143] B. Cole,[35] S. Cole,[108] A. P. Colijn,[107] J. Collot,[55] T. Colombo,[58c] G. Compostella,[101] P. Conde Muiño,[126a,126b] E. Coniavitis,[48] S. H. Connell,[145b] I. A. Connelly,[77] S. M. Consonni,[91a,91b] V. Consorti,[48] S. Constantinescu,[26a] C. Conta,[121a,121b] G. Conti,[30] F. Conventi,[104a,k] M. Cooke,[15] B. D. Cooper,[78] A. M. Cooper-Sarkar,[120] T. Cornelissen,[175] M. Corradi,[20a] F. Corriveau,[87,l] A. Corso-Radu,[163] A. Cortes-Gonzalez,[12] G. Cortiana,[101] G. Costa,[91a] M. J. Costa,[167] D. Costanzo,[139] D. Côté,[8] G. Cottin,[28] G. Cowan,[77] B. E. Cox,[84] K. Cranmer,[110] G. Cree,[29] S. Crépé-Renaudin,[55] F. Crescioli,[80] W. A. Cribbs,[146a,146b] M. Crispin Ortuzar,[120] M. Cristinziani,[21] V. Croft,[106] G. Crosetti,[37a,37b] T. Cuhadar Donszelmann,[139] J. Cummings,[176] M. Curatolo,[47] C. Cuthbert,[150] H. Czirr,[141] P. Czodrowski,[3] S. D'Auria,[53] M. D'Onofrio,[74] M. J. Da Cunha Sargedas De Sousa,[126a,126b] C. Da Via,[84] W. Dabrowski,[38a] A. Dafinca,[120] T. Dai,[89] O. Dale,[14] F. Dallaire,[95] C. Dallapiccola,[86] M. Dam,[36] J. R. Dandoy,[31] N. P. Dang,[48] A. C. Daniells,[18] M. Danninger,[168] M. Dano Hoffmann,[136] V. Dao,[48] G. Darbo,[50a] S. Darmora,[8] J. Dassoulas,[3] A. Dattagupta,[61] W. Davey,[21] C. David,[169] T. Davidek,[129] E. Davies,[120,m] M. Davies,[153] P. Davison,[78] Y. Davygora,[58a]

E. Dawe,[88] I. Dawson,[139] R. K. Daya-Ishmukhametova,[86] K. De,[8] R. de Asmundis,[104a] S. De Castro,[20a,20b] S. De Cecco,[80] N. De Groot,[106] P. de Jong,[107] H. De la Torre,[82] F. De Lorenzi,[64] L. De Nooij,[107] D. De Pedis,[132a] A. De Salvo,[132a] U. De Sanctis,[149] A. De Santo,[149] J. B. De Vivie De Regie,[117] W. J. Dearnaley,[72] R. Debbe,[25] C. Debenedetti,[137] D. V. Dedovich,[65] I. Deigaard,[107] J. Del Peso,[82] T. Del Prete,[124a,124b] D. Delgove,[117] F. Deliot,[136] C. M. Delitzsch,[49] M. Deliyergiyev,[75] A. Dell'Acqua,[30] L. Dell'Asta,[22] M. Dell'Orso,[124a,124b] M. Della Pietra,[104a,k] D. della Volpe,[49] M. Delmastro,[5] P. A. Delsart,[55] C. Deluca,[107] D. A. DeMarco,[158] S. Demers,[176] M. Demichev,[65] A. Demilly,[80] S. P. Denisov,[130] D. Derendarz,[39] J. E. Derkaoui,[135d] F. Derue,[80] P. Dervan,[74] K. Desch,[21] C. Deterre,[42] P. O. Deviveiros,[30] A. Dewhurst,[131] S. Dhaliwal,[107] A. Di Ciaccio,[133a,133b] L. Di Ciaccio,[5] A. Di Domenico,[132a,132b] C. Di Donato,[104a,104b] A. Di Girolamo,[30] B. Di Girolamo,[30] A. Di Mattia,[152] B. Di Micco,[134a,134b] R. Di Nardo,[47] A. Di Simone,[48] R. Di Sipio,[158] D. Di Valentino,[29] C. Diaconu,[85] M. Diamond,[158] F. A. Dias,[46] M. A. Diaz,[32a] E. B. Diehl,[89] J. Dietrich,[16] S. Diglio,[85] A. Dimitrievska,[13] J. Dingfelder,[21] F. Dittus,[30] F. Djama,[85] T. Djobava,[51b] J. I. Djuvsland,[58a] M. A. B. do Vale,[24c] D. Dobos,[30] M. Dobre,[26a] C. Doglioni,[49] T. Dohmae,[155] J. Dolejsi,[129] Z. Dolezal,[129] B. A. Dolgoshein,[98,a] M. Donadelli,[24d] S. Donati,[124a,124b] P. Dondero,[121a,121b] J. Donini,[34] J. Dopke,[131] A. Doria,[104a] M. T. Dova,[71] A. T. Doyle,[53] E. Drechsler,[54] M. Dris,[10] E. Dubreuil,[34] E. Duchovni,[172] G. Duckeck,[100] O. A. Ducu,[26a,85] D. Duda,[175] A. Dudarev,[30] L. Duflot,[117] L. Duguid,[77] M. Dührssen,[30] M. Dunford,[58a] H. Duran Yildiz,[4a] M. Düren,[52] A. Durglishvili,[51b] D. Duschinger,[44] M. Dyndal,[38a] C. Eckardt,[42] K. M. Ecker,[101] R. C. Edgar,[89] W. Edson,[2] N. C. Edwards,[46] W. Ehrenfeld,[21] T. Eifert,[30] G. Eigen,[14] K. Einsweiler,[15] T. Ekelof,[166] M. El Kacimi,[135c] M. Ellert,[166] S. Elles,[5] F. Ellinghaus,[83] A. A. Elliot,[169] N. Ellis,[30] J. Elmsheuser,[100] M. Elsing,[30] D. Emeliyanov,[131] Y. Enari,[155] O. C. Endner,[83] M. Endo,[118] R. Engelmann,[148] J. Erdmann,[43] A. Ereditato,[17] G. Ernis,[175] J. Ernst,[2] M. Ernst,[25] S. Errede,[165] E. Ertel,[83] M. Escalier,[117] H. Esch,[43] C. Escobar,[125] B. Esposito,[47] A. I. Etienvre,[136] E. Etzion,[153] H. Evans,[61] A. Ezhilov,[123] L. Fabbri,[20a,20b] G. Facini,[31] R. M. Fakhrutdinov,[130] S. Falciano,[132a] R. J. Falla,[78] J. Faltova,[129] Y. Fang,[33a] M. Fanti,[91a,91b] A. Farbin,[8] A. Farilla,[134a] T. Farooque,[12] S. Farrell,[15] S. M. Farrington,[170] P. Farthouat,[30] F. Fassi,[135e] P. Fassnacht,[30] D. Fassouliotis,[9] M. Faucci Giannelli,[77] A. Favareto,[50a,50b] L. Fayard,[117] P. Federic,[144a] O. L. Fedin,[123,n] W. Fedorko,[168] S. Feigl,[30] L. Feligioni,[85] C. Feng,[33d] E. J. Feng,[6] H. Feng,[89] A. B. Fenyuk,[130] P. Fernandez Martinez,[167] S. Fernandez Perez,[30] S. Ferrag,[53] J. Ferrando,[53] A. Ferrari,[166] P. Ferrari,[107] R. Ferrari,[121a] D. E. Ferreira de Lima,[53] A. Ferrer,[167] D. Ferrere,[49] C. Ferretti,[89] A. Ferretto Parodi,[50a,50b] M. Fiascaris,[31] F. Fiedler,[83] A. Filipčič,[75] M. Filipuzzi,[42] F. Filthaut,[106] M. Fincke-Keeler,[169] K. D. Finelli,[150] M. C. N. Fiolhais,[126a,126c] L. Fiorini,[167] A. Firan,[40] A. Fischer,[2] C. Fischer,[12] J. Fischer,[175] W. C. Fisher,[90] E. A. Fitzgerald,[23] M. Flechl,[48] I. Fleck,[141] P. Fleischmann,[89] S. Fleischmann,[175] G. T. Fletcher,[139] G. Fletcher,[76] T. Flick,[175] A. Floderus,[81] L. R. Flores Castillo,[60a] M. J. Flowerdew,[101] A. Formica,[136] A. Forti,[84] D. Fournier,[117] H. Fox,[72] S. Fracchia,[12] P. Francavilla,[80] M. Franchini,[20a,20b] D. Francis,[30] L. Franconi,[119] M. Franklin,[57] M. Fraternali,[121a,121b] D. Freeborn,[78] S. T. French,[28] F. Friedrich,[44] D. Froidevaux,[30] J. A. Frost,[120] C. Fukunaga,[156] E. Fullana Torregrosa,[83] B. G. Fulsom,[143] J. Fuster,[167] C. Gabaldon,[55] O. Gabizon,[175] A. Gabrielli,[20a,20b] A. Gabrielli,[132a,132b] S. Gadatsch,[107] S. Gadomski,[49] G. Gagliardi,[50a,50b] P. Gagnon,[61] C. Galea,[106] B. Galhardo,[126a,126c] E. J. Gallas,[120] B. J. Gallop,[131] P. Gallus,[128] G. Galster,[36] K. K. Gan,[111] J. Gao,[33b,85] Y. Gao,[46] Y. S. Gao,[143,f] F. M. Garay Walls,[46] F. Garberson,[176] C. García,[167] J. E. García Navarro,[167] M. Garcia-Sciveres,[15] R. W. Gardner,[31] N. Garelli,[143] V. Garonne,[119] C. Gatti,[47] A. Gaudiello,[50a,50b] G. Gaudio,[121a] B. Gaur,[141] L. Gauthier,[95] P. Gauzzi,[132a,132b] I. L. Gavrilenko,[96] C. Gay,[168] G. Gaycken,[21] E. N. Gazis,[10] P. Ge,[33d] Z. Gecse,[168] C. N. P. Gee,[131] D. A. A. Geerts,[107] Ch. Geich-Gimbel,[21] M. P. Geisler,[58a] C. Gemme,[50a] M. H. Genest,[55] S. Gentile,[132a,132b] M. George,[54] S. George,[77] D. Gerbaudo,[163] A. Gershon,[153] H. Ghazlane,[135b] B. Giacobbe,[20a] S. Giagu,[132a,132b] V. Giangiobbe,[12] P. Giannetti,[124a,124b] B. Gibbard,[25] S. M. Gibson,[77] M. Gilchriese,[15] T. P. S. Gillam,[28] D. Gillberg,[30] G. Gilles,[34] D. M. Gingrich,[3,e] N. Giokaris,[9] M. P. Giordani,[164a,164c] F. M. Giorgi,[20a] F. M. Giorgi,[16] P. F. Giraud,[136] P. Giromini,[47] D. Giugni,[91a] C. Giuliani,[48] M. Giulini,[58b] B. K. Gjelsten,[119] S. Gkaitatzis,[154] I. Gkialas,[154] E. L. Gkougkousis,[117] L. K. Gladilin,[99] C. Glasman,[82] J. Glatzer,[30] P. C. F. Glaysher,[46] A. Glazov,[42] M. Goblirsch-Kolb,[101] J. R. Goddard,[76] J. Godlewski,[39] S. Goldfarb,[89] T. Golling,[49] D. Golubkov,[130] A. Gomes,[126a,126b,126d] R. Gonçalo,[126a] J. Goncalves Pinto Firmino Da Costa,[136] L. Gonella,[21] S. González de la Hoz,[167] G. Gonzalez Parra,[12] S. Gonzalez-Sevilla,[49] L. Goossens,[30] P. A. Gorbounov,[97] H. A. Gordon,[25] I. Gorelov,[105] B. Gorini,[30] E. Gorini,[73a,73b] A. Gorišek,[75] E. Gornicki,[39] A. T. Goshaw,[45] C. Gössling,[43] M. I. Gostkin,[65] D. Goujdami,[135c] A. G. Goussiou,[138] N. Govender,[145b] H. M. X. Grabas,[137] L. Graber,[54] I. Grabowska-Bold,[38a] P. Grafström,[20a,20b] K-J. Grahn,[42] J. Gramling,[49] E. Gramstad,[119] S. Grancagnolo,[16] V. Grassi,[148] V. Gratchev,[123] H. M. Gray,[30] E. Graziani,[134a] Z. D. Greenwood,[79,o] K. Gregersen,[78] I. M. Gregor,[42] P. Grenier,[143] J. Griffiths,[8] A. A. Grillo,[137] K. Grimm,[72] S. Grinstein,[12,p] Ph. Gris,[34] J.-F. Grivaz,[117] J. P. Grohs,[44]

A. Grohsjean,[42] E. Gross,[172] J. Grosse-Knetter,[54] G. C. Grossi,[79] Z. J. Grout,[149] L. Guan,[33b] J. Guenther,[128] F. Guescini,[49] D. Guest,[176] O. Gueta,[153] E. Guido,[50a,50b] T. Guillemin,[117] S. Guindon,[2] U. Gul,[53] C. Gumpert,[44] J. Guo,[33e] S. Gupta,[120] P. Gutierrez,[113] N. G. Gutierrez Ortiz,[53] C. Gutschow,[44] C. Guyot,[136] C. Gwenlan,[120] C. B. Gwilliam,[74] A. Haas,[110] C. Haber,[15] H. K. Hadavand,[8] N. Haddad,[135e] P. Haefner,[21] S. Hageböck,[21] Z. Hajduk,[39] H. Hakobyan,[177] M. Haleem,[42] J. Haley,[114] D. Hall,[120] G. Halladjian,[90] G. D. Hallewell,[85] K. Hamacher,[175] P. Hamal,[115] K. Hamano,[169] M. Hamer,[54] A. Hamilton,[145a] S. Hamilton,[161] G. N. Hamity,[145c] P. G. Hamnett,[42] L. Han,[33b] K. Hanagaki,[118] K. Hanawa,[155] M. Hance,[15] P. Hanke,[58a] R. Hanna,[136] J. B. Hansen,[36] J. D. Hansen,[36] M. C. Hansen,[21] P. H. Hansen,[36] K. Hara,[160] A. S. Hard,[173] T. Harenberg,[175] F. Hariri,[117] S. Harkusha,[92] R. D. Harrington,[46] P. F. Harrison,[170] F. Hartjes,[107] M. Hasegawa,[67] S. Hasegawa,[103] Y. Hasegawa,[140] A. Hasib,[113] S. Hassani,[136] S. Haug,[17] R. Hauser,[90] L. Hauswald,[44] M. Havranek,[127] C. M. Hawkes,[18] R. J. Hawkings,[30] A. D. Hawkins,[81] T. Hayashi,[160] D. Hayden,[90] C. P. Hays,[120] J. M. Hays,[76] H. S. Hayward,[74] S. J. Haywood,[131] S. J. Head,[18] T. Heck,[83] V. Hedberg,[81] L. Heelan,[8] S. Heim,[122] T. Heim,[175] B. Heinemann,[15] L. Heinrich,[110] J. Hejbal,[127] L. Helary,[22] S. Hellman,[146a,146b] D. Hellmich,[21] C. Helsens,[30] J. Henderson,[120] R. C. W. Henderson,[72] Y. Heng,[173] C. Hengler,[42] A. Henrichs,[176] A. M. Henriques Correia,[30] S. Henrot-Versille,[117] G. H. Herbert,[16] Y. Hernández Jiménez,[167] R. Herrberg-Schubert,[16] G. Herten,[48] R. Hertenberger,[100] L. Hervas,[30] G. G. Hesketh,[78] N. P. Hessey,[107] J. W. Hetherly,[40] R. Hickling,[76] E. Higón-Rodriguez,[167] E. Hill,[169] J. C. Hill,[28] K. H. Hiller,[42] S. J. Hillier,[18] I. Hinchliffe,[15] E. Hines,[122] R. R. Hinman,[15] M. Hirose,[157] D. Hirschbuehl,[175] J. Hobbs,[148] N. Hod,[107] M. C. Hodgkinson,[139] P. Hodgson,[139] A. Hoecker,[30] M. R. Hoeferkamp,[105] F. Hoenig,[100] M. Hohlfeld,[83] D. Hohn,[21] T. R. Holmes,[15] T. M. Hong,[122] L. Hooft van Huysduynen,[110] W. H. Hopkins,[116] Y. Horii,[103] A. J. Horton,[142] J-Y. Hostachy,[55] S. Hou,[151] A. Hoummada,[135a] J. Howard,[120] J. Howarth,[42] M. Hrabovsky,[115] I. Hristova,[16] J. Hrivnac,[117] T. Hryn'ova,[5] A. Hrynevich,[93] C. Hsu,[145c] P. J. Hsu,[151,q] S.-C. Hsu,[138] D. Hu,[35] Q. Hu,[33b] X. Hu,[89] Y. Huang,[42] Z. Hubacek,[30] F. Hubaut,[85] F. Huegging,[21] T. B. Huffman,[120] E. W. Hughes,[35] G. Hughes,[72] M. Huhtinen,[30] T. A. Hülsing,[83] N. Huseynov,[65,c] J. Huston,[90] J. Huth,[57] G. Iacobucci,[49] G. Iakovidis,[25] I. Ibragimov,[141] L. Iconomidou-Fayard,[117] E. Ideal,[176] Z. Idrissi,[135e] P. Iengo,[30] O. Igonkina,[107] T. Iizawa,[171] Y. Ikegami,[66] K. Ikematsu,[141] M. Ikeno,[66] Y. Ilchenko,[31,r] D. Iliadis,[154] N. Ilic,[158] Y. Inamaru,[67] T. Ince,[101] P. Ioannou,[9] M. Iodice,[134a] K. Iordanidou,[35] V. Ippolito,[57] A. Irles Quiles,[167] C. Isaksson,[166] M. Ishino,[68] M. Ishitsuka,[157] R. Ishmukhametov,[111] C. Issever,[120] S. Istin,[19a] J. M. Iturbe Ponce,[84] R. Iuppa,[133a,133b] J. Ivarsson,[81] W. Iwanski,[39] H. Iwasaki,[66] J. M. Izen,[41] V. Izzo,[104a] S. Jabbar,[3] B. Jackson,[122] M. Jackson,[74] P. Jackson,[1] M. R. Jaekel,[30] V. Jain,[2] K. Jakobs,[48] S. Jakobsen,[30] T. Jakoubek,[127] J. Jakubek,[128] D. O. Jamin,[151] D. K. Jana,[79] E. Jansen,[78] R. W. Jansky,[62] J. Janssen,[21] M. Janus,[170] G. Jarlskog,[81] N. Javadov,[65,c] T. Javůrek,[48] L. Jeanty,[15] J. Jejelava,[51a,s] G.-Y. Jeng,[150] D. Jennens,[88] P. Jenni,[48,t] J. Jentzsch,[43] C. Jeske,[170] S. Jézéquel,[5] H. Ji,[173] J. Jia,[148] Y. Jiang,[33b] S. Jiggins,[78] J. Jimenez Pena,[167] S. Jin,[33a] A. Jinaru,[26a] O. Jinnouchi,[157] M. D. Joergensen,[36] P. Johansson,[139] K. A. Johns,[7] K. Jon-And,[146a,146b] G. Jones,[170] R. W. L. Jones,[72] T. J. Jones,[74] J. Jongmanns,[58a] P. M. Jorge,[126a,126b] K. D. Joshi,[84] J. Jovicevic,[159a] X. Ju,[173] C. A. Jung,[43] P. Jussel,[62] A. Juste Rozas,[12,p] M. Kaci,[167] A. Kaczmarska,[39] M. Kado,[117] H. Kagan,[111] M. Kagan,[143] S. J. Kahn,[85] E. Kajomovitz,[45] C. W. Kalderon,[120] S. Kama,[40] A. Kamenshchikov,[130] N. Kanaya,[155] M. Kaneda,[30] S. Kaneti,[28] V. A. Kantserov,[98] J. Kanzaki,[66] B. Kaplan,[110] A. Kapliy,[31] D. Kar,[53] K. Karakostas,[10] A. Karamaoun,[3] N. Karastathis,[10,107] M. J. Kareem,[54] M. Karnevskiy,[83] S. N. Karpov,[65] Z. M. Karpova,[65] K. Karthik,[110] V. Kartvelishvili,[72] A. N. Karyukhin,[130] L. Kashif,[173] R. D. Kass,[111] A. Kastanas,[14] Y. Kataoka,[155] A. Katre,[49] J. Katzy,[42] K. Kawagoe,[70] T. Kawamoto,[155] G. Kawamura,[54] S. Kazama,[155] V. F. Kazanin,[109,d] M. Y. Kazarinov,[65] R. Keeler,[169] R. Kehoe,[40] J. S. Keller,[42] J. J. Kempster,[77] H. Keoshkerian,[84] O. Kepka,[127] B. P. Kerševan,[75] S. Kersten,[175] R. A. Keyes,[87] F. Khalil-zada,[11] H. Khandanyan,[146a,146b] A. Khanov,[114] A. G. Kharlamov,[109,d] T. J. Khoo,[28] V. Khovanskiy,[97] E. Khramov,[65] J. Khubua,[51b,u] H. Y. Kim,[8] H. Kim,[146a,146b] S. H. Kim,[160] Y. Kim,[31] N. Kimura,[154] O. M. Kind,[16] B. T. King,[74] M. King,[167] R. S. B. King,[120] S. B. King,[168] J. Kirk,[131] A. E. Kiryunin,[101] T. Kishimoto,[67] D. Kisielewska,[38a] F. Kiss,[48] K. Kiuchi,[160] O. Kivernyk,[136] E. Kladiva,[144b] M. H. Klein,[35] M. Klein,[74] U. Klein,[74] K. Kleinknecht,[83] P. Klimek,[146a,146b] A. Klimentov,[25] R. Klingenberg,[43] J. A. Klinger,[84] T. Klioutchnikova,[30] E.-E. Kluge,[58a] P. Kluit,[107] S. Kluth,[101] E. Kneringer,[62] E. B. F. G. Knoops,[85] A. Knue,[53] A. Kobayashi,[155] D. Kobayashi,[157] T. Kobayashi,[155] M. Kobel,[44] M. Kocian,[143] P. Kodys,[129] T. Koffas,[29] E. Koffeman,[107] L. A. Kogan,[120] S. Kohlmann,[175] Z. Kohout,[128] T. Kohriki,[66] T. Koi,[143] H. Kolanoski,[16] I. Koletsou,[5] A. A. Komar,[96,a] Y. Komori,[155] T. Kondo,[66] N. Kondrashova,[42] K. Köneke,[48] A. C. König,[106] S. König,[83] T. Kono,[66,v] R. Konoplich,[110,w] N. Konstantinidis,[78] R. Kopeliansky,[152] S. Koperny,[38a] L. Köpke,[83] A. K. Kopp,[48] K. Korcyl,[39] K. Kordas,[154] A. Korn,[78] A. A. Korol,[109,d] I. Korolkov,[12] E. V. Korolkova,[139] O. Kortner,[101] S. Kortner,[101] T. Kosek,[129] V. V. Kostyukhin,[21] V. M. Kotov,[65] A. Kotwal,[45] A. Kourkoumeli-Charalampidi,[154]

C. Kourkoumelis,[9] V. Kouskoura,[25] A. Koutsman,[159a] R. Kowalewski,[169] T. Z. Kowalski,[38a] W. Kozanecki,[136] A. S. Kozhin,[130] V. A. Kramarenko,[99] G. Kramberger,[75] D. Krasnopevtsev,[98] M. W. Krasny,[80] A. Krasznahorkay,[30] J. K. Kraus,[21] A. Kravchenko,[25] S. Kreiss,[110] M. Kretz,[58c] J. Kretzschmar,[74] K. Kreutzfeldt,[52] P. Krieger,[158] K. Krizka,[31] K. Kroeninger,[43] H. Kroha,[101] J. Kroll,[122] J. Kroseberg,[21] J. Krstic,[13] U. Kruchonak,[65] H. Krüger,[21] N. Krumnack,[64] Z. V. Krumshteyn,[65] A. Kruse,[173] M. C. Kruse,[45] M. Kruskal,[22] T. Kubota,[88] H. Kucuk,[78] S. Kuday,[4b] S. Kuehn,[48] A. Kugel,[58c] F. Kuger,[174] A. Kuhl,[137] T. Kuhl,[42] V. Kukhtin,[65] Y. Kulchitsky,[92] S. Kuleshov,[32b] M. Kuna,[132a,132b] T. Kunigo,[68] A. Kupco,[127] H. Kurashige,[67] Y. A. Kurochkin,[92] R. Kurumida,[67] V. Kus,[127] E. S. Kuwertz,[169] M. Kuze,[157] J. Kvita,[115] T. Kwan,[169] D. Kyriazopoulos,[139] A. La Rosa,[49] J. L. La Rosa Navarro,[24d] L. La Rotonda,[37a,37b] C. Lacasta,[167] F. Lacava,[132a,132b] J. Lacey,[29] H. Lacker,[16] D. Lacour,[80] V. R. Lacuesta,[167] E. Ladygin,[65] R. Lafaye,[5] B. Laforge,[80] T. Lagouri,[176] S. Lai,[48] L. Lambourne,[78] S. Lammers,[61] C. L. Lampen,[7] W. Lampl,[7] E. Lançon,[136] U. Landgraf,[48] M. P. J. Landon,[76] V. S. Lang,[58a] J. C. Lange,[12] A. J. Lankford,[163] F. Lanni,[25] K. Lantzsch,[30] S. Laplace,[80] C. Lapoire,[30] J. F. Laporte,[136] T. Lari,[91a] F. Lasagni Manghi,[20a,20b] M. Lassnig,[30] P. Laurelli,[47] W. Lavrijsen,[15] A. T. Law,[137] P. Laycock,[74] O. Le Dortz,[80] E. Le Guirriec,[85] E. Le Menedeu,[12] M. LeBlanc,[169] T. LeCompte,[6] F. Ledroit-Guillon,[55] C. A. Lee,[145b] S. C. Lee,[151] L. Lee,[1] G. Lefebvre,[80] M. Lefebvre,[169] F. Legger,[100] C. Leggett,[15] A. Lehan,[74] G. Lehmann Miotto,[30] X. Lei,[7] W. A. Leight,[29] A. Leisos,[154] A. G. Leister,[176] M. A. L. Leite,[24d] R. Leitner,[129] D. Lellouch,[172] B. Lemmer,[54] K. J. C. Leney,[78] T. Lenz,[21] B. Lenzi,[30] R. Leone,[7] S. Leone,[124a,124b] C. Leonidopoulos,[46] S. Leontsinis,[10] C. Leroy,[95] C. G. Lester,[28] M. Levchenko,[123] J. Levêque,[5] D. Levin,[89] L. J. Levinson,[172] M. Levy,[18] A. Lewis,[120] A. M. Leyko,[21] M. Leyton,[41] B. Li,[33b,x] H. Li,[148] H. L. Li,[31] L. Li,[45] L. Li,[33e] S. Li,[45] Y. Li,[33c,y] Z. Liang,[137] H. Liao,[34] B. Liberti,[133a] A. Liblong,[158] P. Lichard,[30] K. Lie,[165] J. Liebal,[21] W. Liebig,[14] C. Limbach,[21] A. Limosani,[150] S. C. Lin,[151,z] T. H. Lin,[83] F. Linde,[107] B. E. Lindquist,[148] J. T. Linnemann,[90] E. Lipeles,[122] A. Lipniacka,[14] M. Lisovyi,[42] T. M. Liss,[165] D. Lissauer,[25] A. Lister,[168] A. M. Litke,[137] B. Liu,[151,aa] D. Liu,[151] J. Liu,[85] J. B. Liu,[33b] K. Liu,[85] L. Liu,[165] M. Liu,[45] M. Liu,[33b] Y. Liu,[33b] M. Livan,[121a,121b] A. Lleres,[55] J. Llorente Merino,[82] S. L. Lloyd,[76] F. Lo Sterzo,[151] E. Lobodzinska,[42] P. Loch,[7] W. S. Lockman,[137] F. K. Loebinger,[84] A. E. Loevschall-Jensen,[36] A. Loginov,[176] T. Lohse,[16] K. Lohwasser,[42] M. Lokajicek,[127] B. A. Long,[22] J. D. Long,[89] R. E. Long,[72] K. A. Looper,[111] L. Lopes,[126a] D. Lopez Mateos,[57] B. Lopez Paredes,[139] I. Lopez Paz,[12] J. Lorenz,[100] N. Lorenzo Martinez,[61] M. Losada,[162] P. Loscutoff,[15] P. J. Lösel,[100] X. Lou,[33a] A. Lounis,[117] J. Love,[6] P. A. Love,[72] N. Lu,[89] H. J. Lubatti,[138] C. Luci,[132a,132b] A. Lucotte,[55] F. Luehring,[61] W. Lukas,[62] L. Luminari,[132a] O. Lundberg,[146a,146b] B. Lund-Jensen,[147] D. Lynn,[25] R. Lysak,[127] E. Lytken,[81] H. Ma,[25] L. L. Ma,[33d] G. Maccarrone,[47] A. Macchiolo,[101] C. M. Macdonald,[139] J. Machado Miguens,[122,126b] D. Macina,[30] D. Madaffari,[85] R. Madar,[34] H. J. Maddocks,[72] W. F. Mader,[44] A. Madsen,[166] S. Maeland,[14] T. Maeno,[25] A. Maevskiy,[99] E. Magradze,[54] K. Mahboubi,[48] J. Mahlstedt,[107] C. Maiani,[136] C. Maidantchik,[24a] A. A. Maier,[101] T. Maier,[100] A. Maio,[126a,126b,126d] S. Majewski,[116] Y. Makida,[66] N. Makovec,[117] B. Malaescu,[80] Pa. Malecki,[39] V. P. Maleev,[123] F. Malek,[55] U. Mallik,[63] D. Malon,[6] C. Malone,[143] S. Maltezos,[10] V. M. Malyshev,[109] S. Malyukov,[30] J. Mamuzic,[42] G. Mancini,[47] B. Mandelli,[30] L. Mandelli,[91a] I. Mandić,[75] R. Mandrysch,[63] J. Maneira,[126a,126b] A. Manfredini,[101] L. Manhaes de Andrade Filho,[24b] J. Manjarres Ramos,[159b] A. Mann,[100] P. M. Manning,[137] A. Manousakis-Katsikakis,[9] B. Mansoulie,[136] R. Mantifel,[87] M. Mantoani,[54] L. Mapelli,[30] L. March,[145c] G. Marchiori,[80] M. Marcisovsky,[127] C. P. Marino,[169] M. Marjanovic,[13] F. Marroquim,[24a] S. P. Marsden,[84] Z. Marshall,[15] L. F. Marti,[17] S. Marti-Garcia,[167] B. Martin,[90] T. A. Martin,[170] V. J. Martin,[46] B. Martin dit Latour,[14] M. Martinez,[12,p] S. Martin-Haugh,[131] V. S. Martoiu,[26a] A. C. Martyniuk,[78] M. Marx,[138] F. Marzano,[132a] A. Marzin,[30] L. Masetti,[83] T. Mashimo,[155] R. Mashinistov,[96] J. Masik,[84] A. L. Maslennikov,[109,d] I. Massa,[20a,20b] L. Massa,[20a,20b] N. Massol,[5] P. Mastrandrea,[148] A. Mastroberardino,[37a,37b] T. Masubuchi,[155] P. Mättig,[175] J. Mattmann,[83] J. Maurer,[26a] S. J. Maxfield,[74] D. A. Maximov,[109,d] R. Mazini,[151] S. M. Mazza,[91a,91b] L. Mazzaferro,[133a,133b] G. Mc Goldrick,[158] S. P. Mc Kee,[89] A. McCarn,[89] R. L. McCarthy,[148] T. G. McCarthy,[29] N. A. McCubbin,[131] K. W. McFarlane,[56,a] J. A. Mcfayden,[78] G. Mchedlidze,[54] S. J. McMahon,[131] R. A. McPherson,[169,l] M. Medinnis,[42] S. Meehan,[145a] S. Mehlhase,[100] A. Mehta,[74] K. Meier,[58a] C. Meineck,[100] B. Meirose,[41] B. R. Mellado Garcia,[145c] F. Meloni,[17] A. Mengarelli,[20a,20b] S. Menke,[101] E. Meoni,[161] K. M. Mercurio,[57] S. Mergelmeyer,[21] P. Mermod,[49] L. Merola,[104a,104b] C. Meroni,[91a] F. S. Merritt,[31] A. Messina,[132a,132b] J. Metcalfe,[25] A. S. Mete,[163] C. Meyer,[83] C. Meyer,[122] J-P. Meyer,[136] J. Meyer,[107] R. P. Middleton,[131] S. Miglioranzi,[164a,164c] L. Mijović,[21] G. Mikenberg,[172] M. Mikestikova,[127] M. Mikuž,[75] M. Milesi,[88] A. Milic,[30] D. W. Miller,[31] C. Mills,[46] A. Milov,[172] D. A. Milstead,[146a,146b] A. A. Minaenko,[130] Y. Minami,[155] I. A. Minashvili,[65] A. I. Mincer,[110] B. Mindur,[38a] M. Mineev,[65] Y. Ming,[173] L. M. Mir,[12] T. Mitani,[171] J. Mitrevski,[100] V. A. Mitsou,[167] A. Miucci,[49] P. S. Miyagawa,[139] J. U. Mjörnmark,[81] T. Moa,[146a,146b]

K. Mochizuki,[85] S. Mohapatra,[35] W. Mohr,[48] S. Molander,[146a,146b] R. Moles-Valls,[167] K. Mönig,[42] C. Monini,[55] J. Monk,[36] E. Monnier,[85] J. Montejo Berlingen,[12] F. Monticelli,[71] S. Monzani,[132a,132b] R. W. Moore,[3] N. Morange,[117] D. Moreno,[162] M. Moreno Llácer,[54] P. Morettini,[50a] M. Morgenstern,[44] M. Morii,[57] M. Morinaga,[155] V. Morisbak,[119] S. Moritz,[83] A. K. Morley,[147] G. Mornacchi,[30] J. D. Morris,[76] S. S. Mortensen,[36] A. Morton,[53] L. Morvaj,[103] H. G. Moser,[101] M. Mosidze,[51b] J. Moss,[111] K. Motohashi,[157] R. Mount,[143] E. Mountricha,[25] S. V. Mouraviev,[96,a] E. J. W. Moyse,[86] S. Muanza,[85] R. D. Mudd,[18] F. Mueller,[101] J. Mueller,[125] K. Mueller,[21] R. S. P. Mueller,[100] T. Mueller,[28] D. Muenstermann,[49] P. Mullen,[53] Y. Munwes,[153] J. A. Murillo Quijada,[18] W. J. Murray,[170,131] H. Musheghyan,[54] E. Musto,[152] A. G. Myagkov,[130,bb] M. Myska,[128] O. Nackenhorst,[54] J. Nadal,[54] K. Nagai,[120] R. Nagai,[157] Y. Nagai,[85] K. Nagano,[66] A. Nagarkar,[111] Y. Nagasaka,[59] K. Nagata,[160] M. Nagel,[101] E. Nagy,[85] A. M. Nairz,[30] Y. Nakahama,[30] K. Nakamura,[66] T. Nakamura,[155] I. Nakano,[112] H. Namasivayam,[41] R. F. Naranjo Garcia,[42] R. Narayan,[31] T. Naumann,[42] G. Navarro,[162] R. Nayyar,[7] H. A. Neal,[89] P. Yu. Nechaeva,[96] T. J. Neep,[84] P. D. Nef,[143] A. Negri,[121a,121b] M. Negrini,[20a] S. Nektarijevic,[106] C. Nellist,[117] A. Nelson,[163] S. Nemecek,[127] P. Nemethy,[110] A. A. Nepomuceno,[24a] M. Nessi,[30,cc] M. S. Neubauer,[165] M. Neumann,[175] R. M. Neves,[110] P. Nevski,[25] P. R. Newman,[18] D. H. Nguyen,[6] R. B. Nickerson,[120] R. Nicolaidou,[136] B. Nicquevert,[30] J. Nielsen,[137] N. Nikiforou,[35] A. Nikiforov,[16] V. Nikolaenko,[130,bb] I. Nikolic-Audit,[80] K. Nikolopoulos,[18] J. K. Nilsen,[119] P. Nilsson,[25] Y. Ninomiya,[155] A. Nisati,[132a] R. Nisius,[101] T. Nobe,[157] M. Nomachi,[118] I. Nomidis,[29] T. Nooney,[76] S. Norberg,[113] M. Nordberg,[30] O. Novgorodova,[44] S. Nowak,[101] M. Nozaki,[66] L. Nozka,[115] K. Ntekas,[10] G. Nunes Hanninger,[88] T. Nunnemann,[100] E. Nurse,[78] F. Nuti,[88] B. J. O'Brien,[46] F. O'grady,[7] D. C. O'Neil,[142] V. O'Shea,[53] F. G. Oakham,[29,e] H. Oberlack,[101] T. Obermann,[21] J. Ocariz,[80] A. Ochi,[67] I. Ochoa,[78] S. Oda,[70] S. Odaka,[66] H. Ogren,[61] A. Oh,[84] S. H. Oh,[45] C. C. Ohm,[15] H. Ohman,[166] H. Oide,[30] W. Okamura,[118] H. Okawa,[160] Y. Okumura,[31] T. Okuyama,[155] A. Olariu,[26a] S. A. Olivares Pino,[46] D. Oliveira Damazio,[25] E. Oliver Garcia,[167] A. Olszewski,[39] J. Olszowska,[39] A. Onofre,[126a,126e] P. U. E. Onyisi,[31,r] C. J. Oram,[159a] M. J. Oreglia,[31] Y. Oren,[153] D. Orestano,[134a,134b] N. Orlando,[154] C. Oropeza Barrera,[53] R. S. Orr,[158] B. Osculati,[50a,50b] R. Ospanov,[84] G. Otero y Garzon,[27] H. Otono,[70] M. Ouchrif,[135d] E. A. Ouellette,[169] F. Ould-Saada,[119] A. Ouraou,[136] K. P. Oussoren,[107] Q. Ouyang,[33a] A. Ovcharova,[15] M. Owen,[53] R. E. Owen,[18] V. E. Ozcan,[19a] N. Ozturk,[8] K. Pachal,[142] A. Pacheco Pages,[12] C. Padilla Aranda,[12] M. Pagáčová,[48] S. Pagan Griso,[15] E. Paganis,[139] C. Pahl,[101] F. Paige,[25] P. Pais,[86] K. Pajchel,[119] G. Palacino,[159b] S. Palestini,[30] M. Palka,[38b] D. Pallin,[34] A. Palma,[126a,126b] Y. B. Pan,[173] E. Panagiotopoulou,[10] C. E. Pandini,[80] J. G. Panduro Vazquez,[77] P. Pani,[146a,146b] S. Panitkin,[25] L. Paolozzi,[49] Th. D. Papadopoulou,[10] K. Papageorgiou,[154] A. Paramonov,[6] D. Paredes Hernandez,[154] M. A. Parker,[28] K. A. Parker,[139] F. Parodi,[50a,50b] J. A. Parsons,[35] U. Parzefall,[48] E. Pasqualucci,[132a] S. Passaggio,[50a] F. Pastore,[134a,134b,a] Fr. Pastore,[77] G. Pásztor,[29] S. Pataraia,[175] N. D. Patel,[150] J. R. Pater,[84] T. Pauly,[30] J. Pearce,[169] B. Pearson,[113] L. E. Pedersen,[36] M. Pedersen,[119] S. Pedraza Lopez,[167] R. Pedro,[126a,126b] S. V. Peleganchuk,[109] D. Pelikan,[166] H. Peng,[33b] B. Penning,[31] J. Penwell,[61] D. V. Perepelitsa,[25] E. Perez Codina,[159a] M. T. Pérez García-Estañ,[167] L. Perini,[91a,91b] H. Pernegger,[30] S. Perrella,[104a,104b] R. Peschke,[42] V. D. Peshekhonov,[65] K. Peters,[30] R. F. Y. Peters,[84] B. A. Petersen,[30] T. C. Petersen,[36] E. Petit,[42] A. Petridis,[146a,146b] C. Petridou,[154] E. Petrolo,[132a] F. Petrucci,[134a,134b] N. E. Pettersson,[157] R. Pezoa,[32b] P. W. Phillips,[131] G. Piacquadio,[143] E. Pianori,[170] A. Picazio,[49] E. Piccaro,[76] M. Piccinini,[20a,20b] M. A. Pickering,[120] R. Piegaia,[27] D. T. Pignotti,[111] J. E. Pilcher,[31] A. D. Pilkington,[84] J. Pina,[126a,126b,126d] M. Pinamonti,[164a,164c,dd] J. L. Pinfold,[3] A. Pingel,[36] B. Pinto,[126a] S. Pires,[80] M. Pitt,[172] C. Pizio,[91a,91b] L. Plazak,[144a] M.-A. Pleier,[25] V. Pleskot,[129] E. Plotnikova,[65] P. Plucinski,[146a,146b] D. Pluth,[64] R. Poettgen,[83] L. Poggioli,[117] D. Pohl,[21] G. Polesello,[121a] A. Policicchio,[37a,37b] R. Polifka,[158] A. Polini,[20a] C. S. Pollard,[53] V. Polychronakos,[25] K. Pommès,[30] L. Pontecorvo,[132a] B. G. Pope,[90] G. A. Popeneciu,[26b] D. S. Popovic,[13] A. Poppleton,[30] S. Pospisil,[128] K. Potamianos,[15] I. N. Potrap,[65] C. J. Potter,[149] C. T. Potter,[116] G. Poulard,[30] J. Poveda,[30] V. Pozdnyakov,[65] P. Pralavorio,[85] A. Pranko,[15] S. Prasad,[30] S. Prell,[64] D. Price,[84] L. E. Price,[6] M. Primavera,[73a] S. Prince,[87] M. Proissl,[46] K. Prokofiev,[60c] F. Prokoshin,[32b] E. Protopapadaki,[136] S. Protopopescu,[25] J. Proudfoot,[6] M. Przybycien,[38a] E. Ptacek,[116] D. Puddu,[134a,134b] E. Pueschel,[86] D. Puldon,[148] M. Purohit,[25,ee] P. Puzo,[117] J. Qian,[89] G. Qin,[53] Y. Qin,[84] A. Quadt,[54] D. R. Quarrie,[15] W. B. Quayle,[164a,164b] M. Queitsch-Maitland,[84] D. Quilty,[53] S. Raddum,[119] V. Radeka,[25] V. Radescu,[42] S. K. Radhakrishnan,[148] P. Radloff,[116] P. Rados,[88] F. Ragusa,[91a,91b] G. Rahal,[178] S. Rajagopalan,[25] M. Rammensee,[30] C. Rangel-Smith,[166] F. Rauscher,[100] S. Rave,[83] T. Ravenscroft,[53] M. Raymond,[30] A. L. Read,[119] N. P. Readioff,[74] D. M. Rebuzzi,[121a,121b] A. Redelbach,[174] G. Redlinger,[25] R. Reece,[137] K. Reeves,[41] L. Rehnisch,[16] H. Reisin,[27] M. Relich,[163] C. Rembser,[30] H. Ren,[33a] A. Renaud,[117] M. Rescigno,[132a] S. Resconi,[91a] O. L. Rezanova,[109,d] P. Reznicek,[129] R. Rezvani,[95] R. Richter,[101] S. Richter,[78] E. Richter-Was,[38b] O. Ricken,[21] M. Ridel,[80] P. Rieck,[16] C. J. Riegel,[175] J. Rieger,[54] M. Rijssenbeek,[148] A. Rimoldi,[121a,121b] L. Rinaldi,[20a] B. Ristić,[49]

E. Ritsch,[62] I. Riu,[12] F. Rizatdinova,[114] E. Rizvi,[76] S. H. Robertson,[87,l] A. Robichaud-Veronneau,[87] D. Robinson,[28] J. E. M. Robinson,[84] A. Robson,[53] C. Roda,[124a,124b] S. Roe,[30] O. Røhne,[119] S. Rolli,[161] A. Romaniouk,[98] M. Romano,[20a,20b] S. M. Romano Saez,[34] E. Romero Adam,[167] N. Rompotis,[138] M. Ronzani,[48] L. Roos,[80] E. Ros,[167] S. Rosati,[132a] K. Rosbach,[48] P. Rose,[137] P. L. Rosendahl,[14] O. Rosenthal,[141] V. Rossetti,[146a,146b] E. Rossi,[104a,104b] L. P. Rossi,[50a] R. Rosten,[138] M. Rotaru,[26a] I. Roth,[172] J. Rothberg,[138] D. Rousseau,[117] C. R. Royon,[136] A. Rozanov,[85] Y. Rozen,[152] X. Ruan,[145c] F. Rubbo,[143] I. Rubinskiy,[42] V. I. Rud,[99] C. Rudolph,[44] M. S. Rudolph,[158] F. Rühr,[48] A. Ruiz-Martinez,[30] Z. Rurikova,[48] N. A. Rusakovich,[65] A. Ruschke,[100] H. L. Russell,[138] J. P. Rutherfoord,[7] N. Ruthmann,[48] Y. F. Ryabov,[123] M. Rybar,[129] G. Rybkin,[117] N. C. Ryder,[120] A. F. Saavedra,[150] G. Sabato,[107] S. Sacerdoti,[27] A. Saddique,[3] H. F-W. Sadrozinski,[137] R. Sadykov,[65] F. Safai Tehrani,[132a] M. Saimpert,[136] H. Sakamoto,[155] Y. Sakurai,[171] G. Salamanna,[134a,134b] A. Salamon,[133a] M. Saleem,[113] D. Salek,[107] P. H. Sales De Bruin,[138] D. Salihagic,[101] A. Salnikov,[143] J. Salt,[167] D. Salvatore,[37a,37b] F. Salvatore,[149] A. Salvucci,[106] A. Salzburger,[30] D. Sampsonidis,[154] A. Sanchez,[104a,104b] J. Sánchez,[167] V. Sanchez Martinez,[167] H. Sandaker,[14] R. L. Sandbach,[76] H. G. Sander,[83] M. P. Sanders,[100] M. Sandhoff,[175] C. Sandoval,[162] R. Sandstroem,[101] D. P. C. Sankey,[131] M. Sannino,[50a,50b] A. Sansoni,[47] C. Santoni,[34] R. Santonico,[133a,133b] H. Santos,[126a] I. Santoyo Castillo,[149] K. Sapp,[125] A. Sapronov,[65] J. G. Saraiva,[126a,126d] B. Sarrazin,[21] O. Sasaki,[66] Y. Sasaki,[155] K. Sato,[160] G. Sauvage,[5,a] E. Sauvan,[5] G. Savage,[77] P. Savard,[158,e] C. Sawyer,[120] L. Sawyer,[79,o] J. Saxon,[31] C. Sbarra,[20a] A. Sbrizzi,[20a,20b] T. Scanlon,[78] D. A. Scannicchio,[163] M. Scarcella,[150] V. Scarfone,[37a,37b] J. Schaarschmidt,[172] P. Schacht,[101] D. Schaefer,[30] R. Schaefer,[42] J. Schaeffer,[83] S. Schaepe,[21] S. Schaetzel,[58b] U. Schäfer,[83] A. C. Schaffer,[117] D. Schaile,[100] R. D. Schamberger,[148] V. Scharf,[58a] V. A. Schegelsky,[123] D. Scheirich,[129] M. Schernau,[163] C. Schiavi,[50a,50b] C. Schillo,[48] M. Schioppa,[37a,37b] S. Schlenker,[30] E. Schmidt,[48] K. Schmieden,[30] C. Schmitt,[83] S. Schmitt,[58b] S. Schmitt,[42] B. Schneider,[159a] Y. J. Schnellbach,[74] U. Schnoor,[44] L. Schoeffel,[136] A. Schoening,[58b] B. D. Schoenrock,[90] E. Schopf,[21] A. L. S. Schorlemmer,[54] M. Schott,[83] D. Schouten,[159a] J. Schovancova,[8] S. Schramm,[158] M. Schreyer,[174] C. Schroeder,[83] N. Schuh,[83] M. J. Schultens,[21] H.-C. Schultz-Coulon,[58a] H. Schulz,[16] M. Schumacher,[48] B. A. Schumm,[137] Ph. Schune,[136] C. Schwanenberger,[84] A. Schwartzman,[143] T. A. Schwarz,[89] Ph. Schwegler,[101] Ph. Schwemling,[136] R. Schwienhorst,[90] J. Schwindling,[136] T. Schwindt,[21] M. Schwoerer,[5] F. G. Sciacca,[17] E. Scifo,[117] G. Sciolla,[23] F. Scuri,[124a,124b] F. Scutti,[21] J. Searcy,[89] G. Sedov,[42] E. Sedykh,[123] P. Seema,[21] S. C. Seidel,[105] A. Seiden,[137] F. Seifert,[128] J. M. Seixas,[24a] G. Sekhniaidze,[104a] K. Sekhon,[89] S. J. Sekula,[40] K. E. Selbach,[46] D. M. Seliverstov,[123,a] N. Semprini-Cesari,[20a,20b] C. Serfon,[30] L. Serin,[117] L. Serkin,[164a,164b] T. Serre,[85] M. Sessa,[134a,134b] R. Seuster,[159a] H. Severini,[113] T. Sfiligoj,[75] F. Sforza,[101] A. Sfyrla,[30] E. Shabalina,[54] M. Shamim,[116] L. Y. Shan,[33a] R. Shang,[165] J. T. Shank,[22] M. Shapiro,[15] P. B. Shatalov,[97] K. Shaw,[164a,164b] S. M. Shaw,[84] A. Shcherbakova,[146a,146b] C. Y. Shehu,[149] P. Sherwood,[78] L. Shi,[151,ff] S. Shimizu,[67] C. O. Shimmin,[163] M. Shimojima,[102] M. Shiyakova,[65] A. Shmeleva,[96] D. Shoaleh Saadi,[95] M. J. Shochet,[31] S. Shojaii,[91a,91b] S. Shrestha,[111] E. Shulga,[98] M. A. Shupe,[7] S. Shushkevich,[42] P. Sicho,[127] O. Sidiropoulou,[174] D. Sidorov,[114] A. Sidoti,[20a,20b] F. Siegert,[44] Dj. Sijacki,[13] J. Silva,[126a,126d] Y. Silver,[153] S. B. Silverstein,[146a] V. Simak,[128] O. Simard,[5] Lj. Simic,[13] S. Simion,[117] E. Simioni,[83] B. Simmons,[78] D. Simon,[34] R. Simoniello,[91a,91b] P. Sinervo,[158] N. B. Sinev,[116] G. Siragusa,[174] A. N. Sisakyan,[65,a] S. Yu. Sivoklokov,[99] J. Sjölin,[146a,146b] T. B. Sjursen,[14] M. B. Skinner,[72] H. P. Skottowe,[57] P. Skubic,[113] M. Slater,[18] T. Slavicek,[128] M. Slawinska,[107] K. Sliwa,[161] V. Smakhtin,[172] B. H. Smart,[46] L. Smestad,[14] S. Yu. Smirnov,[98] Y. Smirnov,[98] L. N. Smirnova,[99,gg] O. Smirnova,[81] M. N. K. Smith,[35] M. Smizanska,[72] K. Smolek,[128] A. A. Snesarev,[96] G. Snidero,[76] S. Snyder,[25] R. Sobie,[169,l] F. Socher,[44] A. Soffer,[153] D. A. Soh,[151,ff] C. A. Solans,[30] M. Solar,[128] J. Solc,[128] E. Yu. Soldatov,[98] U. Soldevila,[167] A. A. Solodkov,[130] A. Soloshenko,[65] O. V. Solovyanov,[130] V. Solovyev,[123] P. Sommer,[48] H. Y. Song,[33b] N. Soni,[1] A. Sood,[15] A. Sopczak,[128] B. Sopko,[128] V. Sopko,[128] V. Sorin,[12] D. Sosa,[58b] M. Sosebee,[8] C. L. Sotiropoulou,[124a,124b] R. Soualah,[164a,164c] P. Soueid,[95] A. M. Soukharev,[109,d] D. South,[42] S. Spagnolo,[73a,73b] M. Spalla,[124a,124b] F. Spanò,[77] W. R. Spearman,[57] F. Spettel,[101] R. Spighi,[20a] G. Spigo,[30] L. A. Spiller,[88] M. Spousta,[129] T. Spreitzer,[158] R. D. St. Denis,[53,a] S. Staerz,[44] J. Stahlman,[122] R. Stamen,[58a] S. Stamm,[16] E. Stanecka,[39] C. Stanescu,[134a] M. Stanescu-Bellu,[42] M. M. Stanitzki,[42] S. Stapnes,[119] E. A. Starchenko,[130] J. Stark,[55] P. Staroba,[127] P. Starovoitov,[42] R. Staszewski,[39] P. Stavina,[144a,a] P. Steinberg,[25] B. Stelzer,[142] H. J. Stelzer,[30] O. Stelzer-Chilton,[159a] H. Stenzel,[52] S. Stern,[101] G. A. Stewart,[53] J. A. Stillings,[21] M. C. Stockton,[87] M. Stoebe,[87] G. Stoicea,[26a] P. Stolte,[54] S. Stonjek,[101] A. R. Stradling,[8] A. Straessner,[44] M. E. Stramaglia,[17] J. Strandberg,[147] S. Strandberg,[146a,146b] A. Strandlie,[119] E. Strauss,[143] M. Strauss,[113] P. Strizenec,[144b] R. Ströhmer,[174] D. M. Strom,[116] R. Stroynowski,[40] A. Strubig,[106] S. A. Stucci,[17] B. Stugu,[14] N. A. Styles,[42] D. Su,[143] J. Su,[125] R. Subramaniam,[79] A. Succurro,[12] Y. Sugaya,[118] C. Suhr,[108] M. Suk,[128] V. V. Sulin,[96] S. Sultansoy,[4c] T. Sumida,[68] S. Sun,[57] X. Sun,[33a] J. E. Sundermann,[48] K. Suruliz,[149] G. Susinno,[37a,37b]

M. R. Sutton,[149] S. Suzuki,[66] Y. Suzuki,[66] M. Svatos,[127] S. Swedish,[168] M. Swiatlowski,[143] I. Sykora,[144a] T. Sykora,[129] D. Ta,[90] C. Taccini,[134a,134b] K. Tackmann,[42] J. Taenzer,[158] A. Taffard,[163] R. Tafirout,[159a] N. Taiblum,[153] H. Takai,[25] R. Takashima,[69] H. Takeda,[67] T. Takeshita,[140] Y. Takubo,[66] M. Talby,[85] A. A. Talyshev,[109,d] J. Y. C. Tam,[174] K. G. Tan,[88] J. Tanaka,[155] R. Tanaka,[117] S. Tanaka,[66] B. B. Tannenwald,[111] N. Tannoury,[21] S. Tapprogge,[83] S. Tarem,[152] F. Tarrade,[29] G. F. Tartarelli,[91a] P. Tas,[129] M. Tasevsky,[127] T. Tashiro,[68] E. Tassi,[37a,37b] A. Tavares Delgado,[126a,126b] Y. Tayalati,[135d] F. E. Taylor,[94] G. N. Taylor,[88] W. Taylor,[159b] F. A. Teischinger,[30] M. Teixeira Dias Castanheira,[76] P. Teixeira-Dias,[77] K. K. Temming,[48] H. Ten Kate,[30] P. K. Teng,[151] J. J. Teoh,[118] F. Tepel,[175] S. Terada,[66] K. Terashi,[155] J. Terron,[82] S. Terzo,[101] M. Testa,[47] R. J. Teuscher,[158,l] J. Therhaag,[21] T. Theveneaux-Pelzer,[34] J. P. Thomas,[18] J. Thomas-Wilsker,[77] E. N. Thompson,[35] P. D. Thompson,[18] R. J. Thompson,[84] A. S. Thompson,[53] L. A. Thomsen,[36] E. Thomson,[122] M. Thomson,[28] R. P. Thun,[89,a] M. J. Tibbetts,[15] R. E. Ticse Torres,[85] V. O. Tikhomirov,[96,hh] Yu. A. Tikhonov,[109,d] S. Timoshenko,[98] E. Tiouchichine,[85] P. Tipton,[176] S. Tisserant,[85] T. Todorov,[5,a] S. Todorova-Nova,[129] J. Tojo,[70] S. Tokár,[144a] K. Tokushuku,[66] K. Tollefson,[90] E. Tolley,[57] L. Tomlinson,[84] M. Tomoto,[103] L. Tompkins,[143,ii] K. Toms,[105] E. Torrence,[116] H. Torres,[142] E. Torró Pastor,[167] J. Toth,[85,jj] F. Touchard,[85] D. R. Tovey,[139] T. Trefzger,[174] L. Tremblet,[30] A. Tricoli,[30] I. M. Trigger,[159a] S. Trincaz-Duvoid,[80] M. F. Tripiana,[12] W. Trischuk,[158] B. Trocmé,[55] C. Troncon,[91a] M. Trottier-McDonald,[15] M. Trovatelli,[134a,134b] P. True,[90] L. Truong,[164a,164c] M. Trzebinski,[39] A. Trzupek,[39] C. Tsarouchas,[30] J. C-L. Tseng,[120] P. V. Tsiareshka,[92] D. Tsionou,[154] G. Tsipolitis,[10] N. Tsirintanis,[9] S. Tsiskaridze,[12] V. Tsiskaridze,[48] E. G. Tskhadadze,[51a] I. I. Tsukerman,[97] V. Tsulaia,[15] S. Tsuno,[66] D. Tsybychev,[148] A. Tudorache,[26a] V. Tudorache,[26a] A. N. Tuna,[122] S. A. Tupputi,[20a,20b] S. Turchikhin,[99,gg] D. Turecek,[128] R. Turra,[91a,91b] A. J. Turvey,[40] P. M. Tuts,[35] A. Tykhonov,[49] M. Tylmad,[146a,146b] M. Tyndel,[131] I. Ueda,[155] R. Ueno,[29] M. Ughetto,[146a,146b] M. Ugland,[14] M. Uhlenbrock,[21] F. Ukegawa,[160] G. Unal,[30] A. Undrus,[25] G. Unel,[163] F. C. Ungaro,[48] Y. Unno,[66] C. Unverdorben,[100] J. Urban,[144b] P. Urquijo,[88] P. Urrejola,[83] G. Usai,[8] A. Usanova,[62] L. Vacavant,[85] V. Vacek,[128] B. Vachon,[87] C. Valderanis,[83] N. Valencic,[107] S. Valentinetti,[20a,20b] A. Valero,[167] L. Valery,[12] S. Valkar,[129] E. Valladolid Gallego,[167] S. Vallecorsa,[49] J. A. Valls Ferrer,[167] W. Van Den Wollenberg,[107] P. C. Van Der Deijl,[107] R. van der Geer,[107] H. van der Graaf,[107] R. Van Der Leeuw,[107] N. van Eldik,[152] P. van Gemmeren,[6] J. Van Nieuwkoop,[142] I. van Vulpen,[107] M. C. van Woerden,[30] M. Vanadia,[132a,132b] W. Vandelli,[30] R. Vanguri,[122] A. Vaniachine,[6] F. Vannucci,[80] G. Vardanyan,[177] R. Vari,[132a] E. W. Varnes,[7] T. Varol,[40] D. Varouchas,[80] A. Vartapetian,[8] K. E. Varvell,[150] F. Vazeille,[34] T. Vazquez Schroeder,[87] J. Veatch,[7] F. Veloso,[126a,126c] T. Velz,[21] S. Veneziano,[132a] A. Ventura,[73a,73b] D. Ventura,[86] M. Venturi,[169] N. Venturi,[158] A. Venturini,[23] V. Vercesi,[121a] M. Verducci,[132a,132b] W. Verkerke,[107] J. C. Vermeulen,[107] A. Vest,[44] M. C. Vetterli,[142,e] O. Viazlo,[81] I. Vichou,[165] T. Vickey,[139] O. E. Vickey Boeriu,[139] G. H. A. Viehhauser,[120] S. Viel,[15] R. Vigne,[30] M. Villa,[20a,20b] M. Villaplana Perez,[91a,91b] E. Vilucchi,[47] M. G. Vincter,[29] V. B. Vinogradov,[65] I. Vivarelli,[149] F. Vives Vaque,[3] S. Vlachos,[10] D. Vladoiu,[100] M. Vlasak,[128] M. Vogel,[32a] P. Vokac,[128] G. Volpi,[124a,124b] M. Volpi,[88] H. von der Schmitt,[101] H. von Radziewski,[48] E. von Toerne,[21] V. Vorobel,[129] K. Vorobev,[98] M. Vos,[167] R. Voss,[30] J. H. Vossebeld,[74] N. Vranjes,[13] M. Vranjes Milosavljevic,[13] V. Vrba,[127] M. Vreeswijk,[107] R. Vuillermet,[30] I. Vukotic,[31] Z. Vykydal,[128] P. Wagner,[21] W. Wagner,[175] H. Wahlberg,[71] S. Wahrmund,[44] J. Wakabayashi,[103] J. Walder,[72] R. Walker,[100] W. Walkowiak,[141] C. Wang,[33c] F. Wang,[173] H. Wang,[15] H. Wang,[40] J. Wang,[42] J. Wang,[33a] K. Wang,[87] R. Wang,[6] S. M. Wang,[151] T. Wang,[21] X. Wang,[176] C. Wanotayaroj,[116] A. Warburton,[87] C. P. Ward,[28] D. R. Wardrope,[78] M. Warsinsky,[48] A. Washbrook,[46] C. Wasicki,[42] P. M. Watkins,[18] A. T. Watson,[18] I. J. Watson,[150] M. F. Watson,[18] G. Watts,[138] S. Watts,[84] B. M. Waugh,[78] S. Webb,[84] M. S. Weber,[17] S. W. Weber,[174] J. S. Webster,[31] A. R. Weidberg,[120] B. Weinert,[61] J. Weingarten,[54] C. Weiser,[48] H. Weits,[107] P. S. Wells,[30] T. Wenaus,[25] T. Wengler,[30] S. Wenig,[30] N. Wermes,[21] M. Werner,[48] P. Werner,[30] M. Wessels,[58a] J. Wetter,[161] K. Whalen,[29] A. M. Wharton,[72] A. White,[8] M. J. White,[1] R. White,[32b] S. White,[124a,124b] D. Whiteson,[163] F. J. Wickens,[131] W. Wiedenmann,[173] M. Wielers,[131] P. Wienemann,[21] C. Wiglesworth,[36] L. A. M. Wiik-Fuchs,[21] A. Wildauer,[101] H. G. Wilkens,[30] H. H. Williams,[122] S. Williams,[107] C. Willis,[90] S. Willocq,[86] A. Wilson,[89] J. A. Wilson,[18] I. Wingerter-Seez,[5] F. Winklmeier,[116] B. T. Winter,[21] M. Wittgen,[143] J. Wittkowski,[100] S. J. Wollstadt,[83] M. W. Wolter,[39] H. Wolters,[126a,126c] B. K. Wosiek,[39] J. Wotschack,[30] M. J. Woudstra,[84] K. W. Wozniak,[39] M. Wu,[55] M. Wu,[31] S. L. Wu,[173] X. Wu,[49] Y. Wu,[89] T. R. Wyatt,[84] B. M. Wynne,[46] S. Xella,[36] D. Xu,[33a] L. Xu,[33b,kk] B. Yabsley,[150] S. Yacoob,[145b,ll] R. Yakabe,[67] M. Yamada,[66] Y. Yamaguchi,[118] A. Yamamoto,[66] S. Yamamoto,[155] T. Yamanaka,[155] K. Yamauchi,[103] Y. Yamazaki,[67] Z. Yan,[22] H. Yang,[33e] H. Yang,[173] Y. Yang,[151] L. Yao,[33a] W-M. Yao,[15] Y. Yasu,[66] E. Yatsenko,[5] K. H. Yau Wong,[21] J. Ye,[40] S. Ye,[25] I. Yeletskikh,[65] A. L. Yen,[57] E. Yildirim,[42] K. Yorita,[171] R. Yoshida,[6] K. Yoshihara,[122] C. Young,[143] C. J. S. Young,[30] S. Youssef,[22] D. R. Yu,[15] J. Yu,[8] J. M. Yu,[89] J. Yu,[114] L. Yuan,[67] A. Yurkewicz,[108]

I. Yusuff,[28,mm] B. Zabinski,[39] R. Zaidan,[63] A. M. Zaitsev,[130,bb] J. Zalieckas,[14] A. Zaman,[148] S. Zambito,[57] L. Zanello,[132a,132b] D. Zanzi,[88] C. Zeitnitz,[175] M. Zeman,[128] A. Zemla,[38a] K. Zengel,[23] O. Zenin,[130] T. Ženiš,[144a] D. Zerwas,[117] D. Zhang,[89] F. Zhang,[173] J. Zhang,[6] L. Zhang,[48] R. Zhang,[33b] X. Zhang,[33d] Z. Zhang,[117] X. Zhao,[40] Y. Zhao,[33d,117] Z. Zhao,[33b] A. Zhemchugov,[65] J. Zhong,[120] B. Zhou,[89] C. Zhou,[45] L. Zhou,[35] L. Zhou,[40] N. Zhou,[163] C. G. Zhu,[33d] H. Zhu,[33a] J. Zhu,[89] Y. Zhu,[33b] X. Zhuang,[33a] K. Zhukov,[96] A. Zibell,[174] D. Zieminska,[61] N. I. Zimine,[65] C. Zimmermann,[83] S. Zimmermann,[48] Z. Zinonos,[54] M. Zinser,[83] M. Ziolkowski,[141] L. Živković,[13] G. Zobernig,[173] A. Zoccoli,[20a,20b] M. zur Nedden,[16] G. Zurzolo,[104a,104b] and L. Zwalinski[30]

(ATLAS Collaboration)

[1]*Department of Physics, University of Adelaide, Adelaide, Australia*
[2]*Physics Department, SUNY Albany, Albany, New York, USA*
[3]*Department of Physics, University of Alberta, Edmonton, Alberta, Canada*
[4a]*Department of Physics, Ankara University, Ankara, Turkey*
[4b]*Istanbul Aydin University, Istanbul, Turkey*
[4c]*Division of Physics, TOBB University of Economics and Technology, Ankara, Turkey*
[5]*LAPP, CNRS/IN2P3 and Université Savoie Mont Blanc, Annecy-le-Vieux, France*
[6]*High Energy Physics Division, Argonne National Laboratory, Argonne, Illinois, USA*
[7]*Department of Physics, University of Arizona, Tucson, Arizona, USA*
[8]*Department of Physics, The University of Texas at Arlington, Arlington, Texas, USA*
[9]*Physics Department, University of Athens, Athens, Greece*
[10]*Physics Department, National Technical University of Athens, Zografou, Greece*
[11]*Institute of Physics, Azerbaijan Academy of Sciences, Baku, Azerbaijan*
[12]*Institut de Física d'Altes Energies and Departament de Física de la Universitat Autònoma de Barcelona, Barcelona, Spain*
[13]*Institute of Physics, University of Belgrade, Belgrade, Serbia*
[14]*Department for Physics and Technology, University of Bergen, Bergen, Norway*
[15]*Physics Division, Lawrence Berkeley National Laboratory and University of California, Berkeley, California, USA*
[16]*Department of Physics, Humboldt University, Berlin, Germany*
[17]*Albert Einstein Center for Fundamental Physics and Laboratory for High Energy Physics, University of Bern, Bern, Switzerland*
[18]*School of Physics and Astronomy, University of Birmingham, Birmingham, United Kingdom*
[19a]*Department of Physics, Bogazici University, Istanbul, Turkey*
[19b]*Department of Physics, Dogus University, Istanbul, Turkey*
[19c]*Department of Physics Engineering, Gaziantep University, Gaziantep, Turkey*
[20a]*INFN Sezione di Bologna, Bologna, Italy*
[20b]*Dipartimento di Fisica e Astronomia, Università di Bologna, Bologna, Italy*
[21]*Physikalisches Institut, University of Bonn, Bonn, Germany*
[22]*Department of Physics, Boston University, Boston, Massachusetts, USA*
[23]*Department of Physics, Brandeis University, Waltham, Massachusetts, USA*
[24a]*Universidade Federal do Rio De Janeiro COPPE/EE/IF, Rio de Janeiro, Brazil*
[24b]*Electrical Circuits Department, Federal University of Juiz de Fora (UFJF), Juiz de Fora, Brazil*
[24c]*Federal University of Sao Joao del Rei (UFSJ), Sao Joao del Rei, Brazil*
[24d]*Instituto de Fisica, Universidade de Sao Paulo, Sao Paulo, Brazil*
[25]*Physics Department, Brookhaven National Laboratory, Upton, New York, USA*
[26a]*National Institute of Physics and Nuclear Engineering, Bucharest, Romania*
[26b]*National Institute for Research and Development of Isotopic and Molecular Technologies, Physics Department, Cluj Napoca, Romania*
[26c]*University Politehnica Bucharest, Bucharest, Romania*
[26d]*West University in Timisoara, Timisoara, Romania*
[27]*Departamento de Física, Universidad de Buenos Aires, Buenos Aires, Argentina*
[28]*Cavendish Laboratory, University of Cambridge, Cambridge, United Kingdom*
[29]*Department of Physics, Carleton University, Ottawa, Ontario, Canada*
[30]*CERN, Geneva, Switzerland*
[31]*Enrico Fermi Institute, University of Chicago, Chicago Illinois, USA*
[32a]*Departamento de Física, Pontificia Universidad Católica de Chile, Santiago, Chile*
[32b]*Departamento de Física, Universidad Técnica Federico Santa María, Valparaíso, Chile*

[33a]Institute of High Energy Physics, Chinese Academy of Sciences, Beijing, China
[33b]Department of Modern Physics, University of Science and Technology of China, Anhui, China
[33c]Department of Physics, Nanjing University, Jiangsu, China
[33d]School of Physics, Shandong University, Shandong, China
[33e]Department of Physics and Astronomy, Shanghai Key Laboratory for Particle Physics and Cosmology, Shanghai Jiao Tong University, Shanghai, China
[33f]Physics Department, Tsinghua University, Beijing 100084, China
[34]Laboratoire de Physique Corpusculaire, Clermont Université and Université Blaise Pascal and CNRS/IN2P3, Clermont-Ferrand, France
[35]Nevis Laboratory, Columbia University, Irvington, New York, USA
[36]Niels Bohr Institute, University of Copenhagen, Kobenhavn, Denmark
[37a]INFN Gruppo Collegato di Cosenza, Laboratori Nazionali di Frascati, Italy
[37b]Dipartimento di Fisica, Università della Calabria, Rende, Italy
[38a]AGH University of Science and Technology, Faculty of Physics and Applied Computer Science, Krakow, Poland
[38b]Marian Smoluchowski Institute of Physics, Jagiellonian University, Krakow, Poland
[39]Institute of Nuclear Physics Polish Academy of Sciences, Krakow, Poland
[40]Physics Department, Southern Methodist University, Dallas, Texas, USA
[41]Physics Department, University of Texas at Dallas, Richardson, Texas, USA
[42]DESY, Hamburg and Zeuthen, Germany
[43]Institut für Experimentelle Physik IV, Technische Universität Dortmund, Dortmund, Germany
[44]Institut für Kern- und Teilchenphysik, Technische Universität Dresden, Dresden, Germany
[45]Department of Physics, Duke University, Durham, North Carolina, USA
[46]SUPA - School of Physics and Astronomy, University of Edinburgh, Edinburgh, United Kingdom
[47]INFN Laboratori Nazionali di Frascati, Frascati, Italy
[48]Fakultät für Mathematik und Physik, Albert-Ludwigs-Universität, Freiburg, Germany
[49]Section de Physique, Université de Genève, Geneva, Switzerland
[50a]INFN Sezione di Genova, Genova, Italy
[50b]Dipartimento di Fisica, Università di Genova, Genova, Italy
[51a]E. Andronikashvili Institute of Physics, Iv. Javakhishvili Tbilisi State University, Tbilisi, Georgia
[51b]High Energy Physics Institute, Tbilisi State University, Tbilisi, Georgia
[52]II Physikalisches Institut, Justus-Liebig-Universität Giessen, Giessen, Germany
[53]SUPA - School of Physics and Astronomy, University of Glasgow, Glasgow, United Kingdom
[54]II Physikalisches Institut, Georg-August-Universität, Göttingen, Germany
[55]Laboratoire de Physique Subatomique et de Cosmologie, Université Grenoble-Alpes, CNRS/IN2P3, Grenoble, France
[56]Department of Physics, Hampton University, Hampton, Virginia, USA
[57]Laboratory for Particle Physics and Cosmology, Harvard University, Cambridge, Massachusetts, USA
[58a]Kirchhoff-Institut für Physik, Ruprecht-Karls-Universität Heidelberg, Heidelberg, Germany
[58b]Physikalisches Institut, Ruprecht-Karls-Universität Heidelberg, Heidelberg, Germany
[58c]ZITI Institut für technische Informatik, Ruprecht-Karls-Universität Heidelberg, Mannheim, Germany
[59]Faculty of Applied Information Science, Hiroshima Institute of Technology, Hiroshima, Japan
[60a]Department of Physics, The Chinese University of Hong Kong, Shatin, N.T., Hong Kong, China
[60b]Department of Physics, The University of Hong Kong, Hong Kong, China
[60c]Department of Physics, The Hong Kong University of Science and Technology, Clear Water Bay, Kowloon, Hong Kong, China
[61]Department of Physics, Indiana University, Bloomington, Indiana, USA
[62]Institut für Astro- und Teilchenphysik, Leopold-Franzens-Universität, Innsbruck, Austria
[63]University of Iowa, Iowa City, Iowa, USA
[64]Department of Physics and Astronomy, Iowa State University, Ames, Iowa, USA
[65]Joint Institute for Nuclear Research, JINR Dubna, Dubna, Russia
[66]KEK, High Energy Accelerator Research Organization, Tsukuba, Japan
[67]Graduate School of Science, Kobe University, Kobe, Japan
[68]Faculty of Science, Kyoto University, Kyoto, Japan
[69]Kyoto University of Education, Kyoto, Japan
[70]Department of Physics, Kyushu University, Fukuoka, Japan
[71]Instituto de Física La Plata, Universidad Nacional de La Plata and CONICET, La Plata, Argentina
[72]Physics Department, Lancaster University, Lancaster, United Kingdom

[73a]*INFN Sezione di Lecce, Lecce, Italy*
[73b]*Dipartimento di Matematica e Fisica, Università del Salento, Lecce, Italy*
[74]*Oliver Lodge Laboratory, University of Liverpool, Liverpool, United Kingdom*
[75]*Department of Physics, Jožef Stefan Institute and University of Ljubljana, Ljubljana, Slovenia*
[76]*School of Physics and Astronomy, Queen Mary University of London, London, United Kingdom*
[77]*Department of Physics, Royal Holloway University of London, Surrey, United Kingdom*
[78]*Department of Physics and Astronomy, University College London, London, United Kingdom*
[79]*Louisiana Tech University, Ruston, Louisiana, USA*
[80]*Laboratoire de Physique Nucléaire et de Hautes Energies, UPMC and Université Paris-Diderot and CNRS/IN2P3, Paris, France*
[81]*Fysiska institutionen, Lunds universitet, Lund, Sweden*
[82]*Departamento de Fisica Teorica C-15, Universidad Autonoma de Madrid, Madrid, Spain*
[83]*Institut für Physik, Universität Mainz, Mainz, Germany*
[84]*School of Physics and Astronomy, University of Manchester, Manchester, United Kingdom*
[85]*CPPM, Aix-Marseille Université and CNRS/IN2P3, Marseille, France*
[86]*Department of Physics, University of Massachusetts, Amherst, Massachusetts, USA*
[87]*Department of Physics, McGill University, Montreal, Québec, Canada*
[88]*School of Physics, University of Melbourne, Victoria, Australia*
[89]*Department of Physics, The University of Michigan, Ann Arbor, Michigan, USA*
[90]*Department of Physics and Astronomy, Michigan State University, East Lansing, Michigan, USA*
[91a]*INFN Sezione di Milano, Milano, Italy*
[91b]*Dipartimento di Fisica, Università di Milano, Milano, Italy*
[92]*B.I. Stepanov Institute of Physics, National Academy of Sciences of Belarus, Minsk, Republic of Belarus*
[93]*National Scientific and Educational Centre for Particle and High Energy Physics, Minsk, Republic of Belarus*
[94]*Department of Physics, Massachusetts Institute of Technology, Cambridge, Massachusetts, USA*
[95]*Group of Particle Physics, University of Montreal, Montreal Québec, Canada*
[96]*P.N. Lebedev Institute of Physics, Academy of Sciences, Moscow, Russia*
[97]*Institute for Theoretical and Experimental Physics (ITEP), Moscow, Russia*
[98]*National Research Nuclear University MEPhI, Moscow, Russia*
[99]*D.V. Skobeltsyn Institute of Nuclear Physics, M.V. Lomonosov Moscow State University, Moscow, Russia*
[100]*Fakultät für Physik, Ludwig-Maximilians-Universität München, München, Germany*
[101]*Max-Planck-Institut für Physik (Werner-Heisenberg-Institut), München, Germany*
[102]*Nagasaki Institute of Applied Science, Nagasaki, Japan*
[103]*Graduate School of Science and Kobayashi-Maskawa Institute, Nagoya University, Nagoya, Japan*
[104a]*INFN Sezione di Napoli, Napoli, Italy*
[104b]*Dipartimento di Fisica, Università di Napoli, Napoli, Italy*
[105]*Department of Physics and Astronomy, University of New Mexico, Albuquerque, New Mexico, USA*
[106]*Institute for Mathematics, Astrophysics and Particle Physics, Radboud University Nijmegen/Nikhef, Nijmegen, Netherlands*
[107]*Nikhef National Institute for Subatomic Physics and University of Amsterdam, Amsterdam, Netherlands*
[108]*Department of Physics, Northern Illinois University, DeKalb, Illinois, USA*
[109]*Budker Institute of Nuclear Physics, SB RAS, Novosibirsk, Russia*
[110]*Department of Physics, New York University, New York, New York, USA*
[111]*Ohio State University, Columbus, Ohio, USA*
[112]*Faculty of Science, Okayama University, Okayama, Japan*
[113]*Homer L. Dodge Department of Physics and Astronomy, University of Oklahoma, Norman, Oklahoma, USA*
[114]*Department of Physics, Oklahoma State University, Stillwater, Oklahoma, USA*
[115]*Palacký University, RCPTM, Olomouc, Czech Republic*
[116]*Center for High Energy Physics, University of Oregon, Eugene, Oregon, USA*
[117]*LAL, Université Paris-Sud and CNRS/IN2P3, Orsay, France*
[118]*Graduate School of Science, Osaka University, Osaka, Japan*
[119]*Department of Physics, University of Oslo, Oslo, Norway*
[120]*Department of Physics, Oxford University, Oxford, United Kingdom*
[121a]*INFN Sezione di Pavia, Pavia, Italy*
[121b]*Dipartimento di Fisica, Università di Pavia, Pavia, Italy*
[122]*Department of Physics, University of Pennsylvania, Philadelphia, Pennsylvania, USA*
[123]*Petersburg Nuclear Physics Institute, Gatchina, Russia*
[124a]*INFN Sezione di Pisa, Pisa, Italy*

[124b]*Dipartimento di Fisica E. Fermi, Università di Pisa, Pisa, Italy*
[125]*Department of Physics and Astronomy, University of Pittsburgh, Pittsburgh, Pennsylvania, USA*
[126a]*Laboratorio de Instrumentacao e Fisica Experimental de Particulas - LIP, Lisboa, Portugal*
[126b]*Faculdade de Ciências, Universidade de Lisboa, Lisboa, Portugal*
[126c]*Department of Physics, University of Coimbra, Coimbra, Portugal*
[126d]*Centro de Física Nuclear da Universidade de Lisboa, Lisboa, Portugal*
[126e]*Departamento de Fisica, Universidade do Minho, Braga, Portugal*
[126f]*Departamento de Fisica Teorica y del Cosmos and CAFPE, Universidad de Granada, Granada, Spain*
[126g]*Dep Fisica and CEFITEC of Faculdade de Ciencias e Tecnologia, Universidade Nova de Lisboa, Caparica, Portugal*
[127]*Institute of Physics, Academy of Sciences of the Czech Republic, Praha, Czech Republic*
[128]*Czech Technical University in Prague, Praha, Czech Republic*
[129]*Faculty of Mathematics and Physics, Charles University in Prague, Praha, Czech Republic*
[130]*State Research Center Institute for High Energy Physics, Protvino, Russia*
[131]*Particle Physics Department, Rutherford Appleton Laboratory, Didcot, United Kingdom*
[132a]*INFN Sezione di Roma, Roma, Italy*
[132b]*Dipartimento di Fisica, Sapienza Università di Roma, Roma, Italy*
[133a]*INFN Sezione di Roma Tor Vergata, Roma, Italy*
[133b]*Dipartimento di Fisica, Università di Roma Tor Vergata, Roma, Italy*
[134a]*INFN Sezione di Roma Tre, Roma, Italy*
[134b]*Dipartimento di Matematica e Fisica, Università Roma Tre, Roma, Italy*
[135a]*Faculté des Sciences Ain Chock, Réseau Universitaire de Physique des Hautes Energies - Université Hassan II, Casablanca, Morocco*
[135b]*Centre National de l'Energie des Sciences Techniques Nucleaires, Rabat, Morocco*
[135c]*Faculté des Sciences Semlalia, Université Cadi Ayyad, LPHEA-Marrakech, Morocco*
[135d]*Faculté des Sciences, Université Mohamed Premier and LPTPM, Oujda, Morocco*
[135e]*Faculté des sciences, Université Mohammed V-Agdal, Rabat, Morocco*
[136]*DSM/IRFU (Institut de Recherches sur les Lois Fondamentales de l'Univers), CEA Saclay (Commissariat à l'Energie Atomique et aux Energies Alternatives), Gif-sur-Yvette, France*
[137]*Santa Cruz Institute for Particle Physics, University of California Santa Cruz, Santa Cruz, California, USA*
[138]*Department of Physics, University of Washington, Seattle Washington, USA*
[139]*Department of Physics and Astronomy, University of Sheffield, Sheffield, United Kingdom*
[140]*Department of Physics, Shinshu University, Nagano, Japan*
[141]*Fachbereich Physik, Universität Siegen, Siegen, Germany*
[142]*Department of Physics, Simon Fraser University, Burnaby BC, Canada*
[143]*SLAC National Accelerator Laboratory, Stanford, California, USA*
[144a]*Faculty of Mathematics, Physics & Informatics, Comenius University, Bratislava, Slovak Republic*
[144b]*Department of Subnuclear Physics, Institute of Experimental Physics of the Slovak Academy of Sciences, Kosice, Slovak Republic*
[145a]*Department of Physics, University of Cape Town, Cape Town, South Africa*
[145b]*Department of Physics, University of Johannesburg, Johannesburg, South Africa*
[145c]*School of Physics, University of the Witwatersrand, Johannesburg, South Africa*
[146a]*Department of Physics, Stockholm University, Stockholm, Sweden*
[146b]*The Oskar Klein Centre, Stockholm, Sweden*
[147]*Physics Department, Royal Institute of Technology, Stockholm, Sweden*
[148]*Departments of Physics & Astronomy and Chemistry, Stony Brook University, Stony Brook, New York, USA*
[149]*Department of Physics and Astronomy, University of Sussex, Brighton, United Kingdom*
[150]*School of Physics, University of Sydney, Sydney, Australia*
[151]*Institute of Physics, Academia Sinica, Taipei, Taiwan*
[152]*Department of Physics, Technion: Israel Institute of Technology, Haifa, Israel*
[153]*Raymond and Beverly Sackler School of Physics and Astronomy, Tel Aviv University, Tel Aviv, Israel*
[154]*Department of Physics, Aristotle University of Thessaloniki, Thessaloniki, Greece*
[155]*International Center for Elementary Particle Physics and Department of Physics, The University of Tokyo, Tokyo, Japan*
[156]*Graduate School of Science and Technology, Tokyo Metropolitan University, Tokyo, Japan*
[157]*Department of Physics, Tokyo Institute of Technology, Tokyo, Japan*

[158]*Department of Physics, University of Toronto, Toronto, Ontario, Canada*
[159a]*TRIUMF, Vancouver, British Columbia, Canada*
[159b]*Department of Physics and Astronomy, York University, Toronto, Ontario, Canada*
[160]*Faculty of Pure and Applied Sciences, University of Tsukuba, Tsukuba, Japan*
[161]*Department of Physics and Astronomy, Tufts University, Medford, Massachusetts, USA*
[162]*Centro de Investigaciones, Universidad Antonio Narino, Bogota, Colombia*
[163]*Department of Physics and Astronomy, University of California Irvine, Irvine, California, USA*
[164a]*INFN Gruppo Collegato di Udine, Sezione di Trieste, Udine, Italy*
[164b]*ICTP, Trieste, Italy*
[164c]*Dipartimento di Chimica, Fisica e Ambiente, Università di Udine, Udine, Italy*
[165]*Department of Physics, University of Illinois, Urbana, Illinois, USA*
[166]*Department of Physics and Astronomy, University of Uppsala, Uppsala, Sweden*
[167]*Instituto de Física Corpuscular (IFIC) and Departamento de Física Atómica, Molecular y Nuclear and Departamento de Ingeniería Electrónica and Instituto de Microelectrónica de Barcelona (IMB-CNM), University of Valencia and CSIC, Valencia, Spain*
[168]*Department of Physics, University of British Columbia, Vancouver, British Columbia, Canada*
[169]*Department of Physics and Astronomy, University of Victoria, Victoria, British Columbia, Canada*
[170]*Department of Physics, University of Warwick, Coventry, United Kingdom*
[171]*Waseda University, Tokyo, Japan*
[172]*Department of Particle Physics, The Weizmann Institute of Science, Rehovot, Israel*
[173]*Department of Physics, University of Wisconsin, Madison, Wisconsin, USA*
[174]*Fakultät für Physik und Astronomie, Julius-Maximilians-Universität, Würzburg, Germany*
[175]*Fachbereich C Physik, Bergische Universität Wuppertal, Wuppertal, Germany*
[176]*Department of Physics, Yale University, New Haven, Connecticut, USA*
[177]*Yerevan Physics Institute, Yerevan, Armenia*
[178]*Centre de Calcul de l'Institut National de Physique Nucléaire et de Physique des Particules (IN2P3), Villeurbanne, France*

[a]Deceased.
[b]Also at Department of Physics, King's College London, London, United Kingdom.
[c]Also at Institute of Physics, Azerbaijan Academy of Sciences, Baku, Azerbaijan.
[d]Also at Novosibirsk State University, Novosibirsk, Russia.
[e]Also at TRIUMF, Vancouver BC, Canada.
[f]Also at Department of Physics, California State University, Fresno CA, USA.
[g]Also at Department of Physics, University of Fribourg, Fribourg, Switzerland.
[h]Also at Departamento de Fisica e Astronomia, Faculdade de Ciencias, Universidade do Porto, Portugal.
[i]Also at Tomsk State University, Tomsk, Russia.
[j]Also at CPPM, Aix-Marseille Université and CNRS/IN2P3, Marseille, France.
[k]Also at Università di Napoli Parthenope, Napoli, Italy.
[l]Also at Institute of Particle Physics (IPP), Canada.
[m]Also at Particle Physics Department, Rutherford Appleton Laboratory, Didcot, United Kingdom.
[n]Also at Department of Physics, St. Petersburg State Polytechnical University, St. Petersburg, Russia.
[o]Also at Louisiana Tech University, Ruston LA, USA.
[p]Also at Institucio Catalana de Recerca i Estudis Avancats, ICREA, Barcelona, Spain.
[q]Also at Department of Physics, National Tsing Hua University, Taiwan.
[r]Also at Department of Physics, The University of Texas at Austin, Austin TX, USA.
[s]Also at Institute of Theoretical Physics, Ilia State University, Tbilisi, Georgia.
[t]Also at CERN, Geneva, Switzerland.
[u]Also at Georgian Technical University (GTU),Tbilisi, Georgia.
[v]Also at Ochadai Academic Production, Ochanomizu University, Tokyo, Japan.
[w]Also at Manhattan College, New York NY, USA.
[x]Also at Institute of Physics, Academia Sinica, Taipei, Taiwan.
[y]Also at LAL, Université Paris-Sud and CNRS/IN2P3, Orsay, France.
[z]Also at Academia Sinica Grid Computing, Institute of Physics, Academia Sinica, Taipei, Taiwan.
[aa]Also at School of Physics, Shandong University, Shandong, China.
[bb]Also at Moscow Institute of Physics and Technology State University, Dolgoprudny, Russia.
[cc]Also at Section de Physique, Université de Genève, Geneva, Switzerland.
[dd]Also at International School for Advanced Studies (SISSA), Trieste, Italy.
[ee]Also at Department of Physics and Astronomy, University of South Carolina, Columbia SC, USA.
[ff]Also at School of Physics and Engineering, Sun Yat-sen University, Guangzhou, China.

[gg]Also at Faculty of Physics, M.V.Lomonosov Moscow State University, Moscow, Russia.
[hh]Also at National Research Nuclear University MEPhI, Moscow, Russia.
[ii]Also at Department of Physics, Stanford University, Stanford CA, USA.
[jj]Also at Institute for Particle and Nuclear Physics, Wigner Research Centre for Physics, Budapest, Hungary.
[kk]Also at Department of Physics, The University of Michigan, Ann Arbor MI, USA.
[ll]Also at Discipline of Physics, University of KwaZulu-Natal, Durban, South Africa.
[mm]Also at University of Malaya, Department of Physics, Kuala Lumpur, Malaysia.